Application of linear-array refraction microtremor in determining shear wave velocity in urban settings:

A case study of Nakuru Municipality, Kenya

Mwaura, George Kinyanjui

I56/82719/2015

Department of Geology

School of Physical Sciences

College of Biological and Physical Sciences

University of Nairobi

A dissertation Submitted to the Department of Geology in partial fulfillment of the Requirements for the Degree of Master of Science in Geology (Engineering Geology) at the University of Nairobi

October 2018

Declaration

I hereby declare that this is my original work and has not been submitted by any other person, form or institution for any award.

Candidate: Mwaura George Kinyanjui

Signature:..... Date: .....

This dissertation has been submitted for examination with my approval as the university supervisor

Supervisor: Dr. Z. N. Kuria

Signature:..... Date: .....

Supervisor: Dr. E. W. Dindi

Signature: ..... Date: ....

Declaration of originality form

This form must be completed and signed for all works submitted to the University for Examination.

Name of student: George Kinyanjui Mwaura

Registration Number: I56/82719/2015

College: College of biological and physical sciences

School: Physical sciences

Department: Department of Geology

Course Name: Master of Science in Geology

Title of work: "Application of linear-array refraction microtremor in determining shear wave velocity in urban settings: A case study of Nakuru Municipality, Kenya"

Declaration

1. I understand what plagiarism is and I am aware of the university's policy in this regard
2. I declare that this dissertation is my original work and has not been submitted elsewhere for examination, award of a degree or publication. Where other peoples work or my own work has been used, this has properly been acknowledged and referenced in accordance with the university of Nairobi's requirements
3. I have not sough or used the services of any professional agencies to produce this work
4. I have not allowed, and shall not allow anyone to copy my work with the intension of passing it off as his/her own work.
5. I understand that any false claim in respect to this work shall result in disciplinary action, in accordance with university plagiarism policy.

Signature: .....

Date: .....

Acknowledgements

My gratitude and acknowledgement as this work becomes a success go to the following:

To God first, I give my thanks for every opportunity, grace and for His enabling hand in all my endeavors. For every beginning, and every ending, for this culmination, all glory and honor go to the Almighty God.

A lot of gratitude goes to the University of Nairobi through the Board of Postgraduate studies for the scholarship award and for finding me deserving of the opportunity to study and for all the assistance granted to me. Thank you.

My supervisors, Dr. Z. N Kuria and Dr. E. Dindi for the constant guidance, corrections and patience throughout the research work. This culmination would not have been what it is without you. God bless you boundlessly.

Dr. D. W. Ichang'i, for the constant follow up with my progress, thereby making sure I never went to sleep when I should have been working, and for the constant reminder of the potential in me. God bless you abundantly Sir.

My dear wife, Mary and our two children, Wanjiru and Mwaura for being patient with me when I had to work late nights and through the weekends. My absence was great at times but your understanding was greater.

Lastly but not least, to Kim, Jimmy, Nyotu and Maggy, for your support during the execution of the field work. I have known not a greater commitment in friendship. God bless you boundlessly.

Dedication

To Mum and Dad, a boy grows to a man, but I will always be your boy. To this height, it has taken your prayers, dedication and love. I give it all back.

Who would have thought?

Abstract

This dissertation presents the results of a ReMi survey conducted in Nakuru Municipality, in Nakuru County, Kenya. Nakuru Municipality is located in the tectonically active rift valley of Kenya with a significantly higher risk of seismic activity.

A 12Km profile was done along the Nairobi-Nakuru-Eldoret highway starting at the Njoro junction and ending at Lanet junction and another short one (1.6Km) running nearly N-S and perpendicular to the 12Km one giving a total of 55 ReMi soundings.

A 2-D model with S-wave velocity ranging from a low of 150m/s to a high of 1000m/s was produced. The low velocities represent loose and mechanically weak material. Higher velocities represent the stiff, well cemented and compact material possessing higher mechanical strength. The area is depicted as having a loose soil cover extending to a depth of not more than 20m. The area to the west has the deepest soil cover that reaches about 15m. The central region only has patches of this material with intermittent outcrops of slightly weathered rock on the surface. The area to the east has slightly more of this loose material. These loose soils are represented by velocities ranging between 150-300m/s. Below these soils is a stiff and denser material from a depth of between 10 and 20m. This dense material, presumed to be weathered rock and cemented pyroclastics is shallower in the central part of the profile, that is, the CBD area. This material is represented by V_s velocities between 400-700m/s and extends to more than 100m in most areas. Values greater than 700m/s are attributed to harder and fairly fresh rock that is mostly mapped in the central part of the profile from a depth of 20m to the deepest reaches of the survey probe at about 100m.

Numerous deep faults were identified as low V_s zones gated by high velocity zones on either sides. These zones recorded velocities in the range of 150-400m/s. The V_s30 for the study area falls between 240 and 680m/s. The range between 240-360m/s places the area to the west in class D, while the rest of the study area falls under class C (V_{s30}=360-760m/s) according to the IBC. The measured S-wave and P-wave velocities have also been used to derive geotechnical dynamic soil parameters that include the shear and elastic moduli for the entire survey area.

Table of Contents

List of tables

List if figures

List of symbols and abbreviations

V_s	Shear wave velocity
V_p	P- wave velocity
s/n	Signal to noise
G	Shear modulus
V_{s30}	Averaged shear wave velocity for the first 30m.
E	Young's modulus/Elastic modulus
ρ	Density
ν	Poisons ratio
RQD	Rock Quality Designation
ReMi	Refraction microtremor
SASW	Spectral Analysis of surface waves
MASW	Multichannel analysis of surface waves
ERT	Electrical resistivity tomography
VLF-EM	Very Low Frequency Electromagnetics
SPAC	Spatial autocorrelation
ESAC	Extended spatial autocorrelation
1-D/2-D	One / two dimensional
SPS	Suspension P and S-wave velocity
CBD	Central Business District
IBC	International Building Code
NEHRP	National Earthquake Hazard Reduction Program

1 CHAPTER ONE: INTRODUCTION

1.1 Background information

Engineering site characterization is usually the starting point of any civil engineering project (Siller and Huang, 1997). Otherwise known as geotechnical site investigation, this is a process through which all the relevant information regarding a proposed civil engineering development is acquired (Simons et al., 2002). The Geological and/ or Geotechnical engineers are the first ones on a proposed site for any civil construction to gather this information.

Among the several tasks the Engineering Geologist is expected to deliver on is the characterization of the proposed site with regards to the prevailing geologic conditions, the mechanical properties of the soils and rocks underlying the site (Eddlestone et al., 1995). In addition, the dynamic properties of the soils that determine how the soils respond to the shearing and shaking effects of an earthquake are also determined during the site characterization phase (Luna and Jadi, 2000).

Steeples (2001) noted that site characterization has in the recent past improved greatly due to developments made in geophysical survey techniques and advancements in instrumentation. He also indicates that modern methods of site characterization benefit from improved accuracy and usefulness due to advances made in software used to process data. Uncertainties that were more rampant in earlier days are thus clarified.

One of the latest developments in site characterization is the need to determine some geotechnical parameters in-situ. Luna and Jadi (2000) expressed the need to apply the initial stress conditions in all attempts to characterize soil behavior. In this respect, shear wave velocity is measured in most cases to determine the dynamic properties of soils. Shear wave velocity can provide crucial input to seismic design, including site response analysis and liquefaction potential analysis (Hamman and Eliwa, 2012). In addition, they also indicate that since S-wave velocity is representative of material and structural conditions of the soil, it can, therefore, be used to asses layer structure and consolidation or compaction degree of a particular soil layer. Perez et al., (2011) also highlight the

importance of shear wave velocity measurement in earthquake engineering due to the direct relationship between S-wave velocity and stress and strain properties of soils.

There are basically two categories of methods for measuring shear wave velocity; destructive and non-destructive testing methods. The destructive methods otherwise referred to as Invasive methods involve drilling holes in to the ground for determination of V_s using different approaches. The common methods include downhole and crosshole (Stokoe and Woods, 1972) and suspension logging (Ohya et al., 1984). Seismic cone penetration test (SCPT) (Campanella et al., 1986) is also used in shallow surveys. These methods are expensive and inefficient, especially in urban areas.

The modern and commonly used non-invasive methods include Spectral Analysis of Surface Waves (SASW) by Nazarian et al., (1984), Multichannel Analysis of Surface waves (MASW) developed by Park et al., (1999) and the more recent refraction microtremor (ReMI) introduced by Louie (2001). These methods have grown in popularity partly because they provide for determination of in-situ V_s measurements at an affordable cost, and quickly (Tokeshi et al., 2013). The need to estimate small-strain shear properties of soil in recent times for ground deformation analyses has also propelled the usefulness of these methods (Luna and Jadi, 2000).

Unlike the other methods, ReMi is particularly applicable in urban settings since the other surface wave methods suffer from the high levels of ambient noise from cultural activities (Chan, 2006). ReMi overcomes this challenge by primarily using this ambient seismic noise as the source of data. This combined with the functional simplicity of SASW and the multichannel recording of MASW and the easy linear field set up of a refraction survey allows ReMi to effectively and efficiently be applied in urban settings (Poormirzaee, 2016). According to Louie (2001), with a configuration of 12 to 48 vertical geophones, with a natural frequency of 8-12Hz, one can be able to measure surface wave velocities at frequencies as low as 2Hz and as high as 26Hz. Such a frequency range allows measurement of shear wave velocities up to 100m below the surface (Louie, 2001).

In this work, the ReMi method has been applied to measure shear wave velocity in Nakuru Municipality and produce 1-D and 2-D Vs models. The ReMi technique provides

information of large volumes of the subsurface in one dimension in an effective and efficient manner (Poormirzaee, 2016). Similar to MASW and SASW, ReMi is aimed at obtaining a dispersion curve from the Rayleigh waves, but unlike the other two methods, it uses ambient seismic noise (microtremor). Processing of ReMi data however follows the same procedure as the other surface wave methods Louie, 2001).

The shear wave velocity determined in this project was used to develop 1-D shear wave models and classify the city of Nakuru under the Nationa Earthquake Hazard Reduction Programme (NEHRP) and the International Building Code (IBC) classification scheme as recognized by major world authorities. Shear wave velocity can be used as a basic index in estimating liquefaction resistance because both are affected to a large extent by the same factors (Chen et al., 2008). In-situ Shear wave velocity measurements can therefore be used as a first estimation and prediction of liquefaction potential.

The averaged shear wave velocity for the top 30m of soil (V_s30) or subsurface geologic materials is used in both the NEHRP and IBC site classification schemes (Martin and Diehl, 2004). In these classification schemes, engineering sites are divided into six (6) categories of different soil profile types; **A** through **F** (BSSC, 2015). The classes are based on the assumption or expectation that sites within a particular class will respond in a similar manner in the event of an earthquake (Martin and Diehl, 2004).

1.2 The study area

1.3 Location and description

The project location, Nakuru Municipality, is the Headquarters of Nakuru County. It is located some 160 kilometers Northwest of Kenya's capital City, Nairobi. This is the economic hub of the whole county, being the fourth largest urban center in Kenya (UN, 2011). Figure 1.1 shows the location of Nakuru County, Nakuru Municipality and the study area.

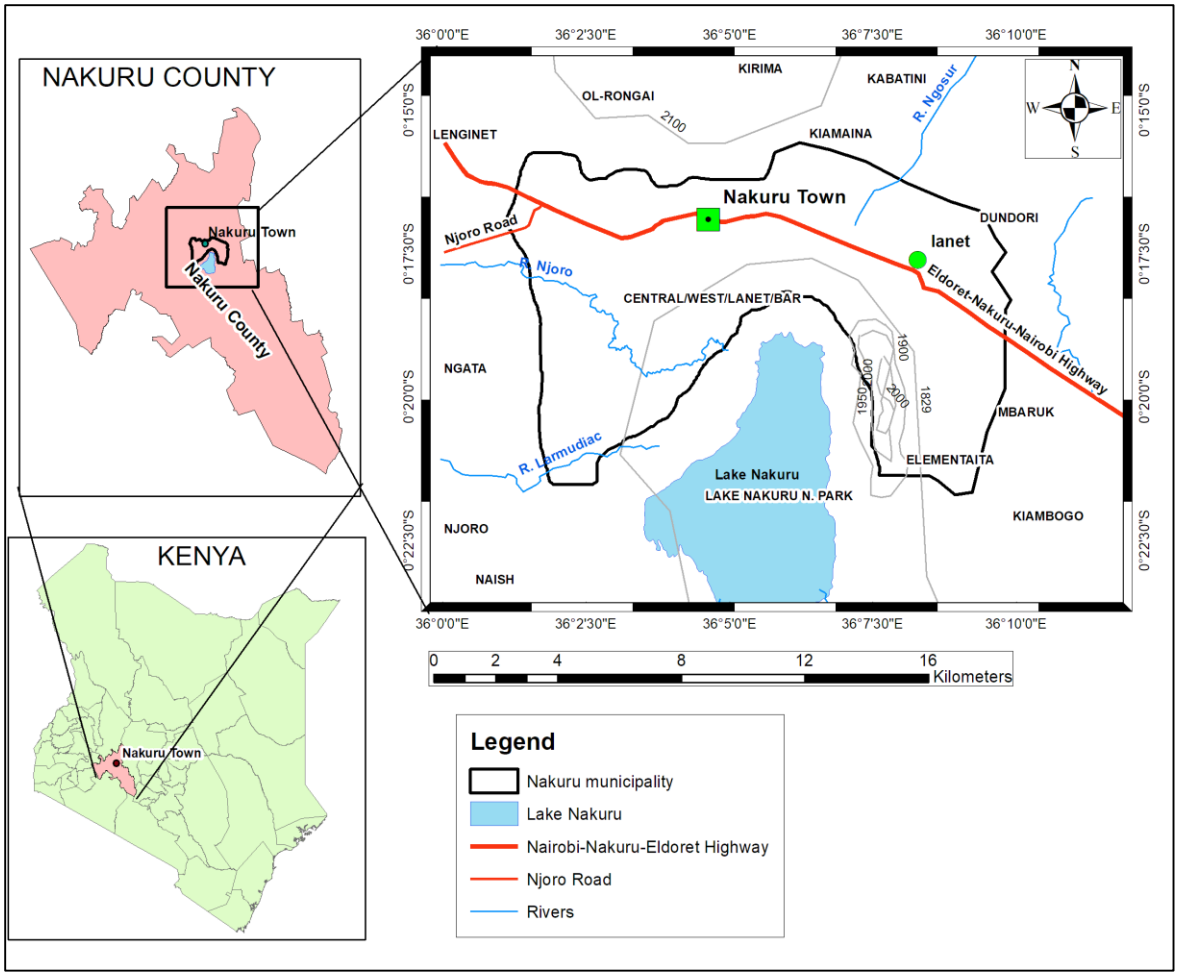

Figure 1.1 Location map of the study area

The economy of Nakuru is dependent on agriculture, manufacturing and tourism. Agricultural activities range from small-medium scale. Coffee, wheat, barley, maize and beans form the bulk of the agricultural produce. Massive silos near Pipeline area by the National Cereals and Produce Board have been built for storage of these produce. Manufacturing industries such as flour milling and grain ginneries get their raw materials from here. Milk is also another product of Nakuru and supports milk processing plants around the city. Major retail stores such as Nakumatt, Uchumi, Naivas and Tuskys have their branches in this city providing goods and services to the people, manufacturing and agricultural sectors.

The United Nations (2011) conducted a study that named Nakuru as Africa's fastest growing city and the fourth in the world. The 2009 Kenya population census listed Nakuru

as having the fourth largest urban population in Kenya at approximately 307, 990 inhabitants (KNBS, 2009). This population is comprised of people from most parts of Kenya and from many regions of the world making it a cosmopolitan Municipality.

1.3.1 Climate

At an altitude of about 1860m.a.s.l. the climate of Nakuru Municipality is typical of the Rift valley ranging from cold and humid to arid and semi-arid. The seasonal migration of the inter-tropical zone (ITCZ) strongly affects the climate of Nakuru. According to Nicholson (2000), rainfall associated with the ITCZ tends to follow the highland sun in the months of March and September. The mean annual rainfall is about 920mm/yr., with the long rains coming in April and May and the short rains between November and December. Temperatures range from a high of 29.3^0C between December and early March to a low of 12^0C between June and July (Kenya meteorological department, 2000).

1.3.2 Vegetation

Nakuru Municipality is surrounded by forests including Menengai crater forest, Mbogoini, Solai, Mau, Bahati and Subukia forests among others. These are a major source of timber and firewood. The forests in the high altitude largely affect the climatic conditions and drainage patterns of the county as a whole. Three vegetation types can be recognized from these forests; the dense near tropical forests and bamboo vegetation of Mau, clumped trees on the grassland areas and shrubs and thickets at valley bottoms and along streams. Eucalyptus forests make up the local artificial forests.

Within the Central Business District (CBD), the main vegetation type includes decorative flowers and trees planted along the road and highway for beautification purposes. Tall trees can also be found within the Nyayo Gardens Park. The tall trees are particularly important on this project as they form part of the environmental noise that is targeted. The trees vibrate when blown by wind and contribute to low frequency signals in the seismic record.

1.3.3 Land Use and Land Resources

Land ownership in Nakuru municipality is either under public or council leases. The peri-urban areas are privately owned without much control on development. Subdivision and transfer of ownership is thus easy in these parts of the Municipality. This has resulted in uncontrolled development without any proper urban planning or management. Tall buildings built on un-investigated liquefiable ground may have resulted from this trend and this poses a risk in the event of an earthquake.

Over time, land use in this Municipality has developed to majorly commercial and industrial rather than from range management and agricultural. Most of the land is either under commercial/industrial or settlement structures.

1.3.4 Settlement structure

Much of the space in Nakuru Municipality has been taken up by the housing sector. Two categories of housing can be recognized from a general point of view: Public and private. Public housing is for government, government corporations and the county staff. This also comprises of rental houses for the county council. Private housing is for individual rental developments or personal occupation by developers (Mwangi, 2003).

The leading provider of housing in Nakuru is the private sector (Mwangi, 2003). This is mainly motivated by the ease of sub-division of land for formal and informal private development, and accelerating the rate of housing development in this sector in the recent past. Flats and high-rise buildings, maisonettes, bungalows, semi-detached housing, terrace, row and informal are the common housing types within and in the peripherals of the Municipality. The distribution of these structures along the study route means that a review of the structural and spatial safety analysis will benefit from the findings of this project.

1.3.5 Physiography and Drainage

Nakuru Municipality is a basin sandwiched between the volcanic landscape of the Menengai crater to the north and the low lying Lake Nakuru to the south. To the north-east is the Bahati escarpment of the Aberdares escarpment (Mwangi, 2003).

The local physiography is rather non-uniform too. The area occupied by the CBD is gently sloping and therefore well drained, with a general slope to the south at an altitude range between 1800-1860meters. The Hyrax hills and the *Milimani* estate regions represent the highest points closest to the CBD.

The drainage system runs from the high slopes of Menengai, Eburru and Mau to the low areas of Lake Nakuru basin. To the west, the east dipping faults of the Mau escarpment bound the Nakuru basin. The west dipping faults separating the intra-rift Bahati-Kinangop plateau from the eastern rift shoulders make up the western borders of the Nakuru basin (Okech, 2012). As noted earlier, the Menengai crater forms the northern bounds. Poor run-off is characteristic of this basin due to the widespread porous surface geology (McCall, 1967). The main rivers flowing in the peripherals of the Municipality include Rivers Njoro, Ngosur, Makalia, Larmudiac, Nderit and Naishi, all of which drain into Lake Nakuru (Figure 2.1). Rivers Njoro, Ngosur and Naishi disappear into faults and form a crucial source of recharge for the aquifer system in Nakuru (Okech, 2012). Springs believed to originate from the Bahati escarpment also flow towards the Lake through underground streams, making surface appearance as the Baharini springs. These springs are rather perennial (Raini, 2005).

The drainage pattern of these rivers is non-uniform. All, except Ngosur River drain the mau escarpment which further drains the Bahati escarpments. Njoro River flows in a dendritic pattern while Makalia and Larmudiac exhibit a trellis pattern. Nderit and Ngosur, and other minor streams that drain Bahati escarpments, Menengai crater and Lion hill flow in rather straight channels (Okech, 2012).

1.3.6 Geology and Structures

The geology of the study area and its environs is comprised of pyroclastics and lava flows of the Tertiary-Quaternary period (McCall, 1967). The main rocks types in this area include the lower Pleistocene Phonolites to the south, the phonolitic trachytes to the Southeast near Lanet, welded vitreous tuffs and ignimbrites north of the Municipality, the glassy, ropy trachyte flows of the Menengai caldera and the agglomeritic tuffs to the south. Surficial and recent deposits include the volcanic soils that cover most of the surface in and around Nakuru Municipality and gravels, tuffs and diatomaceous silts slightly to the

southeast near and around Crescent hill. These soils, if loose, are prone to liquefaction in the event of an earthquake.

Along the study route, volcanic soils are dominant from Lanet in the east to the west at the Njoro junction. Between Lanet and the CBD, pockets of Menengai phonolitic trachytes are encountered, and are observed to be fault controlled. Within the CBD vitreous tuffs and ignimbrites may be observed to outcrop on the road cuts. They are shallowly buried by volcanic soils in this region. To the west, most of the surface is covered by the volcanic soils. These soils are deep in this region with no visible rock outcrops.

1.3.6.1 Structures

Nakuru has a complex structural pattern mainly resulting from the high number and non-uniform orientation of faults (McCall, 1967). The description by McCall (1967) indicates that the patterns displayed by some Cenozoic faults indicate that they may have been controlled by the structural trends of the Basement system. He observes that where it emerges below the Cenozoic formations, the basement system exhibits strongly dominant NNW and NE trends and that normal faults characterized by steep hades represent the Cenozoic-Quaternary faulting, which are near-vertical but may reach up to 60^0. The planes are slightly curved but many of them are predominantly arcuate (McCall, 1967). The presence of these geological structures renders the area rather unstable and highly vulnerable to earthquakes, land subsidence and landslides.

Characteristically the area west of the Municipality has reported cases of subsidence, which could also be expected in the CBD area. Evidence of depressions in the ground and sudden disappearance of surface water into probable fissures, together with vibrations felt on buildings, as a result of heavy commercial vehicles may be indicative of underground cavities (Mwangi, 2003). Ngecu and Nyambok (2000) attributed the incidences of subsidence in the southwest parts of the CBD to the high density of faulting and the unconsolidated silts and pyroclastics that constitute the immediate subsurface cover. Dindi (2015) mapped the faults in the area and noted that all subsidence incidents were located on or near the identified faults. Figure 1.2 is the geological map of the area showing the main rock types and fault patterns

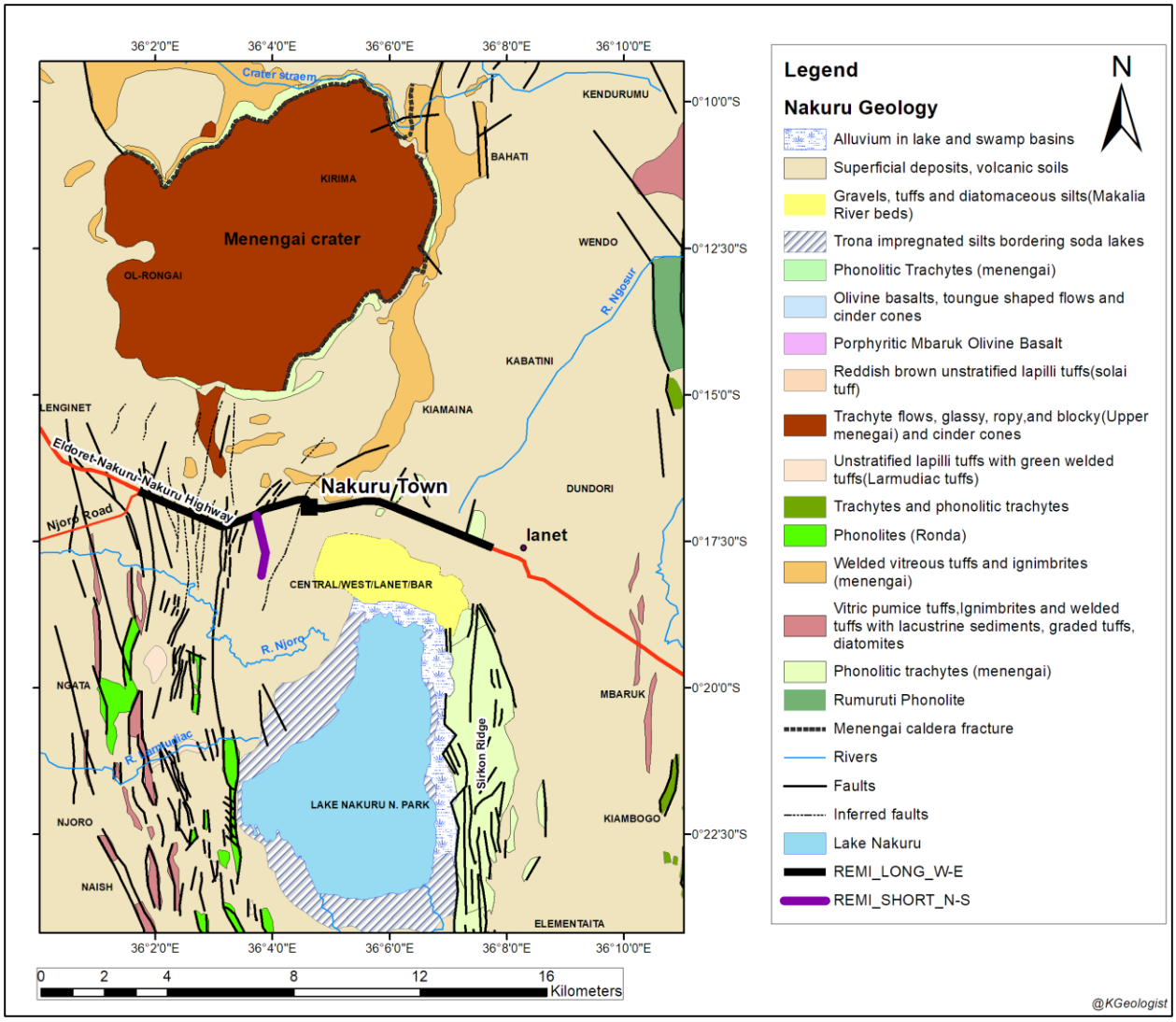

Figure 1.2 Geology of the study area and surrounding areas (McCall 1967)

1.3.7 Soils

The soils within the study area are mainly comprised of volcanic ash, silts and reworked clays and tuffs. Beds of diatomaceous silts and clays and other Lake and river deposits are products of reworked volcanic materials or sub-aqueously deposited pyroclastics (McCall, 1967). These soils are young, poorly developed, porous and light. As a result, the area is characterized by low run-off due to the high porosity of the soils. The geological map (figure 3.2) shows these soils and their distribution in the study area, and it can be observed that they form most of the surface cover.

1.3.8 Surface and Groundwater Resources

1.3.8.1 Surface water

The main rivers in the area have been discussed in section 2.1.6. The Lake Nakuru basin that hosts the Lake Nakuru is the major surface water body in the area. This basin comprises the Lake itself and the Lakeshore and a part of the Njoro River at Kwa Rhoda and Kaptembwa areas.

1.3.8.2 Groundwater

Allen and Darling (1992) suggested that groundwater in the rift receives recharge mainly from rainfall on the flanks of the rift. However, Tole, (1996) noted that this recharge contribution from rainfall is low due to the high levels of evaporation on the floor of the rift, which may even become geothermal waters upon contacting heat sources. The flow and distribution of groundwater in the Nakuru region is controlled by secondary permeability zones such as fractures that are mainly N-S oriented (Olago et al., 2009). This is in agreement with the findings of Clarke et al., (1990) who suggested that the aquifer properties are affected on a small scale by tectonic movements of the rift.

Volcanic areas such Nakuru Municipality tend to have varying depths of groundwater strikes and several aquifers may in fact be encountered on top of each other. The aquifers are mainly confined and their piezometric surfaces vary widely within them (IEA, 2006).

1.4 Problem statement

The use of shear wave velocity (V_s) for evaluating the dynamic properties of soils has been known to be a very important practice for long (Martin and Diehl, 2004). The average shear wave velocity for the top 30m (V_{s30}) has to be determined accurately and efficiently. This data is pertinent to designing of civil structures with earthquake safety considerations, a very important aspect in modern construction requirements. This information is used in the NEHRP provisions and the International Building code (IBC) for site classification (Martin and Diehl, 2004)

Site specific shear wave velocity (V_{s30}) is best determined in-situ. Traditional methods of doing so include borehole measurements such as downhole and crosshole (Stokoe and Woods, 1972) and suspension logging (Ohya et al., 1984). Seismic cone penetration test (SCPT) (Campanella et al., 1986) may also be used (Luna and Jadi, 2000). Notably, all these methods are costly, inefficient, and time consuming and hardly applicable in urban settings due to the high noise levels and the high energy sources required improving the s/n ratio.

Seismic methods such as seismic refraction, SASW (Nazarian and Stokoe, 1984), MASW (Park et al., 1999) are non-invasive and have been favorites for long but are also hindered by the high levels of ambient noise in urban settings that makes it difficult to acquire good quality data. Although cheaper than the invasive methods, these techniques also suffer from technical challenges of data acquisition such as the large energy sources required to considerably improve the signal to noise ratio (Pullammanappallil et al., 2003). They are therefore best applied in seismically quiet sites. Time and size of team required to conduct a day's survey is also a major factor.

There is thus a need for a method to be used in seismic characterization in urban settings, where seismically quiet conditions can hardly be met. The ReMi method is yet to be applied in Kenya for similar projects. This presents us with the opportunity to apply and test it.

Nakuru Municipality, being one of the major economic centers in the country is faced with the challenge of uncertainty in structural integrity of its major infrastructural developments and the safety of its population. This is attributed to limited knowledge and understanding of the geologic materials over which it is built on. The cases of subsidence and earthquake shearing risk for the Municipality are at levels of concern as noted by Ngecu and Nyambok (2000). The population and businesses residing in the buildings may be at risk if the ground they are built on is not properly investigated. This project thus helps in identifying high risk areas and as such advice urban planning regulation. Evidence of volcanic activity derived from the geothermal exploration and drilling program that is quite successful presents significant seismic risk for the Municipality. In addition, the biggest earthquake, which was a Magnitude 6.9, recorded in Kenya on January 6th 1928 occurred

just about 42Km from Nakuru Municipality, in Subukia area (Ambraseys, 1991). The thick cover of unconsolidated sediments presents a major challenge in foundation design and has severally been identified as the major cause of property damage and loss of life in the past (Ngecu and Nyambok, 2000).

This thus poses a great need to understand the seismic characteristics of the soils/geologic materials in the Municipality area as well as produce important geotechnical parameters for use in engineering design of safe civil structures.

1.5 Objectives

The main objective of this project was to determine shear wave velocity for the subsurface geologic materials in Nakuru Municipality and thus be able to classify the Municipality under the National Earthquake Hazard Reduction Program (NEHRP) and the International Building Code (IBC).

The specific objectives of the study were:

1. To evaluate I-D shear wave velocity profiles for Nakuru Municipality along a 12Km section on the main Nairobi-Nakuru-Eldoret highway and the 1.6km Kwa Rhoda feeder road
2. To determine V_s30 and use it to classify Nakuru Municipality according to NEHRP and IBC site classification system
3. To establish the geotechnical character of the geological materials along the major roads traversing the Municipality

1.6 Justification and significance

Nakuru Municipality is located in an earthquake vulnerable region of the tectonically active rift valley and is one of the cities in Kenya with the greatest degree of earthquake hazard (Rao, 2013). The setup of geological structures of the study area includes faults surrounding Nakuru Municipality and a dormant volcano to the north, the Menengai volcano, posing a seismic hazard. The ground cover of unconsolidated silts and pyroclastics also presents a major seismic risk for the Municipality. This is why seismic characterization of the Municipality is very crucial.

For proper earthquake engineering design of any civil structure, a deliberate understanding of the seismic characteristics and dynamic soil properties and the geologic materials at the specific site is of great importance. Shear wave velocity is a crucial parameter in this aspect.

In lieu of the constraints presented by both conventional and modern methods of determining shear wave velocity in urban settings, the refraction microtremor (ReMI) method was employed in this project as a fast, efficient, cheap and accurate method of determining V_s30 in urban settings. This method is non-invasive and non-destructive and only uses the ambient microtremor (noise) as the seismic source. Unlike other seismic methods, such as those requiring explosives, no special permits are required for this type of survey. The fact that the seismic source is readily available in abundance in urban areas makes this technique the most suitable for V_s30 surveys.

The data obtained by this method is representative of a significant ground volume and represents the prevailing in-situ stress conditions of the ground (Fote et al., 2011). This serves as a step towards seismic microzonation of the Municipality and provides primary data for earthquake engineering design and other infrastructural development. It is particularly important for building and regulating policy regarding infrastructural development and human settlement in Nakuru Municipality. Policies such as this informed by scientific evidence have more capability of averting natural disasters such as those occasioned by earthquake caused subsidence and liquefaction. This way, the residents of the area and their properties are protected such calamities. The scientific community also benefits from the data thus obtained for future reference.

2 CHAPTERTWO: LITERATURE REVIEW

2.1 THEORETICAL BACKGROUND

In recent and current times, the analysis of surface waves has been widely utilized in producing shallow earth sub-surface S-wave velocity models. This trend has seen quick and continuous evolution.

Lord Rayleigh (1885) introduced the existence of surface waves and since then, an ever increasing number of researchers have developed interest in the subject. These include researchers drawn from the fields of seismology, geophysics, geotechnical engineering, material science, solid-state physics, microwave engineering, nondestructive testing and ultrasound acoustics (Socco *et al.,* 2010). A review of literature presents leading issues ranging from the historical perspectives, methodology, application and recent trends on the subject. The review focuses on the use of surface waves in geotechnical applications for characterization of civil engineering sites.

2.1.1 Seismic waves

The waves of energy that travel through the earth after an earthquake are referred to as seismic waves. From basic seismology, there are fundamentally two types of seismic waves; those that propagate within a medium (body waves) and those that travel along the shallow parts of the medium (surface waves) (Lillie, 1999). Body waves comprise the compressional waves commonly referred to as P-waves and shear waves commonly referred to as S-waves.

Body waves penetrate deeper in to the earth's interior in form of short pulses of propagating energy following refracted paths that are dependent on the elastic properties of the materials they travel through (Lay and Terry, 1995). P waves are longitudinal and composed of a series of compressions and rarefactions. Particles in their paths thus vibrate back and forth parallel to the direction of the wave travel. Figure 2.1 illustrates this propagation of body waves.

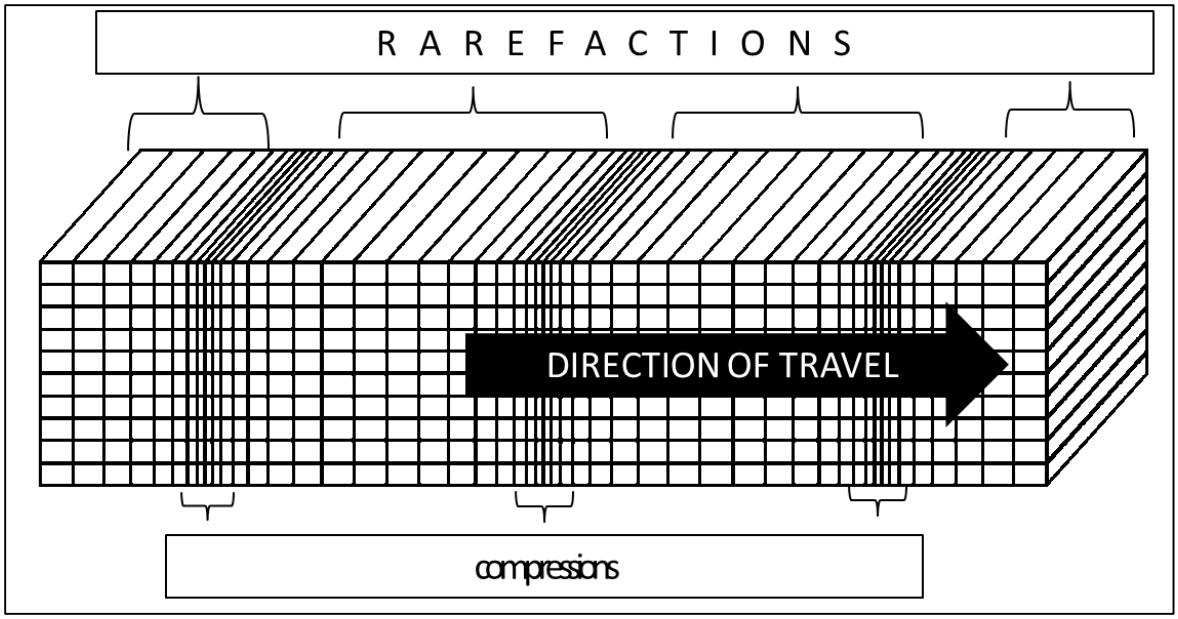

Figure 2.1. Illustration of P-Wave propagation in a medium (modified after Shearer, 2009)

P-wave velocity is given by (Lillie, 1999);

$$V_p = \sqrt{\frac{k+\frac{4}{3}\mu}{\rho}}$$ **where;** **Equation 2-1**

V_p =P-wave velocity

k = Bulk modulus

μ = Shear modulus

ρ = Density

S-waves are transverse waves. Particles in their path are set in motion/vibration perpendicular to the principal direction of travel of the wave. This transverse nature results in polarization of the wave in the vertical and horizontal planes. The vertically polarized component is termed SV while the horizontally polarized component is termed SH (figure 2.2). In isotropic media the two are identical but travel at different speeds in anisotropic media.

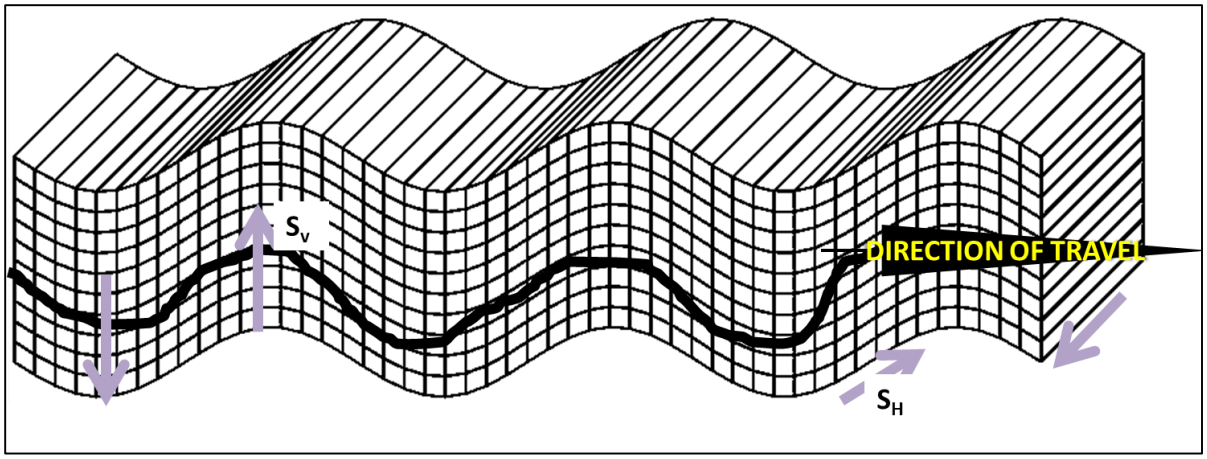

Figure 2.2 Illustration of S-Waves Propagation and SV and SH polarization (Modified after shearer, 2009)

S-wave velocity is given by (Lillie, 1999);

$$V_S = \sqrt{\frac{\mu}{\rho}} \qquad \text{Equation 2-2}$$

The two equations can be interpreted to draw the following generalizations;

1. P-waves will be faster than S-waves for the same material (Lillie, 1999).
2. P and S-waves velocity increase with increase in rigidity; the reason why seismic waves are observed to "speed up" as they travel from the asthenosphere to the lithosphere (higher μ*)* (Lillie, 1999).
3. Fluids have no shear strength (μ=*0);* which means that S-waves cannot travel through fluids and that P-waves travel slower through fluids or the fluid state of material (Lillie, 1999)

2.2 Surface waves

Surface waves travel along the surface of a medium. There are two major types of surface waves: Rayleigh waves and Love waves. These are demonstrated by solving the wave equation when a free surface exists, such as that represented by the earth's surface (Shearer, 2009). As the wave travels along the surface of the earth, the disturbance is greatest at the surface and decreases exponentially with depth.

Rayleigh waves exhibit retrograde elliptical motion. Particles at the top of the ellipse move in opposite direction to the wave travel. On the other hand, Love waves behave like shear

waves. The particles are set in motion in a perpendicularly horizontal (SH) direction to that of the wave propagation (Moro, 2015).

In the analysis of surface waves, Rayleigh waves have achieved quite significant attention. As mentioned before, the basic characteristic of the Rayleigh wave is the retrograde elliptical motion whose amplitude decreases exponentially with depth, the elliptical motion resulting from the superposition of the vertical and horizontal components (Moro, 2015). This is shown in figure 2.4.

Love waves move only in the horizontal plane, transverse to the direction of travel, as compared to the complex nature of Rayleigh waves (figure 2.3 and 2.5). This simplicity is also observed in the computational effort to solve their constitutive equations.

The amplitude of surface waves decreases according to the square root of the distance to the source because their energy is confined to a shallow layer while expanding from the source (Geometric spreading). Body waves lose their energy with distance from the source. The amplitude of the body waves thus reduces greatly compared to surface waves, as a result, surface waves are observed to dominate the data (as noise) in the low-frequency range and are often referred to as ground-roll (Moro, 2015).

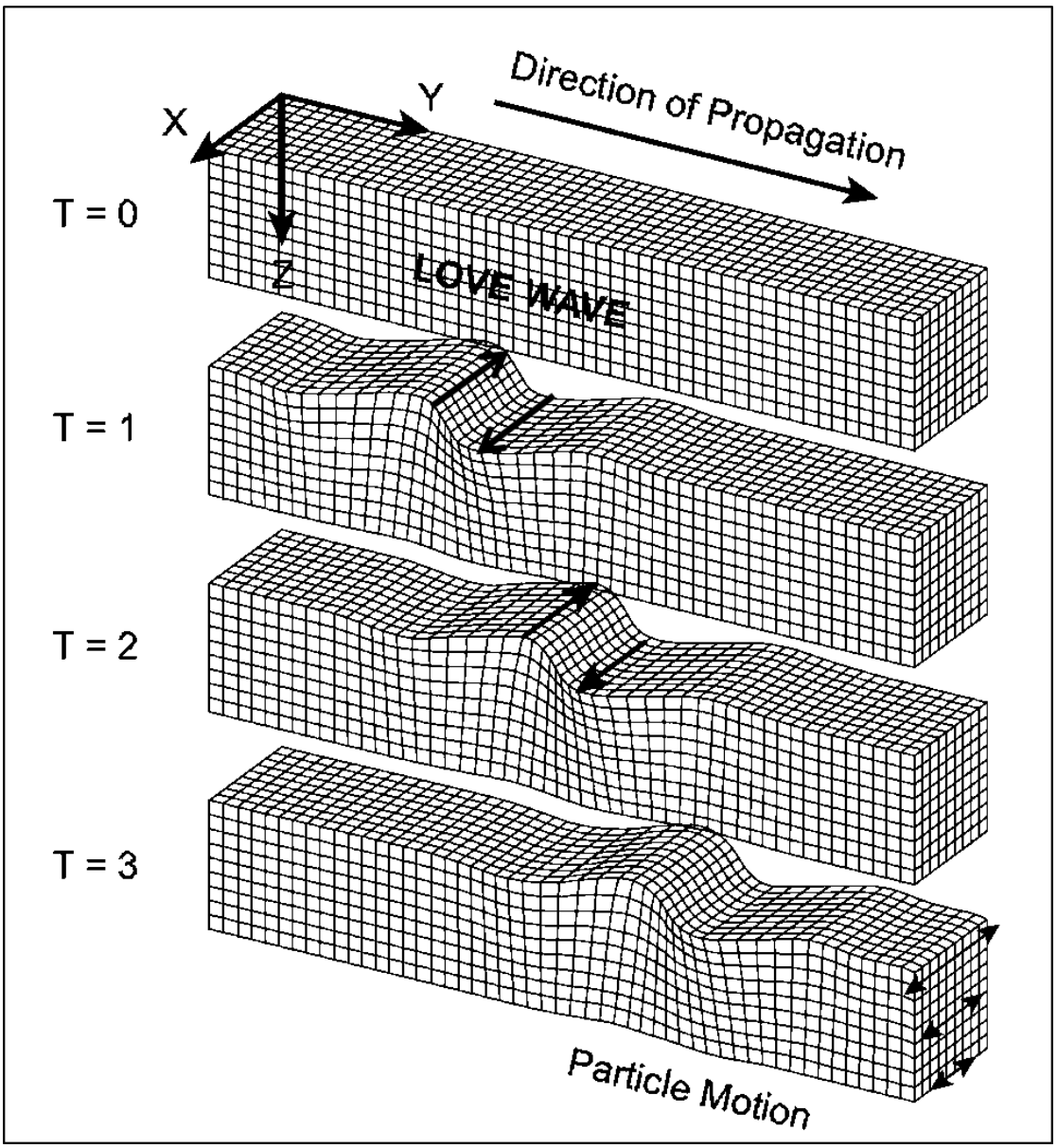

Figure 2.3 Propagation of Love waves at three different times following the wave generation at T=0 (modified from http://www.geo.mtu.edu/UPSeis/waves.html).

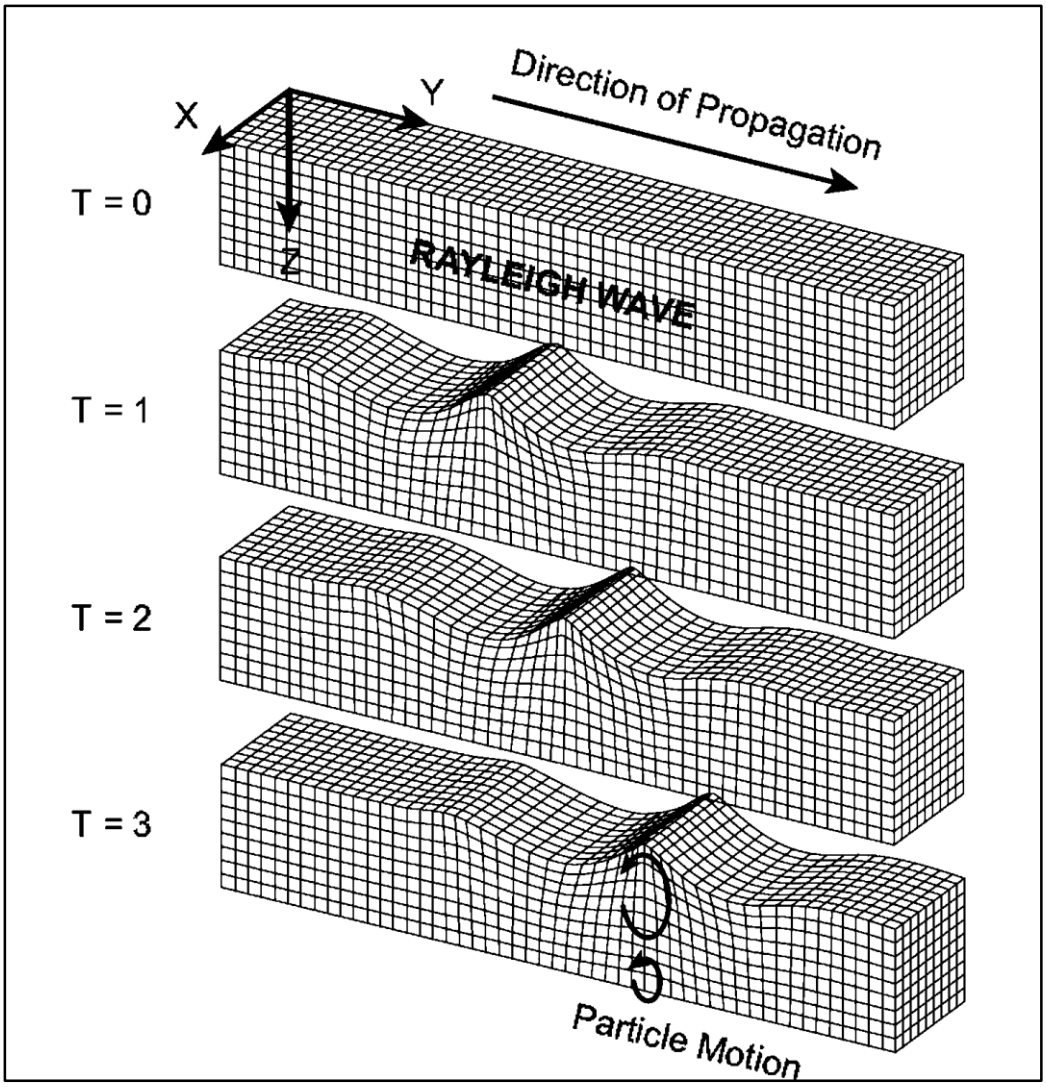

Figure 2.4 Propagation of Rayleigh waves at three different times following the wave generation at T=0 (modified from http://www.geo.mtu.edu/UPSeis/waves.html).

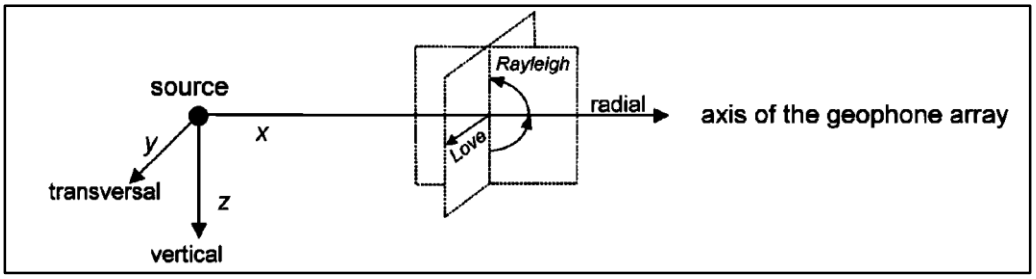

Figure 2.5 Ground motion associated with Rayleigh and Love waves. Rayleigh waves induce particle motion along vertical and radial axes; love waves induce particle motion along the transversal axis only (Moro, 2015).

2.3 Dispersion of Rayleigh waves

One single most useful property of Rayleigh waves is their dispersive nature as they travel in layered media. Surface waves propagate parallel to the earth's surface without spreading their energy into earth's interior. As they travel, their amplitude decreases exponentially with depth, this energy being contained within one wavelength from the surface.

Socco et al., (2010) explains that as the surface wave propagates, it has different harmonics travelling at different wavelengths at different depths. Therefore, in a vertically heterogeneous medium, the surface wave exhibits geometric spreading/dispersion. That is, different frequencies travel at different phase velocities. This dispersive nature of Rayleigh waves as they propagate in vertically heterogeneous media forms the main basis of surface wave measurement. In a homogeneous medium, the different Rayleigh wave frequencies will probe different depths (Figure 2.7) and since the medium is homogeneous, the wavelengths will have the same phase velocity. In such a case, the Rayleigh waves are non-dispersive (figure 2.6)

The propagation in vertically heterogeneous, say layered media, where the individual layers have different mechanical properties, is multimodal in nature (Socco et al., 2010); each frequency travelling in different velocities for the different layers owing to the difference in mechanical properties in the layers the waves are propagating through. The wave will therefore not have a unique velocity, but will have a phase velocity that is very much a function of frequency of propagation.

To observe the relationship between frequency and the phase velocity, a dispersion curve is prepared by plotting frequency on one axis and the phase velocity on the other (Foti et al., 2015). The shape of a dispersion curve will be dependent on local geology. The phase velocity is close to the surface wave velocity in the uppermost layers at low frequencies. At low frequencies, the phase velocity will behave asymptotically to the surface wave velocity of the deeper layers. Inference can thus be easily made that longer wavelengths (low frequency) will penetrate deeper than short wavelengths (high frequency).

For a layered medium where the S-velocity increases with depth, a **normal curve** results in which the phase velocity decreases with frequency. A **reverse dispersion curve** results where the S-wave decreases with depth, in which case the phase velocity increases with frequency. In situations where the geology is complex, the relation between phase velocity and frequency will portray this complexity by producing an **irregular dispersion curve**. The most common scenario however is the normal curve, representing most geological settings. This is illustrated in figures 2.6 to 2.8.

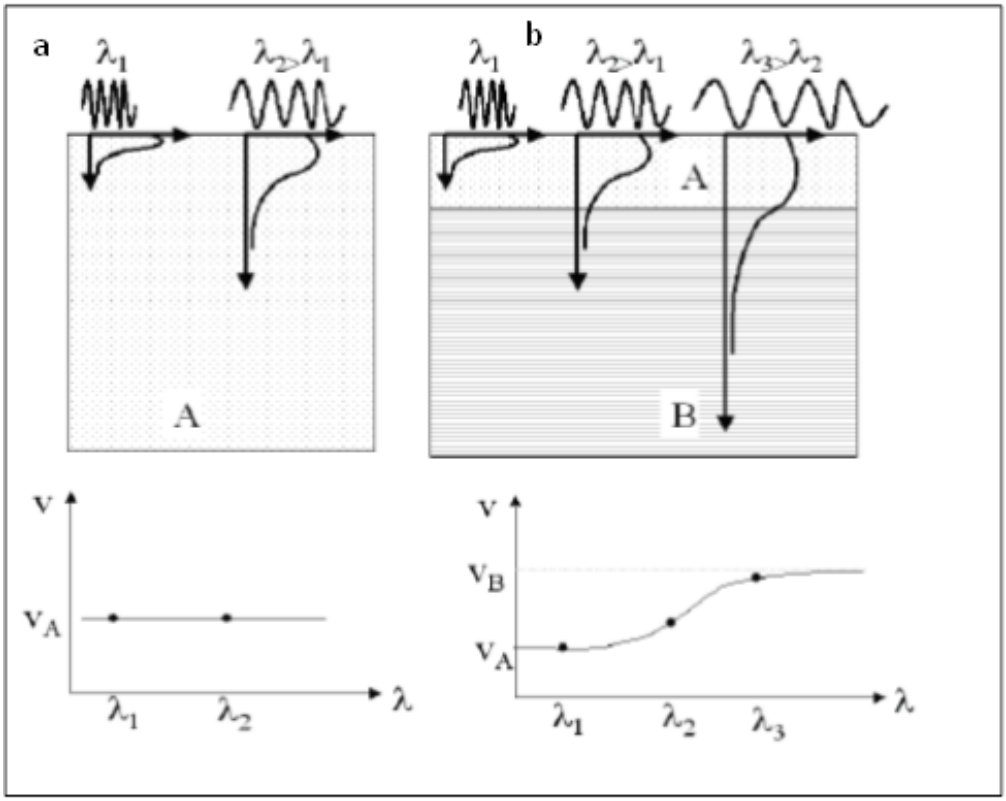

Figure 2.6 (a) S-wave propagation in a homogenous half space (all wavelengths sample same material thus same phase velocity), and (b) in vertically heterogeneous media (phase velocity depends on wavelength as medium properties varies with depth) resulting in dispersion (Pei, 2007)

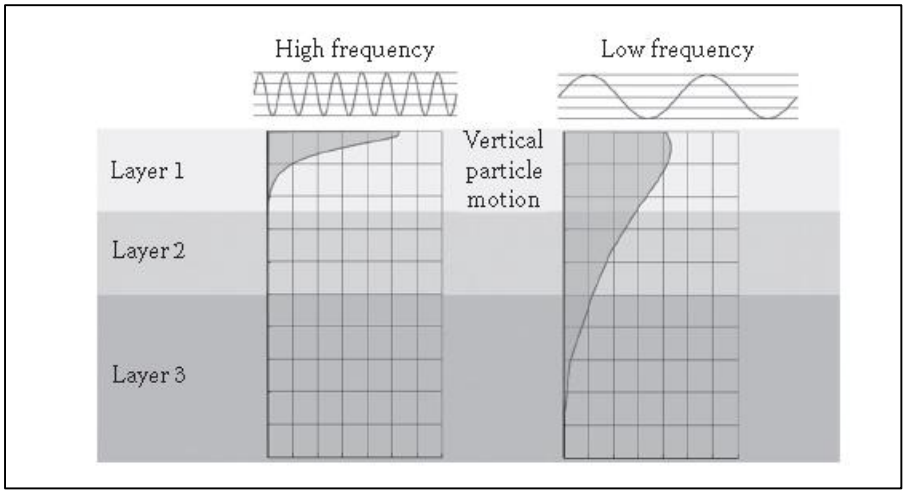

Figure 2.7 Geometric dispersion of Rayleigh waves: Behavior with depth associated with propagation in layered medium. (From Foti et al., 2015)

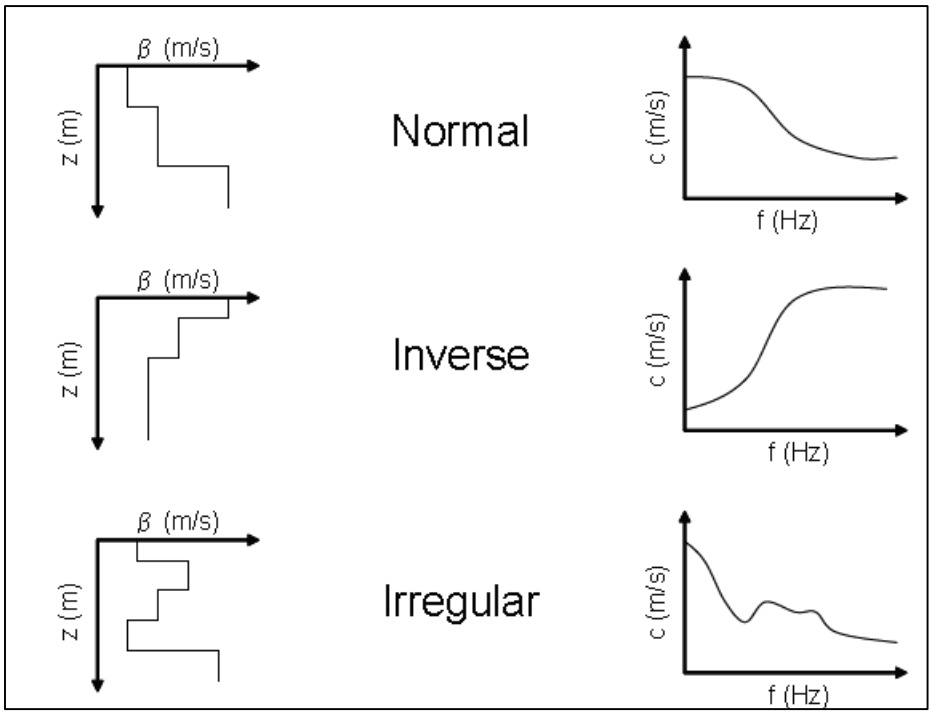

Figure 2.8 Dispersion curve shapes corresponding to different geologic settings (Pei, 2007)

2.4 Measurement of surface wave velocity

The velocity with which surface waves travel through the subsurface (or any media) is what is being referred to as shear wave velocity. Several methodologies have been advanced in the determination or measurement of Shear wave velocity. But before discussing these various methods, it is imperative to note that the ways in which surface waves are measured, that is the different methodologies, are different and independent from the successive inversion procedures of these data (Moro, 2015).

Foti et al., (2011) simplifies the procedure of surface wave measurement. He noted that typically, surface wave data are obtained on the surface by the use of a variable number of receivers. The geometry of deployment of these receivers can be one dimensional (1-D) or two dimensional (2-D). In exploration geophysics and engineering geophysics of the near subsurface, the most common type of receivers are geophones, otherwise referred to as velocity transducers. Foti et all., (2011) notes that accelerometers are also sometimes used but mainly for pavements where the use of geophones is limited due to the high frequencies involved. More so, geophones have an advantage over accelerometers of not requiring a power supply. Another advantage of using geophones is when there is need to record very low frequency signals. This advantage is however countered by the vulnerable nature of low frequency geophones that have a base frequency of less than 2Hz (Foti et al., 2011). These geophones are more bulky due to the heavy suspended mass that is prone to damage during handling and field deployment.

The most common type of devices used for the acquisition and storage of these data are commercial seismographs. Modern systems are designed for field use and even come in scalable acquisition blocks that can be co-used with field computers. This helps as it allows pre-processing of data in the field (Foti et al., 2015).

The wavefield itself (which is the main objective) can be generated in several ways but typically impact sources are used. These have to be adopted in considering the amount of energy and the frequency range on interest. The low cost of impact sources makes them more preferable. Sledge hammers and falling weights are commonly used for high frequencies (10-200Hz) and low frequencies (2-40Hz) respectively.

More appealing substitutes are controlled sources that are capable of producing harmonic waves that provide very high quality signals/data. Others such electromagnetic shakers and truck-mounted vibroseis present the choice for size, but the main drawback here is cost and extended acquisition processes and time.

The latest application in seismic site characterization is seismic noise analysis which is the main focus of this dissertation. This method makes use of background ambient noise (often referred to as microtremor) avoiding the need for a source. This is a passive method that makes use of noise produced by human and vehicular traffic and construction sites. In addition, natural noise such as sea waves, wind and earthquakes comprise other sources (Foti et al., 2011). Low frequencies dominate microtremor data and this makes it effectively applicable for deep characterization up to hundreds of meters, ranges which are not possible with the other relatively high frequency sources (see figure 2.7). However, as Pullammanappallil et al., (2003) noted, the resolution of shallow characterization is very poor with this method due to the high wavelengths in low frequency signals. For this reason, this method may be combined with any of the active methods very easily to fully measure the s-wave velocity for the near surface and deeper levels with relatively high resolution. Piccozzi et al, (2010a) also suggest the use of a larger number of sensors combined with high sampling rates to overcome this limitation.

It has been previously noted that the dispersion property of Rayleigh waves in layered media is the main basis upon which surface waves are measured. Upon this background, there are different methodologies of acquiring dispersion properties data from the field for engineering site characterization. These are discussed in the subsequent sub-headings.

2.4.1 Invasive methods

Invasive methods require data from seismometers that are placed beneath the Earth's surface (in boreholes). Two categories of such exist: those using surface sources and those using down-hole sources.

Surface-source methods as discussed by Boore & Thompson (2007), make use of a source at the surface and a sensor attached to the edges of a cased borehole at varying depths. The surface sources use an active source and the seismic waves are recorded

in the sensors. A three component seismometer is commonly used. The source of the S-wave can either be a wood plank struck with a sledge hammer on the ends or an air-activated slide hammer. The wood plank should be held to the ground by a large weight, preferably a heavy truck. The P-wave is generated by striking a metal plate with a sledge hammer (Liu et al., 1988). Seismic cone penetration method (SCPT) (Campanella et al., 1986) uses an active source mounted near the tip of a special tool (a seismic cone penetrometer) that is pushed into the ground.

Downhole methods will mostly involve crosshole study where a source is activated in one hole and received by sensors in other /another hole (Stokoe and Woods, 1972). In ASTM, (2003), three major limitations of the crosshole method are highlighted: The first and most obvious one is that it is very expensive since it requires multiple holes. The spatial orientation of these holes needs to be known precisely, and this poses a challenge for most people. Secondly, the fact that the velocities are measured in the horizontal direction may not be appropriate for waves traveling vertically, which is the main concern in earthquake engineering. The third limitation is that the velocity model may not extend without gaps from the surface to depth. This method is nevertheless useful for detecting local variations in soil properties, which might be important for liquefaction potential or for foundation design (Pei, 2007).

Suspension P-S logging method by Nighbor and Imai (1994), later replaced crosshole method mainly in earthquake engineering. In this method, a probe is lowered into a hole, where a source that is near the bottom of the probe emits acoustic waves coupled into P- and S-waves at the edges of the borehole. The waves travel in the wall material and are converted into acoustic waves that are then received by two receivers mounted 1m apart. The difference in travel times at the two receivers will give the wave velocity. This method produces good results in uncased boreholes and can be applied for relatively deep boreholes.

The major advantage over the prior methods is that it provides much finer resolution but it also has its limitations. As Pei (2007) noted, it sometimes does not produce accurate velocities near the surface and thus cannot produce a reliable model that extends to the

surface. Another problem is the inability to interpolate across any zones where data are lacking like in the surface based methods.

2.4.2 Noninvasive methods

The major drawback in the invasive methods discussed above is the need and cost of drilling a borehole for the measurements to be made. In lieu of this, noninvasive methods have been developed for obtaining surface wave data more efficiently. These noninvasive techniques are discussed below.

2.4.2.1 Spectral analysis of surface waves (SASW)

Nazarian and Stokoe (1984) and Stokoe et al., (1994) introduced the use of the dispersive properties of ground roll Rayleigh waves to infer the near-surface elastic properties, and the Spectral analysis of surface waves (SASW) was born. This method uses the spectral analysis of ground roll generated by a an active source and receved by a pair of geophones (Park et al., 1999), and “straight forward singal processing tools” (Foti et al., 2014).

Goh et al., (2011) applied SASW in determining rockmass rock quality designation (RQD) value and perform excavation classification analysis as well as site characterization. They noted that there was a 10% difference in RQD determined from SASW and discontinuity study. It was thus recorded that SASW can be applied as a non-destructive, cheap and easy way of earth material characterization. Abdull et al., (2009) aslo applied the same method for rockmass characterization and noted that the SASW is a reliable and cheap method in such applications.

Foti e tal., (2014) explains that to obtain a dispersion curve, the time delay between the arrivals (phase shift) at the two receiver stations for each frequency component of a wave generated by an active source is estimated and that several receiver spacings are required for a site due to the frequency range limitations brought about by the use of two-receiver stations. The individual disperssion curves from each receiver spacing are then combined to produce a single disperssion curve to be used for inversion. This results in a very slow process of data acquisition (Foti at al., 2014).

Another challenge noted by Socco et al., (2010) and Forti et al., (2014) is in the interpretation of the two-receiver measurements where they observed that this process requires some level of engineering knowledge and judgement. The process cannot be automated since the periodicity of the phase shift between receivers leads to the need to interrogate the phase of the cross-power spectrum that is used to calculate or estimate the Rayleigh phase velocity (Poggiagliolmi et al.,1982) and (Nazarian and Desai, 1993) . Limitations related to the effects of incoherent and coherent noise are even more important. Body waves, near-field effects, lateral variations and higher modes cause distortions to the phase velocity for each disperssion curve and these need also to be considered (Foti et al., 2014). Nevertheless, this method has been used in many geotechnical investigations since then and has played a critical role in the historical development of the surface wave methods (Stokoe et al., 1994).

2.4.2.2 Multichannel analysis of surface waves (MASW)

Using multiple receivers is bound to enhance data collection speed and quality. The data processing is thus more robust and less subjective. McMechan and Yedlin (1981) and Gabriels et al., (1987) pioneered this development but their extensive applications became apparent in the late 1990s. Park et al., (1999) at Kansas Geological Survey introduced “Multichannel analysis of surface waves” that is a successor of the older “Spectral Analysis of Surface Waves” (SASW) method.

As Park et al., (2005) illustrate, an array (multichannel) of geophones, usually 24, is used to receive surface waves generated from a sledge hammer or a heavy weight dropped at pre-determined points on the survey line. 1-D and 2-D V_s information is produced both in a very cost-effective and cost efficient manner. From the measured V_s and density (ρ), stiffness parameters are determined (Park et al., 2005). Data is collected in the time-space domain and then transformed into frequency-wavenumber domain. Phase velocities that are associated with different frequencies determined by picking the spectral maxima (Foti et al., 2014).

MASW uses surface waves in low frequencies (usually 1-30Hz) and a shallow depth of probe (a few to a few tens of meters). The low cost associated with the simple field operation and data processing has seen this technique gain popularity in engineering

projects (Park et al., 2005). It has been used in many near surface studies such as studying site-response for the purpose of characterizing specific sites amplification due to earthquakes (Mahajan et al., 2007) and consruction site charactirization (Penumadu and park, 2005) Such studies are important for the design of civil structures in mitigating sesmic hazards. In addition, MASW has become popular in Geotechnical engineering applications especially in detecting the near-surface anomalies and the low velocity layer due to its chances of success over other seismic methods. Noteworthy, surface waves respond effectively to near-surface anomalies, which are the main targets in geotechnical investigations (Mohamed et al., 2013). Shear wave velocity variation at shallow depth is thus best measured using multichannel analysis of surface waves (Mahajan et al., 2007).

This technique however, like its predecessor (SASW) suffers major setbacks: In urban settings in particular, MASW cannot resolve and/or detect velocity reversals and the high ambient noise levels present a high noise to signal ratio that results in poor quality seismic data (Louie, 2001). The much needed large energy sources to improve the signal to energy (s/n) ratio raises environmental and safety concerns. Such technical and financial challenges limit application of these techniques impractical in urban settings (Pulammanappallil et al., 2003).

2.4.2.3 Refraction Microtremor (ReMi)

ReMI, developed by Louie (2001) is a great step towards overcoming the challenges presented by the previously discussed techniques. This method uses standard P-wave recording equipment and the "problematic" ambient noise to measure $V_{s.}$ up to 100 meters depth. By combining standard refraction equipment, a source-free ambient recording, a simple linear array of multiple geophones, a technique to process wavefield transformations and an interactive Rayleigh-wave dispersion modeling tool, 1-D shear wave profiles can be produced with high levels of accuracy and reliability (Louie, 2001). Such a method comes in handy to exploit the strengths of SASW, MASW and array microtremor methods (Pulammanappallil et al., 2003).

As Louie (2001) and Pulammanappallil et al., (2003) indicate, the focus in these methods is on the low-frequency range and thus the need to have geophones with low base frequencies. 4.5Hz has been the minimum value but lower values are also possible

(Pulammanappallil et al., 2003), the only challenge is the cost of the low base frequency geophones (Louie, 2001). The dispersion curve picking is done the same way as in active methods and the assumption that the noise sources are uniformly distributed in space.

Since its introduction (Louie, 2001) ReMI has made some impact in the way surface waves have been used in charactering the subsurface. Most of the applications have been in busy urban settings where other methods have faced challenges.

Cha et al., (2006) applied the ReMI technique for rock mass classification in an urban tunnel design in Busan city, in Korea. In their conclusion, they noted that "the correlations between shear wave velocity from SPS logging and rock mass rating (RMR) or compressive strength were found to be good." They were thus able to derive a relationship between the shear velocity from ReMI and RMR were able to estimate the RMR for the tunnel route for purposes of design using ReMI. The cost of conducting rockmass classification thus goes down significantly by limiting drilling to the most and only crucial zones.

In the city of Ljubl jana, Slovenia's capital, Rošer and Goser (2010) used the ReMI technique alongside other methods to determine Vs30 for purposes of supplementing the existing seismic microzonation maps. The ReMI and ESAC (Extended Spatial Autocorrelation) phase-velocity dispersion curves were found to have very good agreement in this study, thereby advancing the level of reliability of the ReMI method. The duo also note that although V_s30 might be the best parameter for determining seismic site response, many national seismic regulation require it be determined and reported. This parameter also provides valuable information towards seismic microzonation efforts, an exercise highly needed for our major cities, Nakuru being on the forefront due to its tectonic setting.

Rošer and Gosar (2010) go on to indicate that the 1-D models produced can be used for direct 1D modeling of the seismic ground motion. Above all, the ReMI method is easy, quick, cheap and highly effective. In the concluding remarks, Baniasadi et al., (2009) in a study to determine V_s 30 for Bordabad in south-west Tehran, noted the ease of applying the ReMI method in urban settings. The major advantage is the lack of the need to drill a

single hole to determine shear-wave by downhole survey, thereby suppressing survey costs by a considerable margin. The limitations of the ReMI method are only as a result of the frequency range of the noise being recorded and the acquisition parameters selected (Gamal et al., 2011).

High frequencies and short geophone spacing are useful in resolving thin layers in shallow subsurface. For deeper depths, low frequencies and longer arrays are required. Ambient noise may lack the higher frequencies, and thus may need to be supplemented with active source from say, a sledge hammer (Gamal et al., 2011).

Strobbia and Cassiani, (2010) however noted that despite this method being very simple and fast, significant overestimation of the shear wave velocity profile may result if the background noise happens to be travelling in a preferred direction that is not in line with the geophones array.

2.5 [1]Surface wave dispersion analysis

2.5.1 Summary

Several methods exist that are used to process field data to obtain the dispersion curve. A variety of signal processing techniques have been developed over time but all rely on the Fourier transform (Foti et al., 2009). They also note that the Fourier transform is capable of separating the different frequency components for subsequent processing to estimate phase velocities.

The SASW procedure has become more popular in the engineering applications and a significant amount of literature available is based on it. The method however needs meticulous data inspection to deal with problems caused by phase unwrapping of the cross-power spectrum of the two receivers (Socco et al., 2010). The process of unwrapping is bound to introduce errors on the data set as noted by Rosenblad and Bertel (2008), and this makes automation of the process difficult (Nazarian and Desai, 1993). According to Foti et al., (2000), this problem may be overcome by considering the two

[1] All figures used in this section are from Foti et al., (2015)

station procedure as a special case of *f-k* analysis and perform it with “two receivers and an infinite zero padding” after which the fast Fourier transform (FFT) can be applied in an easier way (Socco et al., 2010).

In the works of Grandjean and Birti (2006) and Neducza (2007), they were able to show that the quality of experimental dispersion curve from the field can be improved by stacking in the spectral domain when many data are available, in addition to the wavefield transform.

With regard to passive data, spatial autocorrelation (SPAC) procedure is more common. Socco et al., (2010) explains that SPAC and extended autocorrelation (ESPAC) are capable of providing more stable results in the low frequency range and are also applicable with fewer receivers, the only problem arising from the assumption of a uniform distribution of the ambient noise source. The frequency-wavenumber can in such a case be used to validate such an assumption. For this reason, the two procedures should be employed together (Asten and Henstridge, 1984).

If active and passive data sets were acquired from the same site, they will produce differing dispersion curves corresponding to the different frequency ranges. Merging the two dispersion curves increases the amount of information (resolution) gathered about the subsurface (Battaglia et al., 2008).

2.5.2 Inversion

The final step in interpretation of Rayleigh dispersion is the solution of the Rayleigh inverse problem. There are basically two inversion methods used in the interpretation of the shear wave velocity profile from the dispersion curve(s) obtained from field data. One is the simple conversion method. This method is based on two main assumptions; one is that the shear wave velocity is nearly equal to approximately 110% of the Rayleigh wave phase velocity, and that the effective penetration depth is one third (1/3) or one half (1/2) of the wavelength of the Rayleigh wave.

The second method, which is more advanced, is back-calculation. This method involves two main steps:

1. Construction of the experimental dispersion curve.
2. Use of an algorithm to minimize the error between the theoretical and experimental dispersion curve. This method is the actual back-calculation, otherwise known as inversion

Whichever method is used, the experimental dispersion curve is always the first step and the level of accuracy that is to be expected in the inversion process will definitely depend on the accuracy of construction of the measured/experimental dispersion curve (Lu and Zhang, 2004).

In most applications, the experimental dispersion curve is always considered as that of the fundamental Rayleigh mode. The fundamental mode is the mode in the lowest frequency range. This assumption is however not applicable where irregular velocity-depth profiles are encountered. This is when the normal characteristic of shear wave velocity increasing with depth is not the case. For this reason, Tokimatsu et al., (1992) proposed that the dispersion curve be chosen from multimode Rayleigh waves. This dispersion curve will be treated as the theoretical dispersion curve and compared with the experimental/ measured dispersion curve. Ganji et al., (1998) also proposed another method of constructing the dispersion curve of multimode Rayleigh waves. The method constructs the theoretical dispersion curve from the cross-power spectrum of two pairs of signals, similar to the process of constructing the experimental dispersion curve. The aforementioned problem of 'unwrapping' presents itself in this process. Since the phases of the cross-power spectrum are always relative phases ($\Delta\varphi$) with values between -180^0 and $+180^0$, the actual phase for each frequency must be found using the relation $\varphi=\Delta\varphi + n \times 360^0$ to produce a dispersion curve. This is what is referred to as unwrapping.

Another problem is the 'spurious 360^0' cycles, a term coined by Al-Hunaidi, (1998). When more than one mode of Rayleigh wave dominates the surface wave motion, a phenomenon referred to as mode jumping is observed. This is the jump from one mode to another in correspondence to a slight change in frequency. This phenomenon may cause the picking of a dispersion curve be incorrect and hence the subsequent inversion will also result in error due to the presence of the spurious 360^0. The multichannel analysis

helps in overcoming the problems discussed related to SASW. In MASW, it is possible to obtain separate dispersion curves for the various modes in the frequency range.

Foti et al., (2015) indicates that generally, the techniques applied in solving nonlinear optimization problems such as the inversion of experimental dispersion curve can be broadly divided into two methods; Global search (GS) and local search (LS) methods.

According to Foti et al., (2015), Local search (LS) procedures iteratively start from an initial guess of the solution and proceed to generate a sequence of better estimates that converge to the solution under suitable conditions. Most of these methods are calculus-based that tend to linearize a nonlinear function during each iteration until a stationary point is reached. LS techniques require that the functions be sufficiently smooth so that the *frechet derivatives* exist and are continuous but still, only if the initial guess is as close as possible to the solution, will the sequence of approximations of the solutions converge. The most important limitation of the LS procedures is that there exists no simple criterion to determine whether it is a local or global stationary point in the solution space even if a stationary point is successfully found.

GS procedures help in addressing this ambiguity. The global stationary search is done through a search through the whole of the solution space, either systematically in a grid format or randomly similar to the Monte Carlo simulations. GS methods are generally computationally intensive compared to LS methods, but they are more robust and dependable in finding the farthest points in the solution space.

2.5.3 SPAC AND ReMi

This dissertation has focus on the use of microtremor data to obtain Rayleigh dispersion properties of the subsurface. The spatial Autocorrelation (SPAC) method developed by Aki (1957, 1965) is the commonly used method for calculating dispersion curves from microtremor data. The initial applications used were limited to circular array geometry. The extended spatial autocorrelation (ESAC) method by Ohori et al., (2002) removes the restrictions of array geometry.

Microtremor data is usually recorded in 2D arrays. This receiver geometry allows for the determination of the direction of propagation of the surface wave that is being generated by unknown and uncontrolled sources. Refraction microtremor (ReMi) as proposed by Louie (2001) uses a linear array of geophones. One limitation that is apparent in this method is the possible presence of a single source. This is because the measured apparent velocity will depend on the unknown angle (θ) between the array and the source direction as shown in figure 2.9

Figure 2.9 In a linear array, a plane wave depicts an apparent wavelength that is longer that the true velocity. The apparent velocity also is higher than the true velocity.

Foti et al., (2015) explains that a single plane wave recorded in the x-direction will have an apparent velocity equal to the true velocity divided by Cosθ, which will be greater than or equal to the actual velocity. Then the apparent wavenumber K_x can be written as K_x=K.Cosθ. Since the array length is finite, we can ignore the spectral leakage. A single frequency will appear as a spike in the wavenumber spectrum.

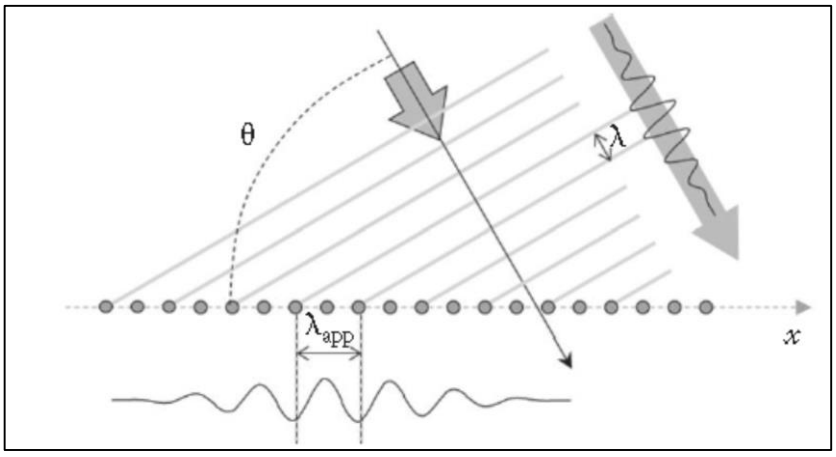

This shortcoming can be overcome if we have an isotropic and diffused wavefield with signals coming from evenly distributed sources directions. This means that a single frequency, the K_x-K_y spectrum will have a polar symmetry. Figure 2.10 represents the spectrum of a perfectly diffused wavefield with unit wavenumber.

A linear array will detect both the in-line energy along the x-axis with positive and negative

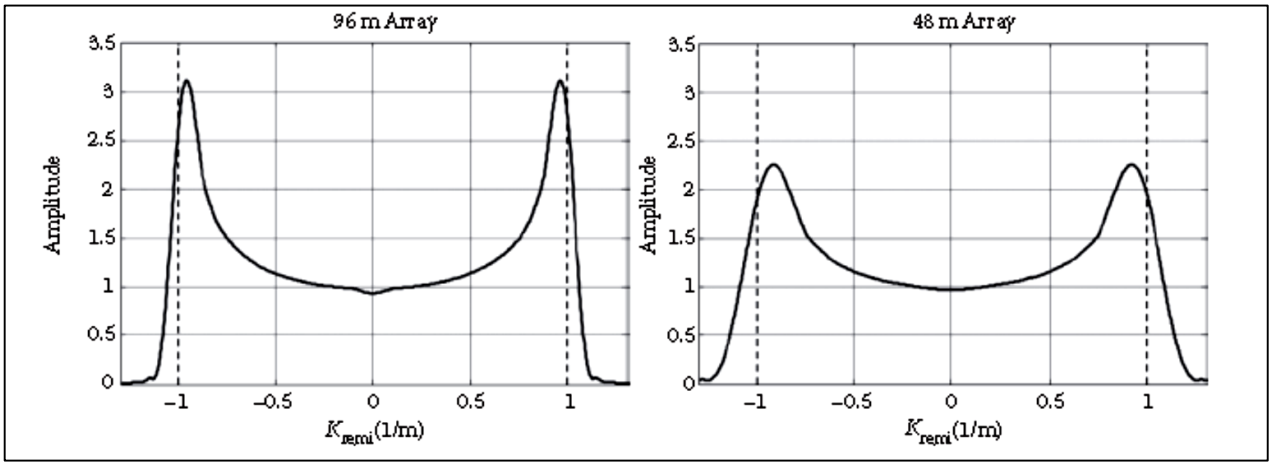

wavenumbers and the energy travelling with lower apparent wavenumbers. If we consider

Figure 2.10 A theoretical ReMi wavenumber spectra for two different lengths of the linear array for a perfectly isotropic microtremor wave field.

an array in the x-direction, the spectrum of the Kx is written as equation 2-3. (Foti et al., 2014)

$$P(E) = \frac{1}{\sqrt{1-\cos^2}} \frac{1}{\pi}$$

Equation 2-3

The linear array, with its finite length comes with its own complications in the ReMI spectrum. The example presented by Foti et al., (2014) is shown in figure 2.11. It presents the ReMI spectra for a given frequency for plane waves with uniform directional and for two array lengths of 48 and 96m. The maximum of the 1D spectrum for any finite array length will be at a smaller wavenumber that the true value as can be seen in the figure. The vertical dashed lines represent the true unit wavenumber while the maxima are at the values of *k* that is smaller than the true wavenumber of the wavefield.

In figure 2.12 (a), the resultant ReMi spectrum in the *f-k* domain is shown, assuming a

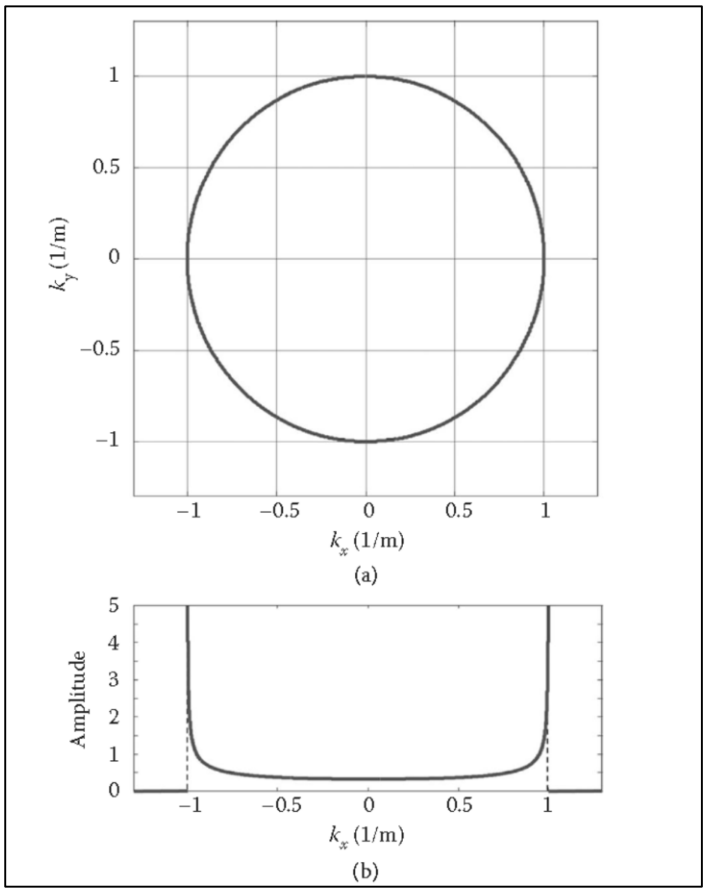

Figure 2.11 (a) Shows the ideal spectrum of a well diffused wave field with unit wavenumber in the Kx-Ky domain. (b) Is the corresponding spectrum in a linear array in which the spectral maxima are on the true wavenumber

perfectly isotropic diffused wave. The spectrum will be symmetrical for a homogenous wavefield. This single property is normally used to check for the assumption of uniform microtremor distribution, which is the basis upon which ReMi is built.

The process of identifying the true wavenumber from ReMi is rather complex. As can be seen in figure 2.12(b), the true wavenumber is plotted as a dotted line at each frequency. Louie (2001) proposed a manual picking of the maxima and where the spectral amplitude decreases abruptly. This method is however subjective and is prone to errors in the picked wavenumber and consequently in the phase velocity.

The method proposed by Strobbia and Cassiani (2011) involves automatic identification of the true wavenumber from the experimental spectrum. This method can also be used to check the assumption of uniform noise distribution too in the measured data. The method involves four major steps:

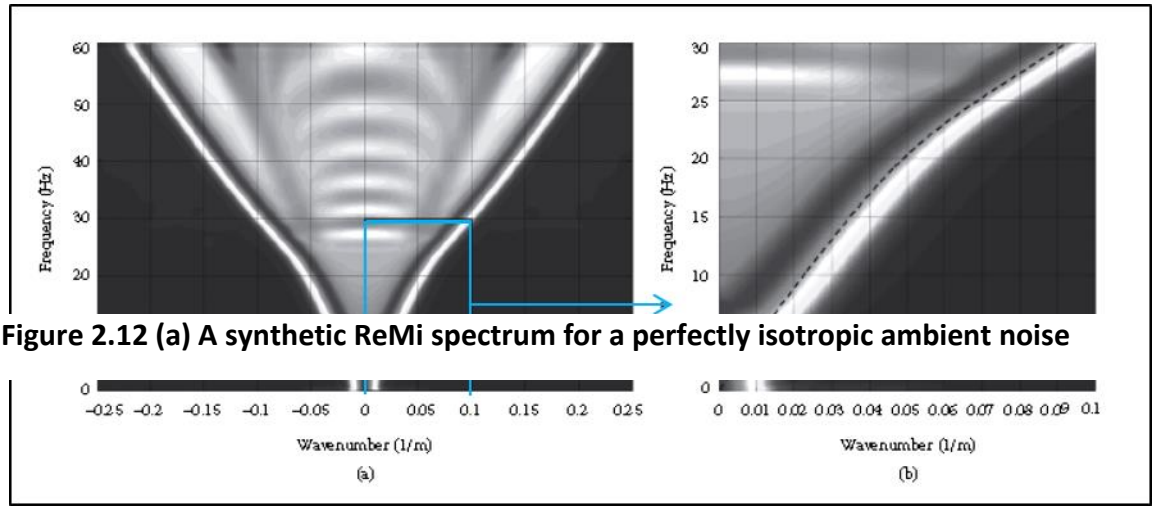

Figure 2.12 (a) A synthetic ReMi spectrum for a perfectly isotropic ambient noise

1. The data is segmented into normalized and overlapping sub-windows
2. The elementary spectrum (f-k or f-p) for each window is computed, normalized and stacked. Positive and negative quadrants are plotted.
3. The frequency range of interest is picked. The spectrum is normalized and split into two parts (positive and negative wavenumbers) which can be independently inverted, fitting the data with the theoretical shape of the spectrum.
4. The two inverted wavenumbers are compared to check the assumption of uniform noise distribution

Foti et al., (2015) also presents another example of a ReMi spectrum computed from a 15 minute microtremor record on a 24-channel array (figure 2.13). Upon inspecting the spectrum qualitatively, he noted an acceptable symmetry and suggests the presence of higher modes as secondary local maxima. In figure 2.14, an example of fitting a section of the spectrum at a frequency of 30 Hz is presented.

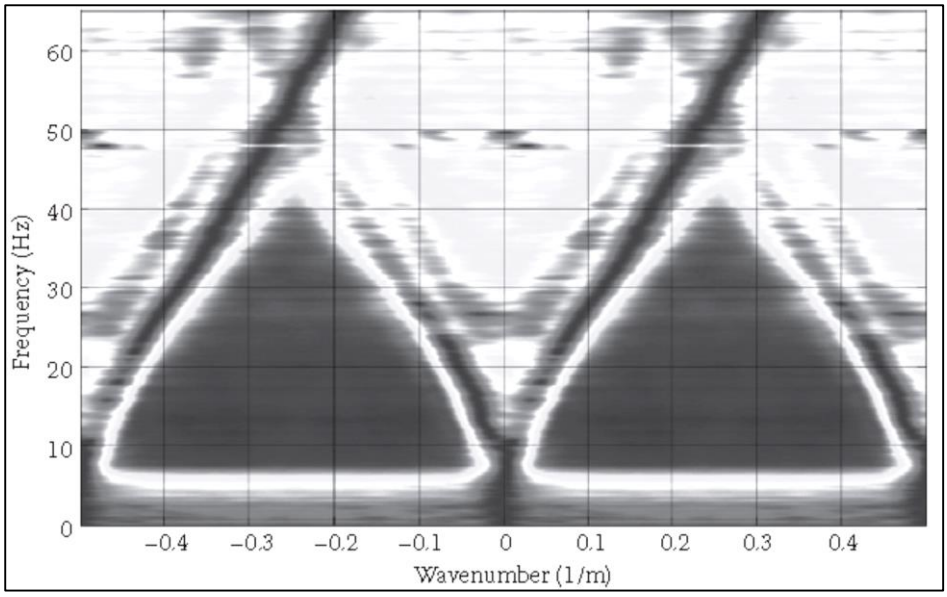

Figure 2.13 An experimental ReMi spectrum where the basic assumption of uniform seismic source distribution is verified from the symmetry of the spectrum

Figure 2.15 shows the result of the inversion for the whole frequency range. In (a), the wavenumbers for the positive and negative quadrants are shown while (b) shows the corresponding misfit. The two dispersion curves are shown in (c), alongside a curve from an active acquisition obtained from the same array. It is out rightly apparent that there is no significant disagreement between the active and passive data sets.

In the event that the source is nearly in-line with the array, the spectral shape resembles that of a single source. In this case the spectral maximum is expected on the true wavenumber; and the ReMi spectrum should be treated as an active source spectrum.

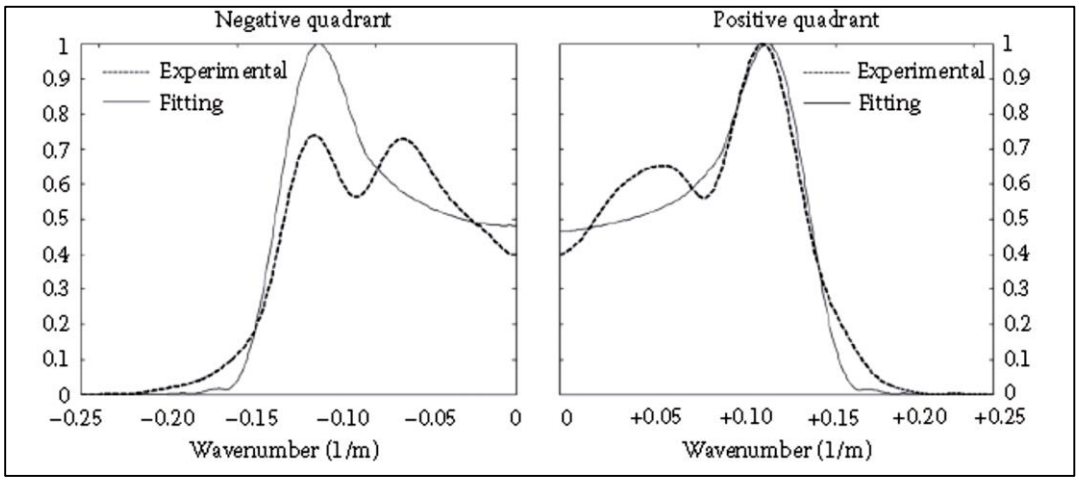

Figure 2.14 The two quadrants from figure 2.13 are inverted independently to estimate the wavenumber. The fitting of a section at 30Hz is shown

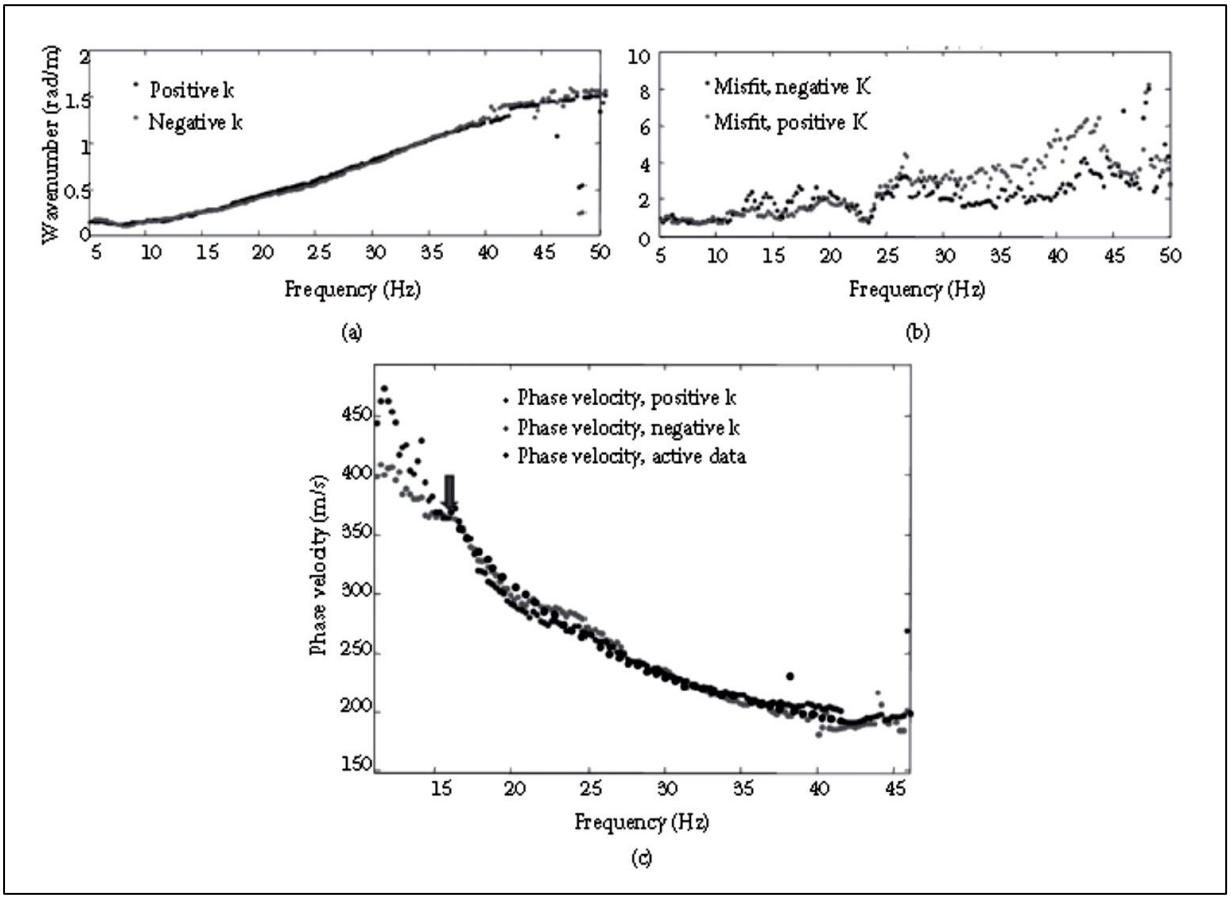

Figure 2.15 (a) Estimated wavenumbers for the +ve and -ve quadrants; (b) misfit between the measured and theoretical functions; (c) the dispersion curves from ReMi and active source tests for the same site

2.6 Ambiguities in surface wave analysis for shallow investigations

Dispersion analysis presents quite a number of problems, majority of which are directly linked to uncertainties arising from the measured data and during processing.

Noise in the measured data may be associated to coherent and uncorrelated noise (ambient noise). Geometric problems such as the location of receivers, tilting and ground coupling also introduce significant levels of uncertainties. O' Neill (2003) did a study of the influence of several sources of ambiguities using numerical simulations. From his studies, receiver/geophone tilt and ground coupling result in minimal influence. Location errors, static shift and Additive Gaussian noise were found to constitute a significant level of ambiguities in the measured dispersion curve.

Foti et al., (2014), noted that when using transform-based methods, the estimation of the ambiguity is not negligibly small, and difficulties will actually manifest in an attempt to quantify the influence of the error in data and how it is propagated through data processing steps starting at acquisition to the calculation of the dispersion curve.

In multichannel surveys, the ambiguity is easily determined by directly measuring the statistical distribution of raw and derived surface wave data. This process is however time and effort intensive but it avoids simplification of assumptions such as small variances of raw data and is free of major technical challenges (Foti et al., 2014).

Generally, estimating the uncertainty in surface wave measurements is not straightforward. This exercise is highly dependent on the specific technique used to calculate the dispersion and attenuation curves as discussed by Foti et al., (2014). The technical challenges may include instrument inaccuracies, testing configuration errors, the mode of data acquisition and errors arising from any subjective decisions by the operator.

Foti et al., (2015) gives a detailed coverage on the estimation of the uncertainties associated with different surface wave measurement methods. This is however beyond the scope of this project.

3 CHAPTER THREE: MATERIALS AND METHODS

3.1 Introduction

This chapter discusses the various tools used in this work. This includes both hardware and software. A brief discussion on the use and application of each of these tools is given. The methodological approach taken to achieve each of the set objectives is also given.

3.2 Materials/ equipment

3.2.1 Pasi seismograph model 16S24-N and its components

The equipment used for seismic data acquisition was PASI Mod.16S24-N (24 channels) equipment (Figure 3.1)**.** This is a completely integrated and rugged system with built-in PC, daylight-visible color 10.6" LCD touch screen, and printer with a built-in PC for data processing.

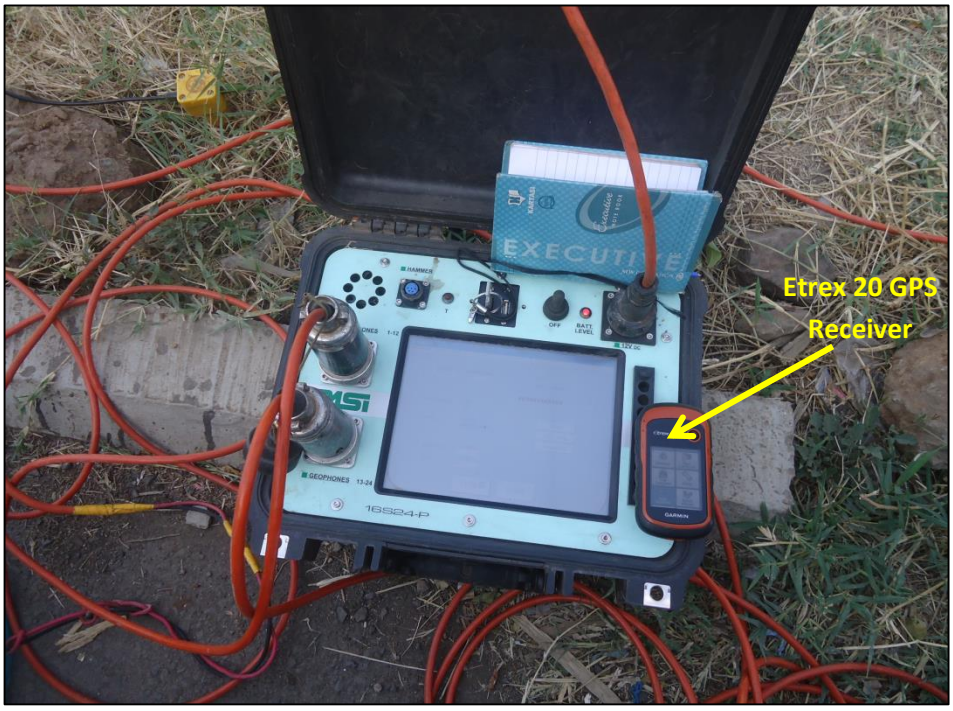

Figure 3.1 PASI Model16S24-N seismograph

The main highlighted features as per the manufacturer include;

- Filter Activation: in acquisition or post-acquisition
- Antialiasing filters: active, LPF, 8^{th} in Butterworth order; attenuation -48dB/oct (-160dB/dec); f_0=5/8 fnyq; accuracy. ±1% cutting frequency
- Enhancement with/without total/partial preview
- Geophone polarity inversion
- Marker for the determination of the video points position on the time scale;
- possibility to save the first arrivals on file for data download to PC
- A.G.C. Automatic Gain Control
- Delay: Pre-trigger 0-10ms (step of 1ms); Post-trigger 0-16000ms (step of 1ms)
- Display in wiggle-trace or variable area
- Noise-monitor with “real time” cascade display
- Automatic or manual trace-size for each channel
- Automatic recording of acquisition
- Data download to PC via USB
- Automatic calibrations
- Data codification in SEG-2 format

The complete equipment set comprises of 24 Geophones, Trigger geophone, Trigger cable, two 12 takeout cables measuring 120m each, at connector spacing of 10m intervals, a sledge hammer and a striking aluminum plate. These are depicted in the following set of photos in figure 3.2.

3.2.2 SeisImager/SW software

SeisImager/SW is an easy-to-use, yet powerful program that allows analysis of multi-channel active and passive source (microtremor) surface wave data. Some of the procedures that the software performs include:

- Input and display data.
- Control how data is displayed.
- Make changes/corrections to data files and save them.

- Calculate and edit dispersion curves.
- Invert data for a one-dimensional shear wave velocity curve.
- Invert data for a two-dimensional shear wave velocity cross-section.
- Display results in graphical form.

SeisImager is the master program comprising four modules (Pickwin, Plotrefa, WaveEq, and GeoPlot) for surface wave and refraction data analysis. The Surface Wave Analysis Wizard automatically calls on specific functions from Pickwin, WaveEq, and GeoPlot as required through the analysis steps.

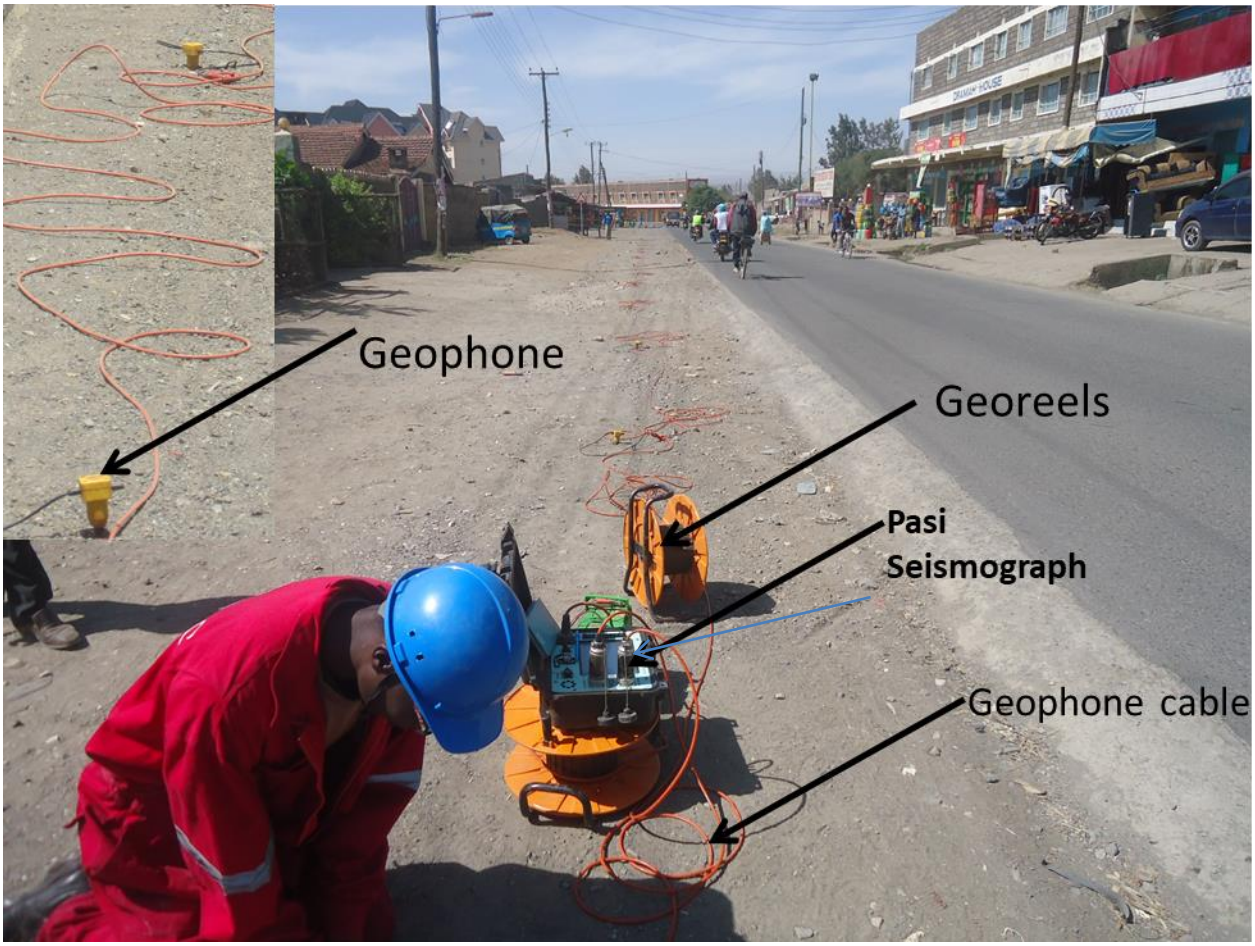

Figure 3.2 The various components of the Pasi seismograph for seismic survey (equipment obtained from Regional Geophysical survey Ltd)

3.2.3 Other equipment/materials

Support equipment such as garmin etrex 20-GPS and a digital camera were used. The GPS was used to record the coordinates of each measurement location while the digital camera was used to capture field photographs. e-trex 20 takes coordinates with an accuracy of $\pm$3m.

3.2.4 Maps and reports

The geological map used in this work and the geological background information were obtained from the Mines and Geological Department in Nairobi for the specific work titled "Geology of the Nakuru-Thomson's Falls-Lake Hannington Area". The map was geo-referenced and digitized for the specific area of study, while the report for the work was used as the main source information regarding the geology description of the area.

3.3 Methodology

The project involved desktop study, field data acquisition followed by data analysis and processing. The desk top study involved the review of the areas previous geological work.

3.3.1 Field work

The field work exercise was conducted between March 8th and March 15th 2017. The main activities included field deployment of the complete setup for data acquisition. This involved laying out the 24 geophones spaced out at 5m for each sounding. The geophones were planted in the ground up to 4 inches deep, ensuring good coupling with the ground and verticality. They were then connected to the seismic cable which is in turn connected to the seismograph. This was set up along the main Nairobi-Nakuru-Eldoret highway, between Lanet area and the Njoro exit junction. This represents a total distance of 12Km with a total of 50 soundings. This profile was chosen because it strands through the entire CBD and covers most of the built up areas. The profile also runs along the busy highway, thereby presenting a good source of seismic energy for the ReMI survey. In addition, seismic data was acquired along a 1.6Km profile perpendicular to the main profile in a more or less North-South direction. 5 measurements were taken each measuring 115m. This 1.6Km profile runs north-south starting at the Nakumatt downMunicipality roundabout, running south to the '*Kwa Rhoda*' area, towards Lake Nakuru National Park. This short profile was meant to collect data for the section of the Municipality that is built up towards the lake sediments and provide a fair coverage of the

Municipality. These two profiles are provided a fair coverage of the built environment around the Municipality for proper seismic characterization. Figure 3.5 shows the distribution of the ReMi stations along the main profile and the short profile.

Figure 3.3 Google earth image showing the locations of the ReMI soundings

3.3.2 ReMi data acquisition

The geometry adopted was a linear array, with 24 geophones spaced out at 5m. This gives a total array length of 115m. The recording parameters are presented in the table 3-1. Figure 3.4 is a photograph taken during the field work.

Table 3-1 ReMi survey design parameters

PARAMETER	SETTING
Spread/array configuration	Linear

Array size	115m (depth of probe about 1times this length)
Geophone interval	5m
Total number of geophones	24
Geophone type	10Hz base frequency
Trigger	Semi-automatic; Initial manual and subsequent automatic 20-stack recording
Record length	32 seconds(s)
Sample interval	2 milliseconds (ms)
No. of records	20

Figure 3.4 A photo taken during the field exercise showing the field layout of the linear ReMi array

This setup provided a good probe to a depth approximately equal to the array length of 115m.

3.3.3 ReMI data processing

Processing of ReMi data involved three main steps:

i. Velocity spectral analysis
ii. Rayleigh phase-velocity dispersion picking
iii. Shear wave velocity modeling

3.3.3.1 Velocity spectral analysis

A ρ-f image, otherwise termed 'velocity spectrum' was first generated from the recorded microtremor (ambient noise) data. This was done by computing a surface-wave phase velocity dispersion-ratio image by ρ-T and Fourier transform across all vectors (Louie, 2001). This transformation (ρ-f) separates Rayleigh waves from other arrivals in the record.

3.3.3.2 Rayleigh phase-velocity dispersion picking

In order to ensure best practice, the lowest-velocity envelope (fundamental mode) was picked being of the lower limit of the apparent phase velocity, which is always assumed to be the true phase velocity. This assumption is the fundamental idea behind the ReMI technique using a linear 1-D array (Louie, 2001).

3.3.3.3 Shear velocity modelling

A non-linear inversion modelling using least squares method was used to determine the shear wave velocity profile from the ρ-f image and dispersion curve. The microtremor data collected from the field in this project was analyzed and modeled using SeisImager/SW 2013 software. This program uses the Spatial autocorrelation (SPAC) method that assumes that the signal wavefront is planar, stable, and isotropic (coming from all directions) making it independent of source locations (SeisImager/SW manual, 2009).

3.3.4 Input and data display

During analysis and processing of ReMi data, all the records acquired were input. In this project, 20 records were taken. In SeisImager, all the records are input together at once. Figure 3.7 shows the display in SeisImager/SW of a single record. Other records are viewed by scrolling through the display.

In this window, one is able to control and change how the traces are displayed by

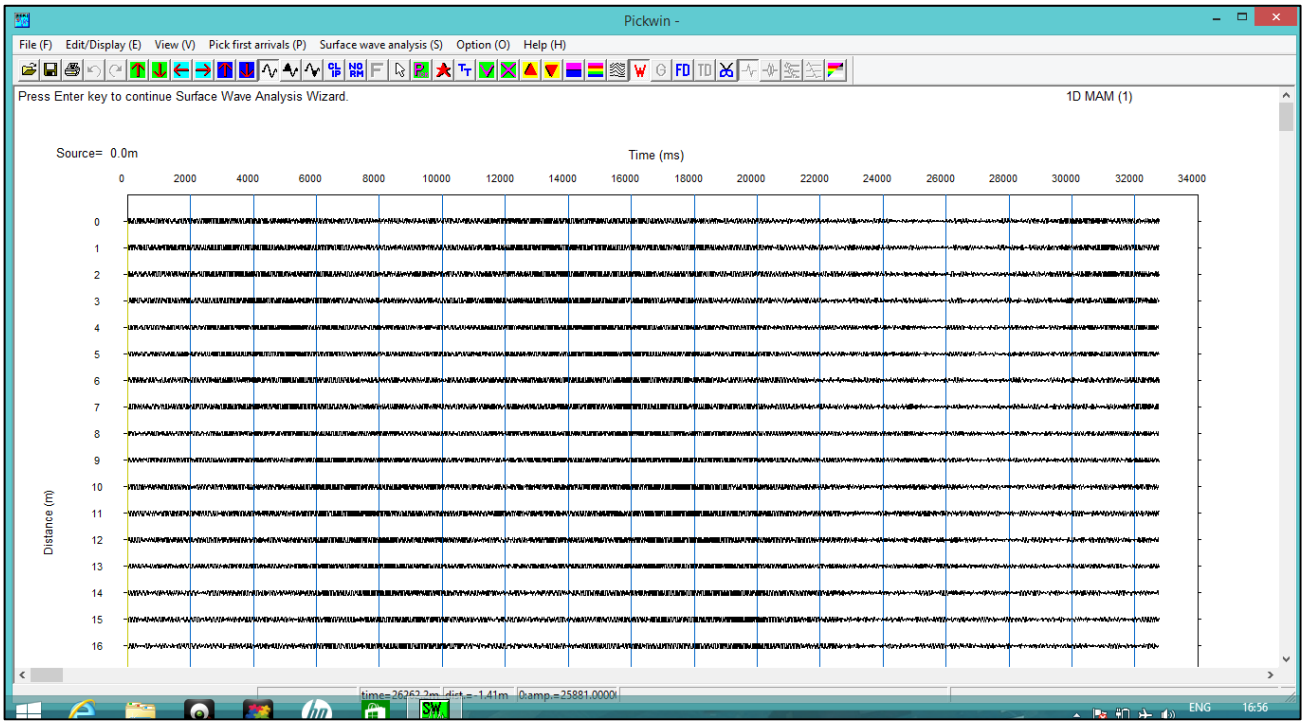

Figure 3.5 Screenshot of the display in SeisImager/Sw for a single microtremor record.

enlarging the traces. Corrections on geometry parameters and edits are done here before proceeding to subsequent steps, after which there is an option to save the changes into the record.

3.3.5 Calculation of the dispersion curve

The first step in the calculation of the dispersion curve was calculation of the phase velocity. In SeisImager/SW, there is the provision to choose/trim the end of the phase velocity to suit the maximum velocity expected for the particular site. The frequency range was selected next. Setting a higher value for the maximum allows for the extent of the fundamental mode to be seen.

The parameters for picking the maximum amplitudes were then set. These defined the dispersion curve on the phase velocity-frequency plot. At this point the minimum frequency targeted was chosen, which was guided by the natural frequency of the geophones used during data acquisition. In ReMi surveys, low natural frequency

geophones (between 2-10Hz) are used to allow deeper investigations. The lower the frequency used, the deeper the probe depth.

Figure 3.8 shows the phase velocity-frequency (ρ-f) plot with the automatically determined maximum amplitudes shown as red dots displayed after the calculations using SPAC.

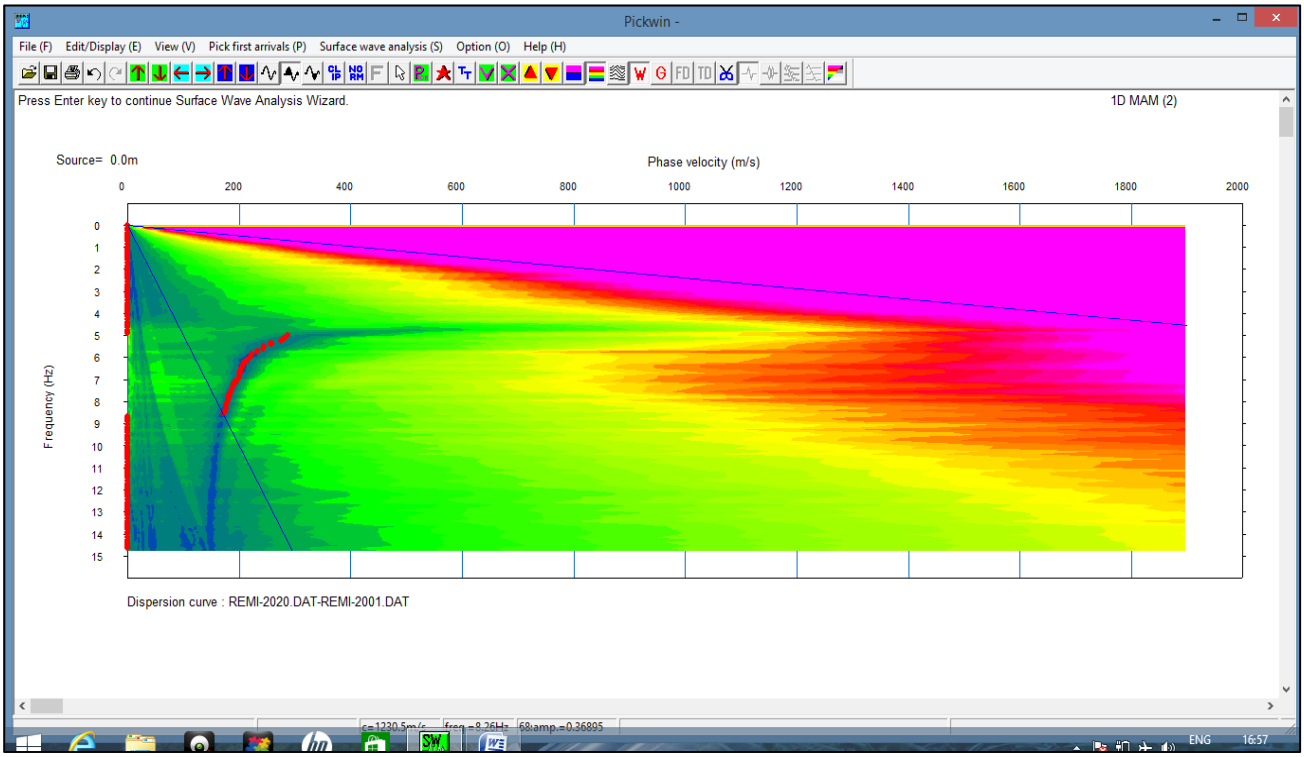

Figure 3.6 p-f plot showing the automatically picked maximum amplitudes for each frequency

The dark blue colors represent the maximum amplitudes, and a normal dispersion curve is observed in this case. Figure 3.9 is an actual dispersion curve for S1 site for the current project. This too is a normal dispersion curve with the phase velocity increasing with decreasing frequency. In this particular sounding, data was recorded to a minimum frequency of about 5Hz and a maximum frequency of about 9Hz.

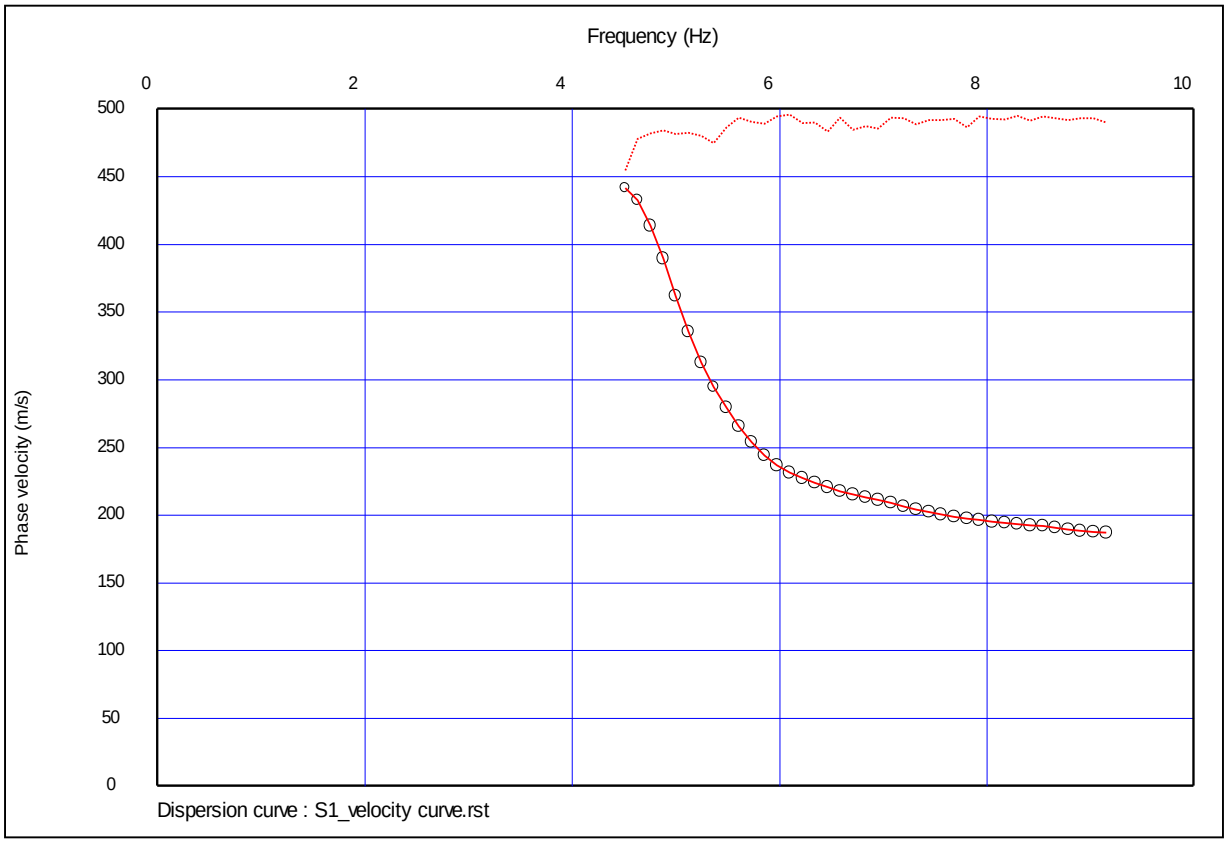

Figure 3.7 Sample dispersion curve for site S_1 of the project study area

The automatically picked dispersion curve was edited for refinement and correction of bad picks. Some frequencies may also have been omitted and may be picked as well, a process that is manual. The next step was the development of the shear wave velocity model.

3.3.6 Shear wave velocity modeling

After the dispersion curve was edited to satisfaction and saved, the shear wave velocity model was produced. The final step in editing the dispersion curve involved removing noisy picks on the low and high frequency ends of the curve using a gate provided by the software in the WaveEq module. Once done, the initial shear wave velocity model with depth was calculated. SeisImager has a default setting that calculates the initial model from the one-third wavelength approximation. In ReMi surveys, the array length is used

as the estimated maximum depth. Figure 3.10 shows the initial model generated after all these parameters were been defined.

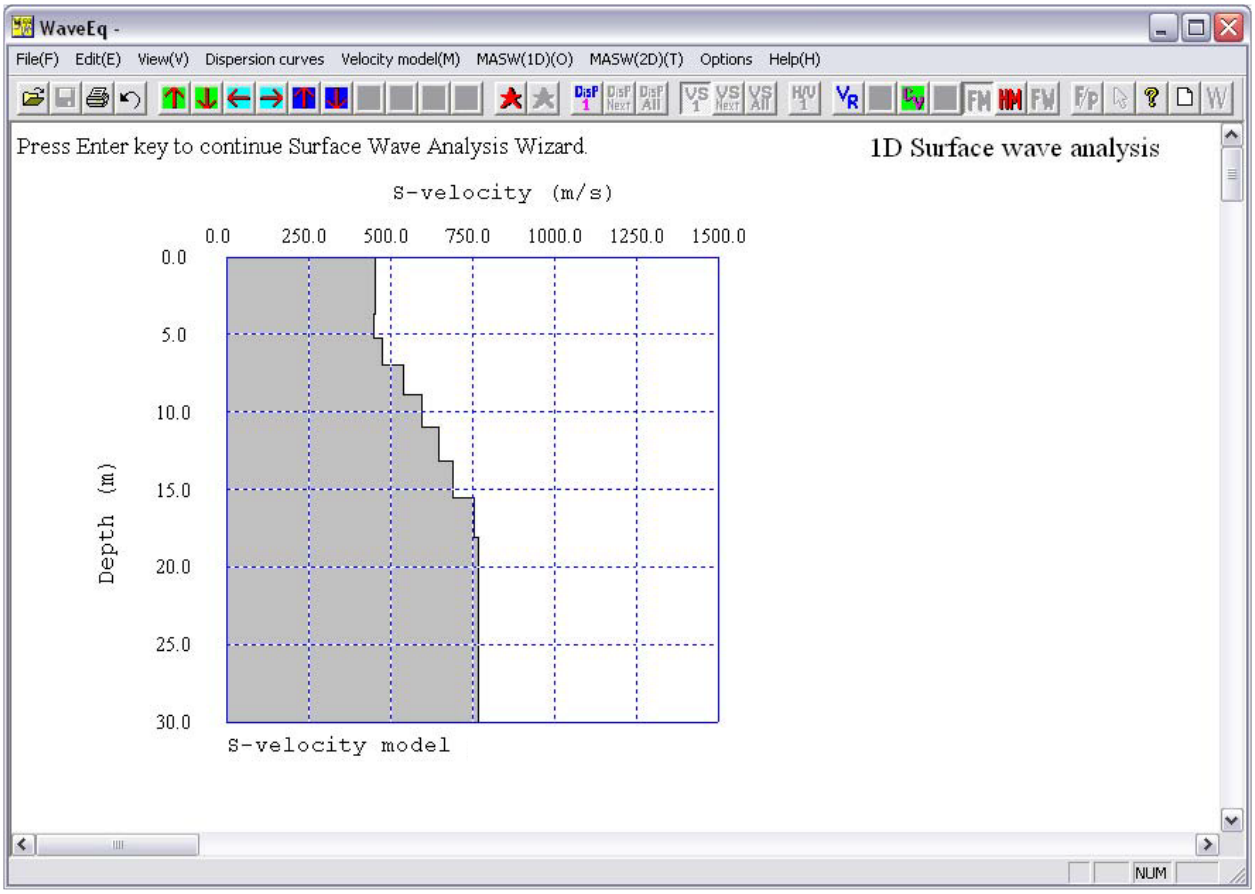

Figure 3.8 The initial surface wave velocity model prior to inversion.

After the initial model had been generated and displayed, the next and final step was inversion. In SeisImager/Sw waveEq module, the process is automated and only the number of iterations can be modified at the user's discretion. A default value of 5 is always set but one may choose to increase this value. The objective here is to have the module iterate the number of times chosen to converge on the best fit of the initial model with the observed/measured data. Once all this was done, inversion was done and once completed, the final V_s curve was displayed as shown in figure 3.9. The Inverted surface wave velocity curve is the final result of a one-dimensional surface wave survey. This curve is what is interpreted to provide information regarding the subsurface.

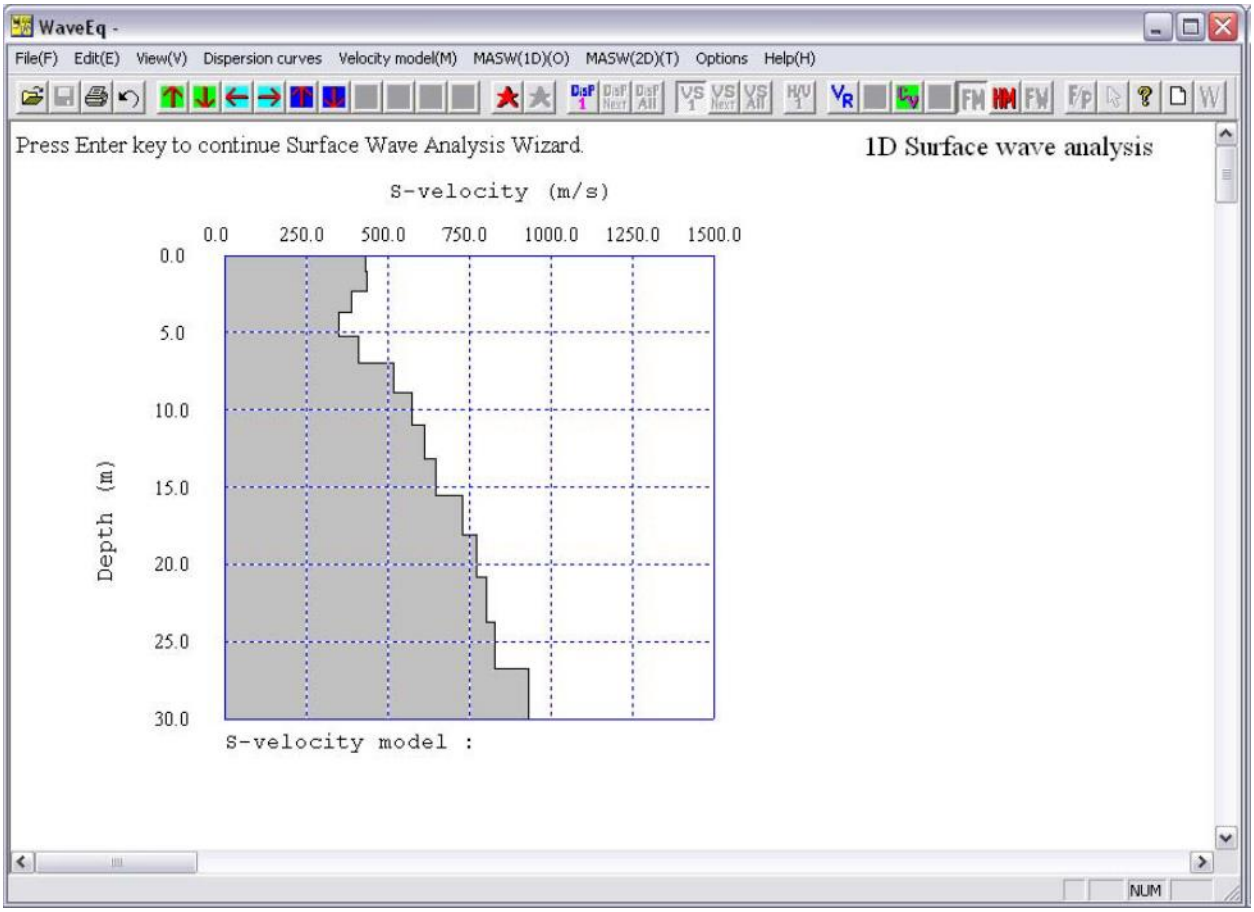

Figure 3.9 The inverted V_s curve of the initial model in figure 3.10

3.3.7 Derivation of geotechnical parameters

It is a rare event that the surface wave velocity curve is the ultimate objective of any survey. In almost all cases, the dynamic soil properties are the main objective. These geotechnical soil properties are mathematically derived from the S-wave velocity obtained from the preceding steps, particularly the Vs curve.

The main dynamic soils parameters derived from seismic surface wave velocity tests are the elastic modulus, and the shear modulus, G.

For the purpose of determining site response parameters the following mathematical relations were applied as:

Poisson ratio, $\nu = \frac{Vp^2 - 2Vs^2}{2(Vp^2 - Vs^2)}$ (Luna and Jadi, 2000)

Shear Modulus $G = \rho V_s^2$ (Luna and Jadi, 2000)

Young modulus $E = 2G(1 + \nu)$ (Luna and Jadi, 2000)

Where ν= poisons ratio, G= shear modulus, E= Elastic/young's Modulus, ρ= density of the soil and V_p and V_s are the P wave and Shear wave velocities respectively, determined from field measurements.

The density, ρ, of the material is computed from the relation;

$\rho = 0.31 V_p^{0.25}$ proposed by Gardener et al., (1974) and V_p is in m/sec.

3.3.8 2D shear wave velocity models

To obtain the 2D shear wave velocity models that helped in presenting a summarized 1D analysis, the inverted 1-D S-wave models were combined in Surfer 2009. Such a model presents a 2D section of the entire survey profile with clear correlation and comparisons between individual 1-D measurements.

3.3.9 IBC site classification

The automation in SeisImager/SW analysis software allows for determination of the V_{s30} that is used by the International building code (IBC) to classify a site based on its measured average shear wave velocity for the top 30m. The values so determined were then plotted on a shaded contour map. Table 3.2 shows the classification scheme by IBC 2009.

Table 3-2 Site class definitions (International Building Code IBC-2009)

Site class	Average shear wave velocity (v_s[1])	Average standard Penetration resistance (N^1 or N_{ch}[1])	Average undrained shear strength in the case of cohesive soils (su^1)
A : Hard Rock	>1500 m/s	Not applicable	Not applicable
B: Rock	760 to 1500 m/s	Not applicable	Not applicable
C:Very dense soil or soft rock	370 to 760 m/s	>50	>100kPa
D: Stiff soil	180 to 370 m/s	15 to 50	50 to 100 kPa
E: Soft soil	<180 m/s	<15	<50 kPa
	Any profile with more than 3 m of soil having Plasticity Index PI>20, Moisture content ω≥40% Average undrained shear strength su < 24 kPa		
F:Soils requiring site-specific evaluation	Soils vulnerable to potential failure or collapse (liquefiable, quick- or highly sensitive clays, collapsible weakly cemented soils) More than 3 m of peat and/or highly organic clays More than 7.5m of very high plasticity clays (PI>75) More than 37m of soft to medium clays		

4 CHAPTER FOUR: RESULTS AND DISCUSSION

4.1 Introduction

This chapter presents the results of the study followed by a discussion and subsequent analysis of the same. The ReMi survey for the 50 locations along the 12Km section of the main Nairobi-Nakuru-Eldoret highway and the 5 locations along the 1.6Km section are herein presented and discussed successively. The results from the survey include the 2-D shear wave velocity models, Derived geotechnical parameters and the NEHRP/IBC classification for each measurement site. The derived geotechnical parameters and the 1D profile for each measurement locations are provided in the appendix I. Appendix II is a table of the coordinates of the measurement locations in UTM WGS 84 datum.

4.2 Results and discussions

The results from the one dimensional shear wave velocity models were combined in surfer 2009 software (Golden softwares) to produce a composite 2-D model for the entire survey profile.

4.2.1 Main profile

The main profile runs along the main Nairobi-Nakuru-Eldoret highway stretching a distance of 12Km.This profile was divided into three sections on the basis of geology and geological structures, mainly faults as can be inferred from the geological map (figure 4.1). As such, three sections have been discussed;

1. The first section represents about 2.9 Km between S1-S10, from the Njoro road junction to the second roundabout where the profile takes a bend to the northeast. The section is intended to highlight the influence of the faults in the section on the shear wave velocities
2. The second section strands the Nakuru CBD without devoid of mapped structures. The objective was to map the continuum with no geological structures or identify geological structures in cases where such features are buried.
3. The last section starts near the junction to Nyahururu and terminating at the Lanet junction (S25-S50). The objective was to capture the few mapped faults in this zone.

The interpretation of the velocity profile was done with reference to geology and structures thus the geological map is presented in figure 4.1.

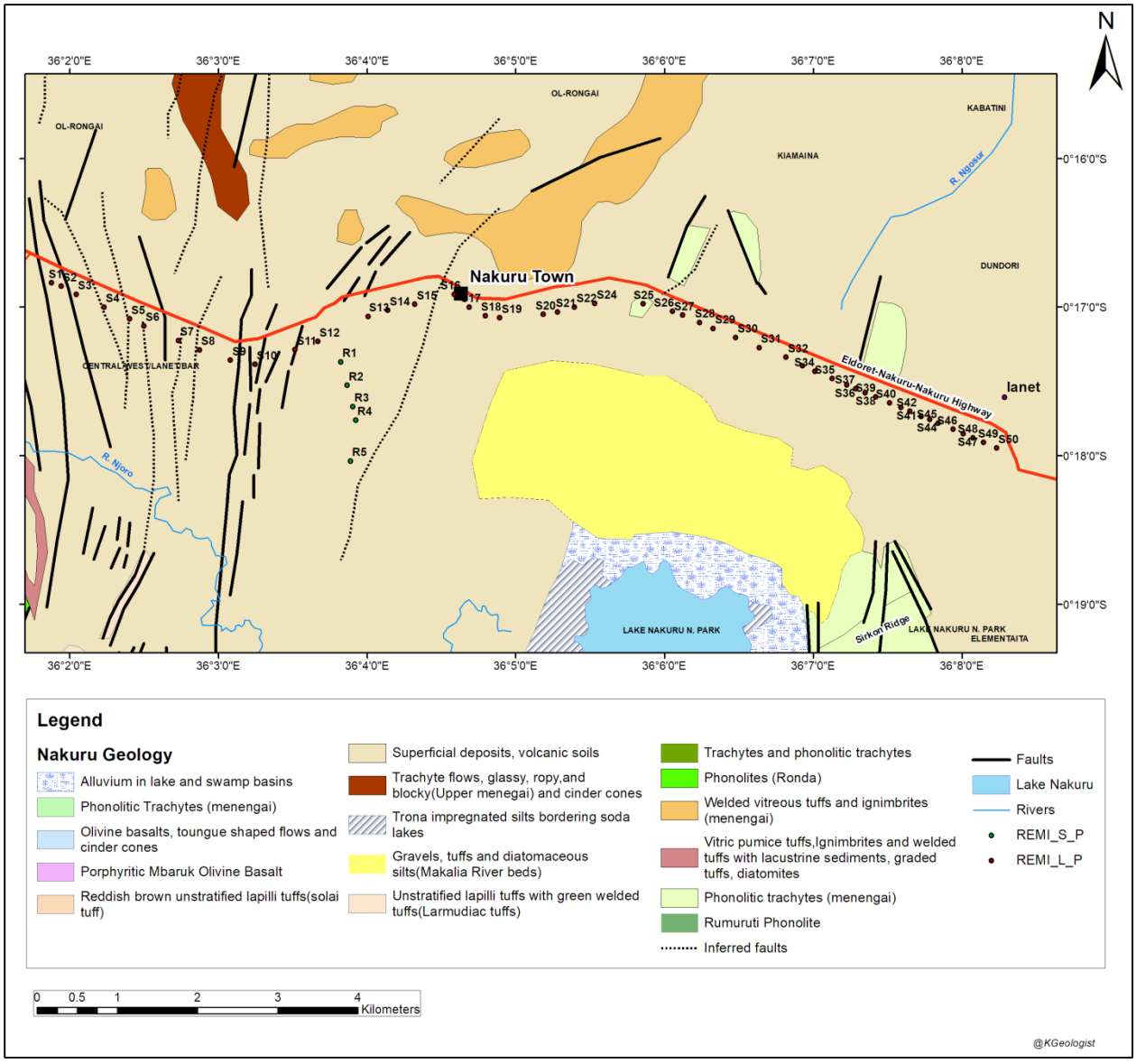

Figure 4.1 Geological map of the study area. The faults are marked as the dark lines, inferred faults as dashed lines, while the ReMi points are marked as dots along the highway (Modified after Macall (1967), Ngecu and Nyambok (2000))

Figure 4.2 is a Google earth image of the survey area with the ReMi points plotted on it along the highway.

Figure 4.2 Google earth image of the survey area. The ReMi points are plotted as blue circles

The results of the 1-D ReMi survey are presented in the appendix section in from of Surface wave velocity curves. Depth is plotted on the y-axis and velocity in m/s on the x-axis. The curve was plotted as formation layers exhibiting different velocities up to a 100m. This different velocity layers are interpreted in terms of geology exhibiting varying mechanical properties.

4.2.1.1 First section between S1-S10

The ReMi section between S1 and S10 starts at the Njoro junction, near the newly built interchange, where S1 is located. S10 is located near the second roundabout that has an exit to Nakuru industrial area. Figure 4.3 is the Google earth image of this section.

Figure 4.3 Google earth image of section 1 (S1-S10). The black lines are the previously mapped faults in the area (from the geological map).

The 2-D model of the section is presented in figure 4.4. From the model, this section records a range of V_S between 160m/s to 700m/s. The range between 160-360m/s is represented by the blue-purplish colors and is the lowest velocity zone. This zone wedges out eastwards with a very irregular bottom with minor crests and troughs. The thickest part is to the west near S1 where a maximum thickness of about 20m is attained and tapers out to the east where it becomes indistinctly defined at S10. This zone is interpreted to represent the loose volcanic soils and/or weathered material.

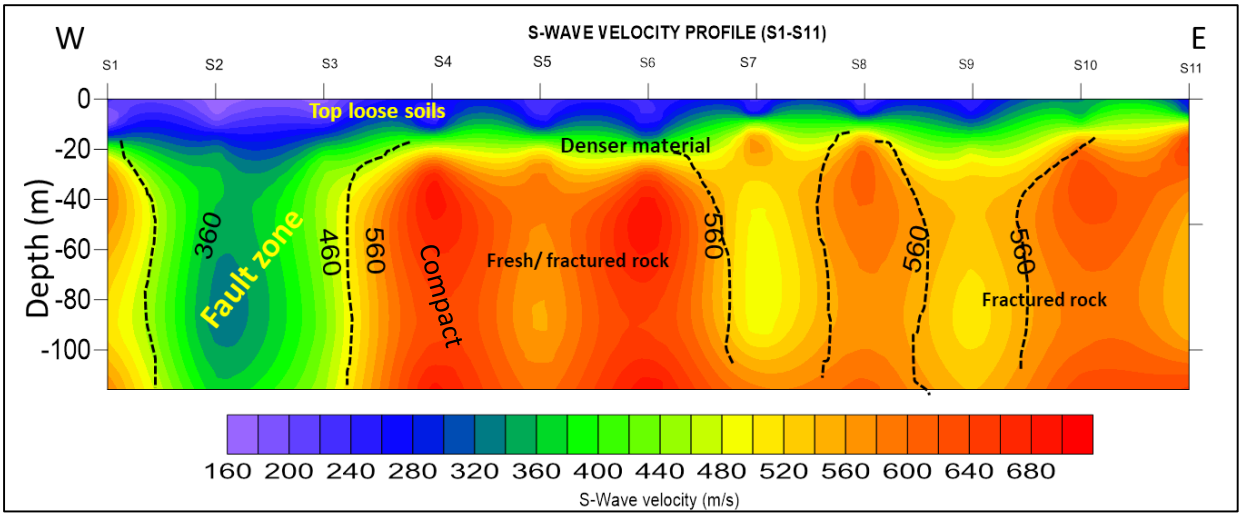

Figure 4.4 2-D S-wave velocity model between S1-S11

Below this loose soil layer is layer with intermediate velocity values (360-480m/s) marked by the green tinge. This zone represents highly weathered rock mass. This zone is expected to be composed of denser saprolitic material and weathered rock with a thickness between 5-10m. The basal layer is represented by velocities between 480-700m/s. This is the zone shown by the orange-reddish colors. Most of the eastern part of the profile from S3 is dominated by this range. This range is interpreted to represent the fractured and possibly marginally weathered but dense material.

Characteristically, to the west, between S1-S4, is a fault zone that is interpreted and that is rather coincident with a mapped fault in the geological map. The faulted zone is represented by a low velocity area characteristic of mechanically weak geologic material (similar to highly weathered) bounded on both sides by high velocities that represent mechanically competent and dense material. Further east, zones marked by yellow colorations indicate fractured zones whose matrix is not weathered. The identified faults also coincide with the mapped faults in the geological map for the area. These are located between S6, S7, and at S9. This section provided scientific evidence of the nature of fractures on seismic velocity models.

4.2.1.2 Second Section between S11-S25

This section covers the main CBD area to the junction of the Nyeri-Nyahruru road, near section 58. The profile covers a distance of about 4.57km from S11 to S25. Figure 4.5 is the Google earth image of the section.

Figure 4.5 Google earth image of the section S11-S25

This section, as can be readily observed in the geological map (figure 4.1) and figure 4.5 has a single mapped fault that is rather extensive in the SW-NE trend.

The interpreted S-wave velocity model is presented in figure 4.6. The profile records a higher range of S-wave velocity (200-1100m/s) compared to the previous section (160-700m/s). The higher velocity range is expected to mean improved mechanical competence in the geologic materials for this section.

The western end of the profile between S11 to S16 has a relatively thick cover of loose material reaching a depth of about 10m. This section also hosts the interpreted fault zone between S13-S16 that extends to the maximum probed depth of 115m. This zone records the lowest V_s (200-400m/s) for the whole depth as compared to other similar zones in this profile. This faulted zone coincides with the mapped fault in the geological map. To the west and east of the zone are two high velocity zones recording value higher than 900m/s. representing rather dense material.

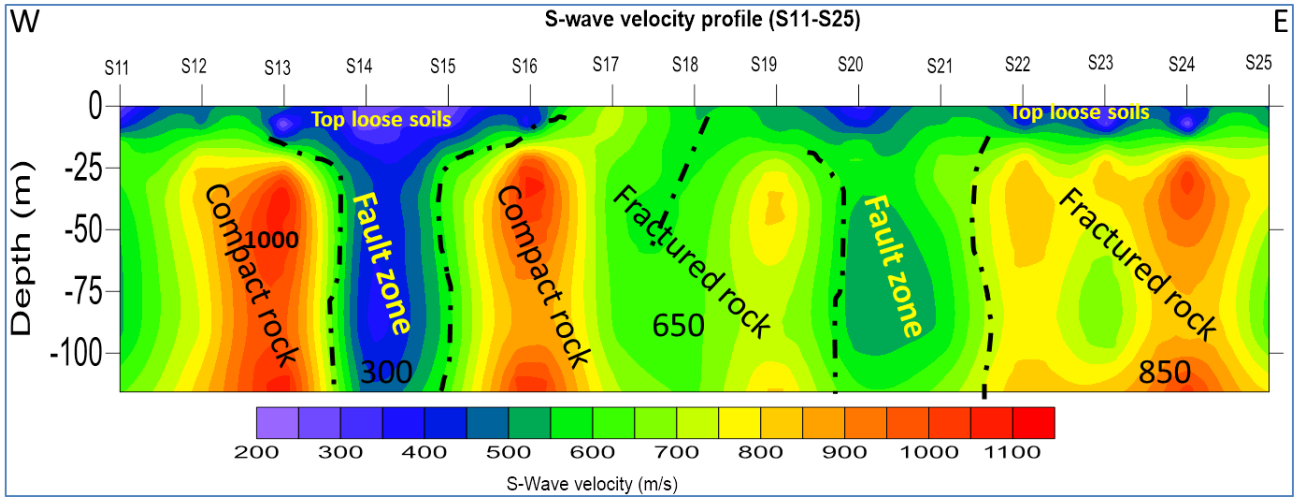

Figure 4.6 2-D S-wave velocity model between S11-S25

The zone between S17 and S20 with velocities between 600-800m/s is interpreted as representing the fractured rock. The fractures may extend to considerable depths as can be seen in the inferred fracture at S18. There is another fault zone between S19-S21 that has rather low velocities compared to the surrounding areas.

4.2.1.3 Third Section between S25-S50

This represents the last section of the entire 12Km profile measuring a total distance of 4.76Km. This section ends at the Lanet junction to Ndundori and Lanet barracks. Few faults have been mapped on the geological map, and have also been overlaid on the Google earth image in figure 4.7 showing the location of the measurements for the section.

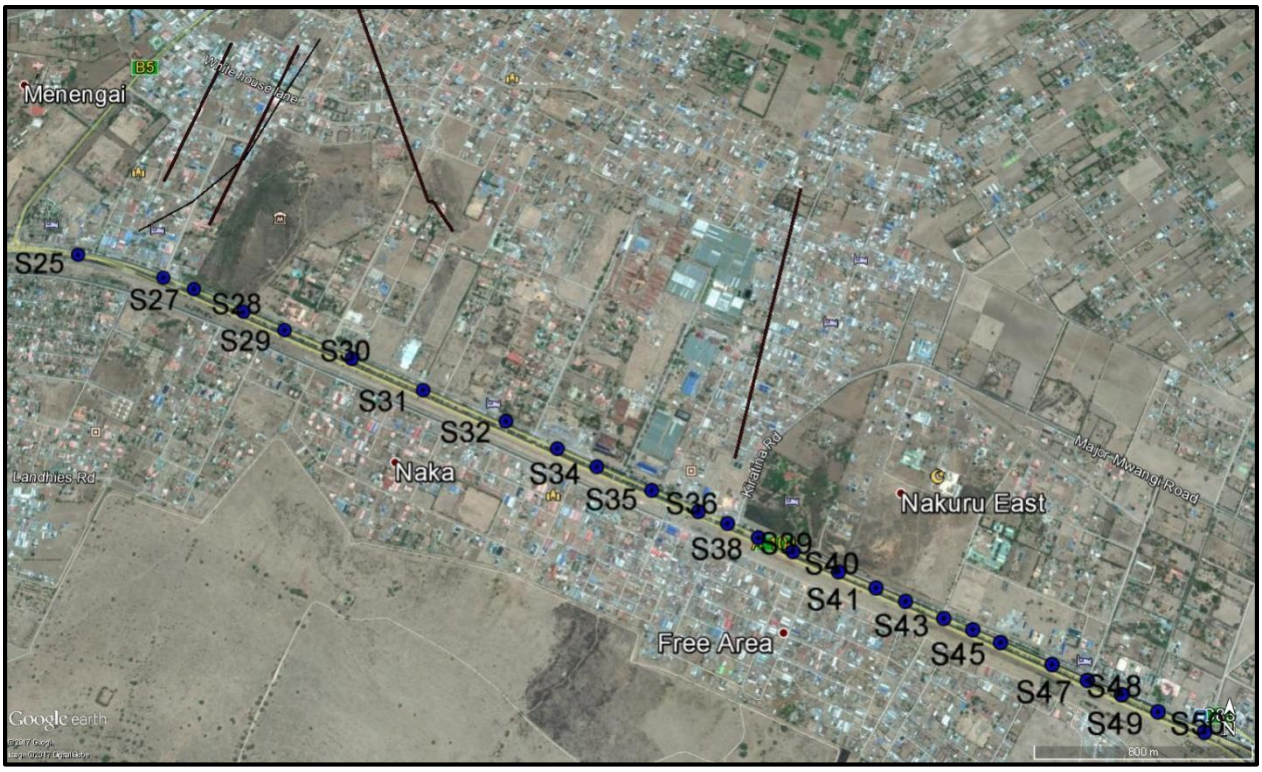

Figure 4.7 Google earth image of the survey area with faults overlain as the thick dark lines

The interpreted Vs model (figure 4.8) exhibits a rather complex model with dominating velocities between 250-650 m/s. The Vs range is between 250m/s to 1000m/s. The lower end representing the faulted zones while the intermediate (650m/s) representing the fractured zones. The Central part has a high velocity zone (>850m/s) and stands out as the outlier in this section of the profile. Three fault zones corresponding to the V_s have been marked between S27-S34, S38-S43-S47. These zones all extend to the maximum depth of probe. The fault zone at S27 coincides with the fault mapped in the geological map but the faults in the map do not however extend to the highway. This coincidence then could suggest that these faults may in-fact be extensive. Another fault line mapped in the geological map is in close coincidence with that in this profile at S38. This can be readily observed in figures 4.7 and 4.1.

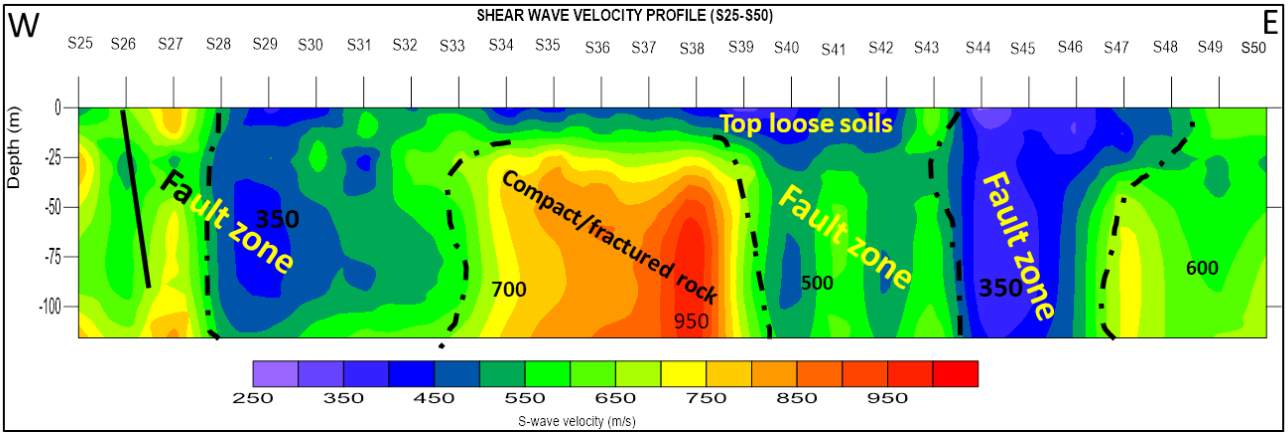

Figure 4.8 2-D S-wave velocity model between S25-

4.2.1.4 The combined profile

The combined profile consists of the three discussed sections. A combined profile gives a better view for the entire survey distance and allows a complete characterization of the earth's subsurface. The interpreted model (figure 4.9) gives a range of 150m/s to 1050m/s.

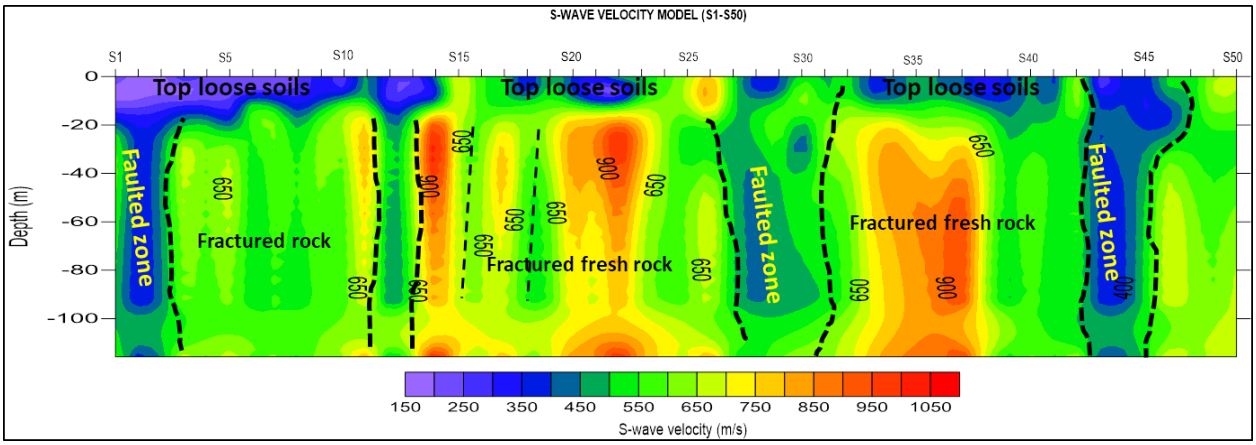

Figure 4.9 The combined S-wave velocity model for the 12Km profile

The highly weathered fault zones occur with some regular intervals and surrounded by fractured zones. The areas underlain by compact rock occupy very narrow ranges indicating the instability zones often observed in Nakuru Municipality.

4.2.2 The North-South profile

This profile runs along the *Kwa Rhoda* road a distance of about 1.36Km. The interpreted S-wave velocity model for this profile (figure 4.10) exhibits a range of velocities from 200m/s to 1000m/s. The low values between 200 and 450m/s are representative of the top loose soils that are dominant in the mid-section of the profile and extend to a maximum depth of about 20m between R2 and R3. Either ends of the profile do not have thick cover of the soils. The Intermediate values between 459 and 700m/s represent denser materials, either fractured or weathered rock or very dense sediments. In the middle of the profile, below R2 is what is interpreted as a probe within a wide W-E trending fault zone that is rare on the geological map. It has very gentle slopes and actually resembles a syncline buried by sediments. The characteristic feature of the fault zone is that it tapers with depth. The higher values >700m/s are representative of the hard and competent rock. This occurs from a depth of 20m below R1 and about 40m below R3.

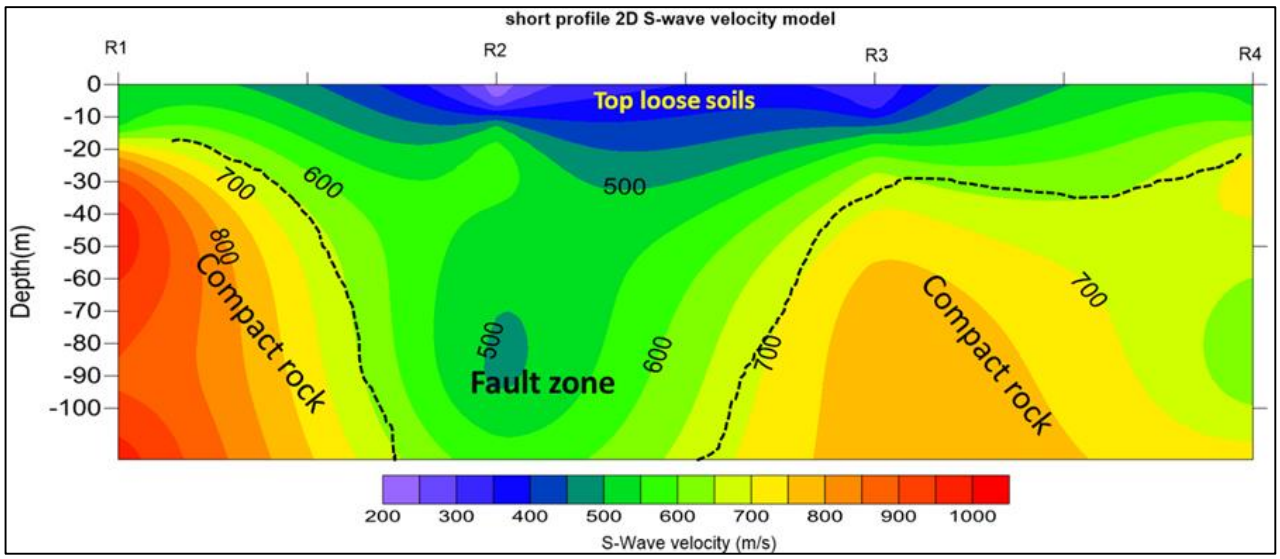

Figure 4.10 2-D S-wave velocity profile for the S-N profile

4.2.3 IBC classification (V_{s30})

The average shear wave velocity for the top 30m (V_{s30}) was calculated for all the 55 measurement locations and plotted as a contour map (figure 4.11) and overlaid on the geological map (Figure 4.1) for correlation puposes. As can be observed from the map,

the V_{s30} ranges between 240m/s and 680m/s. Generally, the study area falls under two classes according to the IBC (2009). To the west of the study area, near the Njoro junction, the lowest values are recorded that place this area under category D (<370m/s). This category represents stiff soils while the rest of the area falls under category C (370-760m/s) representing very dense soils and/or soft rock. The V_{s30} for the study area also tends to replicate the lithological and structural variations.

It can be inferred from the map (figure 4.11) that the highly faulted area to the west records the lowest S-wave velocity values. This area also has the deepest sediment cover compared to the east. The mid-section and the area to the east which are not as faulted as the west record higher values (class C). Observations made on the ground also confirm visible outcrops and shallow buried rock in this area.

The significance of site classification is noticed in the factorization of the identified site class in seismic design criteria as provided in the Building Seismic Safety Council (2015). The soil structure interaction for seismic design is also elaborated in this publication. Site coefficients and risk-targeted maximum considered earthquake spectral response acceleration parameters are adjusted for the determined site class effects in accordance with guidelines provided in the manual.

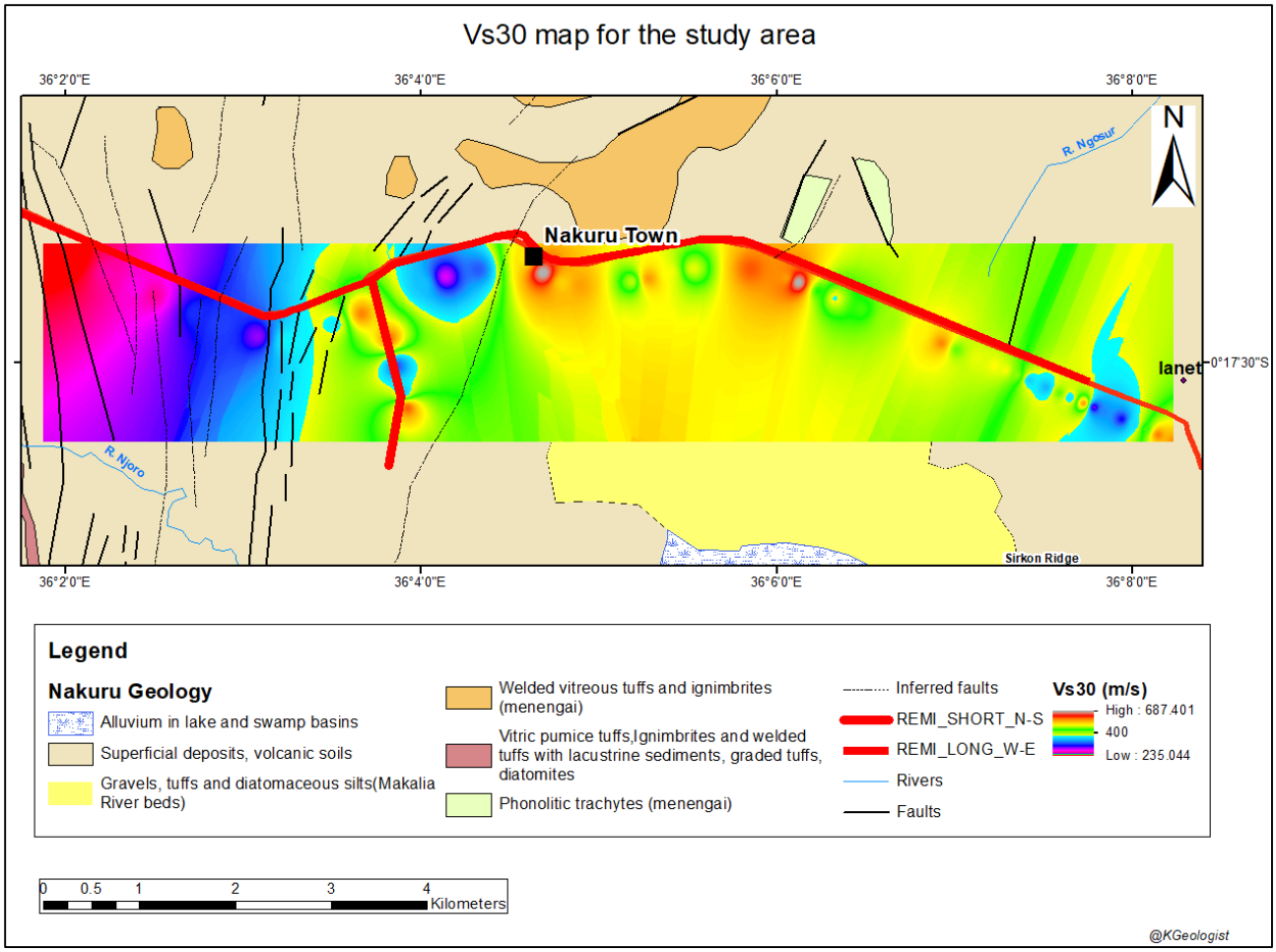

Figure 4.11 Vs30 map overlaid on the geological map

4.3 Discussion

The findings of this research project are twofold:

1. Numerous fault zones and general zones of weakness in the ground characterize the subsurface in the area of study. 1-D Shear wave velocity models from the ReMi survey were combined to produce 2-D shear wave velocity models for the two profiles. Vertical low S-wave velocity zones enveloped on both sides by high S-wave velocity zones were identified and interpreted as fault/weak zones. Numerous such zones have been identified and marked on the models.
2. The area of study falls under class D to the west and C to the east according to the IBC (2009) based on the averaged shear wave velocity for the top 30m (V_{s30}). It ranges between 240 and 360m/s and 360-700m/s to the east.

Although ReMI is essentially a one-dimensional survey method, combining these numerous 1-D models to produce a 2-D model allows for easy correlation with each other across the entire profile. A correlation of these resultant models with findings from previous works in the vicinity of the study area shows that they compare rather well. Dindi (2015) did a study on the faults using Magnetics and VLF-EM in the area southwest of Nakuru Municipality. In this study, he was able to map faults and confirm with ground observations. Buried faults, otherwise not very evident on the surface were also identified based on the observable faults. Some of the faults identified in his work extend farther north and intersect the main profile for the current work. The fault observed in his work at the farthest point west extends to and intersects the main ReMi profile at S1 zone and is identified as a fault owing to the low S-wave velocities recorded in this area.

Other faults identified in this project, particularly in the first and third sections (S1-S10 and S25-S50) coincide with those mapped in the geological mapping exercise by McCall (1967) in which he also conducted magnetic survey traverses to identify the faults.

The structural map by Ngecu and Nyambok (2000) contains more mapped fractures, fissures and faults than found in the geological map by McCall (1967). This has been incorporated to the geological map for better correlation. Nearly all the mapped faults in their map coincide with those identified by the ReMI survey. This greatly helps in

identifying more fault zones, presumably buried and not obvious on the surface that can be readily observed in the ReMi profiles. This fault mapping is crucial for future urban development panning and more so in the infrastructural developments such as roads and bridges.

The use of S-wave velocity measured from ReMi to classify sites has been done previously and compared to other methods such as MASW and down hole measurements. Stephenson et al.,(2005) did a blind comparative study for these three methods with the main objective being to determine how closely MASW and ReMi match the downhole measurements. From their work they note that the surface methods match the borehole results to within 15% to a depth of about 260m. In some instance, they were able to match the results to within 3% to a depth of 100m. From their findings, they conclude that MASW and ReMi can be appropriate for shear wave velocity estimation. It is on this premise that the S-wave velocities estimated in the current project using ReMi method have been deemed suitable for classifying Nakuru the study area according the IBC (2009) standards.

The V_s so determined and this classification are important parameters in building codes. V_s is used by the earthquake engineering community in design applications and hazards calculation particularly in urban settings.

5 CHAPTE FIVE: CONCLUSIONS AND RECOMMENDATIONS

5.1 CONCLUSIONS

The ReMi method of determining shear wave velocity models of the subsurface was applied in this project based on its effectiveness in doing so in urban settings. This method records ambient seismic noise (microtremors) to be later analyzed to produce the shear wave velocity models.

The main objective of this project was to determine shear wave velocity for the subsurface geologic materials in Nakuru Municipality and thus be able to classify the Municipality under the National Earthquake Hazard Reduction Program (NEHRP) and the International Building Code (IBC).

The results of the whole exercise have been presented and discussed in chapter four and from this;

- 1-D shear wave velocity models were produced. These were collated and combined to produce a composite 2-D model for better correlation of the results from one measurement location to the next. This method allows for trends to be established and anomalies easily detected. From the composite model, faulted and fractured zones were identified as the zones with the lowest s-wave velocities compared to high velocity zones that are observed enveloping them. A comparison with the geological map shows a good correspondence between the identified fault zones and previously mapped faults on the geological map. Four major fault zones were identified along the entire 12Km section. The first zone is located near the Njoro Junction (between S1 and S5). The second zone is located between S9 and S15. This is near the Egerton university retirement benefits scheme construction. The third major zone is between S25 and SS31. This covers the area where Nyahururu road joins the Nairobi-Nakuru highway. The fourth fault zone is located between S42 and S45 which covers the area between shiners high school and cool rivers hotel.

- The V_{s30} classification for Nakuru Municipality and specifically the study depicts the area to the west (Njoro junction) classified as category D with Vs30 range between 240-360 m/s. The central and eastern areas fall under category C, with Vs30 in the range 360-700m/s. This classification reflects the nature of geologic materials in the earths subsurface. Class D zones are expected to have stiff soils, and probably highly weathered pyroclastic rock. The volcanic soils consist of pyroclastic and are very loose on the surface. Such soils are known to achieve little cementation even at great depths. Class C area is expected to comprise densely packed soils and fairly fresh pyroclastic rock (tuffs).
- The main Nairobi-Nakuru-Eldoret highway that passes through Nakuru Municipality has also been geotechnically mapped and dynamic soil properties of the subsurface determined for the entire study profile. These include shear modulus, Elastic (Young's) modulus and poisson's ratio. These are tabulated in the appendices with other results. The shear modulus follows the same trend as the shear wave velocity as this parameter is in direct relation to S-wave velocity. Such parameters are crucial for road design as they apply to the very nature of dynamic loading by traffic.

5.2 Research limitations

ReMi is a 1-D survey method. Surface wave velocity variation is thus measured against depth only. In the interest of observing lateral variations then, correlation of the individual ReMi 'soundings' has to be made. This ultimately results in interpolation between the survey points and thus has the potential of introducing errors owing to the complex nature of geology and the possibility of significant changes within short distances. This is often overlooked. In the current work, the spacing of about 115m between measurement locations was adopted and considered sufficient on the scale of the survey. It is however important to note that this was not always practical due to infrastructural and natural barriers such as roundabouts, road junctions and tight bends. This was compensated for by earlier planning of the survey so that not many points coincided with such restrictions.

In surface wave measurements, the frequency range of interest is very crucial since it determines the depth of probe and the resolution as well. In the current project, it was

noted during analysis of the dispersion curves that the lowest frequency recorded was between 5 and 10Hz. The objective in ReMi surveys is to record even lower frequencies to ensure that the desired depths are achieved. In lieu of this, it is approximated that only 85% of this was achieved in this project, and thus the presumed depth of 100m.

A direct correlation with previous seismic studies in the area would have provided a better assessment but this was not available. The only available geophysical studies are the VLF-EM and magnetics by Dindi (2015) which serve to provide alternate methods for correlation.

5.3 RECOMMENDATIONS

Following the study results and experiences during the whole research project, the following recommendations emanate:

- Geophones with a natural frequency of 4.5 HZ or lower are recommended in future studies so that lower frequencies below 5Hz can be recorded to improve on depth coverage and resolution.
- It is highly recommended that a follow up of the findings of this work be done with other geophysical methods such as Electrical resistivity tomography (ERT) and VLF-EM to correlate with and possibly validate the findings of ReMi, particularly location of structures such as faults.
- A combination of active with passive surface wave methods is recommended to record the high frequencies in the shallow subsurface up to about 30m and thus improve the resolution of this depth range.
- A policy framework for Nakuru Municipality and the County at large should be developed that requires builders and developers to conduct seismic characterization of any site intended for any civil construction.
- It is also recommended that Municipality planners consider IBC and other site classification schemes in their mandate

REFERENCES

Abdul R. S., Goh, T.L. & Abdul G. R.,2009. Application of spectral analysis of surface wave (SASW) for characterization of rock mass in engineering geology: case study in Malaysia. Geosea 2009, 11th Regional Congress on Geology, Mineral and Energy Resources of Southeast Asia, 62.

Aki, K., 1957. Space and time spectra of stationary stochastic waves, with special reference to microtremors. *Bull Earthquake Res Inst* 35, 416–456.

Aki, K., 1965. A note on the use of microseisms in determining the shallow structure of the Earth's crust. *Geophysics* 30,.665–666.

Allen, D.J.; Darling, W.G., 1992. Geothermics and hydrogeology of the Kenya Rift Valley between Lake Baringo and Lake Turkana. Nottingham, UK, British Geological Survey, 133. (SD/92/001) (Unpublished)

Al-Hunaidi, O., 1998. Evolution based genetic algorithm for the analysis of nondestructive surface wave test on pavements. *Nondestr Test Eval* 31, .273–280.

Ambraseys, N.N., 1991. Earthquake hazard in the Kenya Rift : the Subukia earthquake 1928. Geophysics Journal International, (105), .253–269.

ASTM (American Society for Testing and Materials) D4428/D4428M-00, 2003. Standard Test Methods for Crosshole Seismic Testing, Vol 04.08 Soil and Rock (I).

Asten, M. W., and Henstridge J. D., 1984. Array estimators and the use of microseisms for reconnaissance of sedimentary basins. *Geophysics* 49(11),1828–1837.

Baniasadi, E., Riahi, M. A. and Chaychizadeh, S., 2009. Determination of 1-D Shear-Wave Velocity Profile using the Refraction Microtremor Method, in *First International Petroleum Conference & Exhibition*. Shiraz, Iran,4–6.

Battaglia, J., Zollo, A., Virieux, J., and Dello Iacono, D., 2008. Merging Active and Passive Data Sets in Travel-Time Tomography: The Case Study of Campi Flegrei Caldera (Southern Italy), Geophysical Prospecting, 56, 555–573,

Boore, D. M., and Thompson E. M., 2007. On using surface-source downhole-receiver logging to determine seismic slownesses, Soil Dynamics and Earthquake Engineering 97

Campanella, R.G., Robertson, P.K., Gillespie, D., 1986. Seismic cone penetration test. In: Proceedings of In-Situ'86. GSP 6. ASCE, Reston, VA, 116–130.

Cha, Y.H, Kang, J.S. and Jo, C. H., 2006. Application of linear-array microtremor surveys for rock mass classification in urban tunnel design, *Exploration geophysics*, 37(1),108–113.

Chen, Yun-min, Zhou, Yan-guo and Ke, H., 2008. Shear Wave Velocity-Based Liquefaction Resistance Evaluation : Semi-Theoretical Considerations and Experimental Validations, *The 14th World Conference on Earthquake Engineering*,1–8.

Claprood, M., Asten, M. W. and Kristek, J., 2011. Using the SPAC microtremor method to identify 2D effects and evaluate 1D shear-wave velocity profile in Valleys, *Bulletin of the Seismological Society of America*, 101(2), 826–847.

Dindi, E.,2015. An assessment of the performance of the geophysical methods as a tool for the detection of zones of potential subsidence in the area southwest of Nakuru Municipality, Kenya, *Environmental Earth Sciences*, 73(7), 3643–3653.

Eddleston,M., Walthall, S., Cripps, J. C.& Culshaw, M. G. (eds),1995. Engineering Geology of Construction. Geological Society Engineering Geology Special Publication No. 10, 389-401

Foti, S., 2000. Multistation method for geotechnical characterization using surface waves, Multistation method for geotechnical characterization using surface waves.

Foti, S., Parolai, S., Albarello, D. and Picozzi, M., 2011. Application of Surface-Wave Methods for Seismic Site Characterization, *Surveys in Geophysics*, 32(6), 777–825.

Foti, S., 2012. Combined use of Geophysical Methods for Geotechnical Site Characterization, (September), 43–61

Foti, S., Lai, C., Rix, G. and Strobbia, C., 2015. *Surface Wave Methods for Near-Surface Site Characterization*.

Foti, S., Parolai, S., Albarello, D. and Picozzi, M., 2011. Application of Surface-Wave Methods for Seismic Site Characterization, *Surveys in Geophysics*, 32(6), 777–825.

Gabriels, P., Snieder R., and Nolet G.,1987. In situ measurement of shear wave velocity in sediments with higher-mode Rayleigh waves. *Geophys Prospect* 35, 187–196.

Gardner, G.H.F., Gardner, L.W., and Gregory, A.R., 1974. Formation velocity and density – the diagnostic basics for stratigraphic traps: Geophysics, 39, 770-780.

Gamal, M. A. and Pullammanappallil, S., 2011. Validity of the Refraction Microtremors (ReMi) Method for Determining Shear Wave Velocities for Different Soil Types in Egypt', *International Journal of Geosciences*, 2(4), 530–540.

Ganji, V., Gucunski N. and Nazarian S., 1998. Automated inversion procedure for spectral analysis of surface waves. *J Geotech Geoenviron Eng* 124, 757–770.

Goh, T. L., Samsudin, A. R., & Rafek, A. G., 2011. Application of spectral analysis of surface waves (SASW) method: Rock mass characterization. Sains Malaysiana, 40(5), 425–430.

Grandjean G., Bitri A., 2006. 2 M-SASW: multifold multichannel seismic inversion of local dispersion of Rayleigh waves in laterally heterogeneous subsurfaces: application to the Super-Sauze earthflow, France. Near Surface Geophys 4, 367–375

Hammam, A. H. and Eliwa, M., 2013. Comparison between results of dynamic & static moduli of soil determined by different methods, *HBRC Journal*. Housing and Building National Research Center, 9(2), 144–149.

Huang Y.T, Siller T.J., 1997. Fuzzy representation and reasoning in geotechnical site characterization. Comput Geotech, 21(1), 65–86

International Building Code, 2009. International Code Council

IEA (Institute of Economic Affairs), 2006. A rapid assessment of Kenya's water, sanitation and sewerage framework. IEA, Nairobi, Kenya.

Kenya Meteorological Department, 2000. Unpublished Synoptic and rain station data. Ministry of Information, Transport and Communications, Nairobi, Kenya.

KNBS. (2009) Republic of Kenya, 2009. KENYA POPULATION AND HOUSING CENSUS24th/25th August, 2009.

Kramer, S.L., 1996. Geotechnical Earthquake Engineering: Prentice Hall, Upper Sadle River, New Jersey.191-215

Lay, T. and Terry, C. W., 1995. *Modern Global Seismology*. San Diego, California: Academic Press.

Lillie, R. J., 1999. *Whole earth geophysics: an introductory textbook for geologists and geophysicists*. Upper Saddle River, N.J., Prentice Hall.

Liu, H. P., Warrick R.E., Westerlund R.E., Fletcher J. B., and Maxwell G. L., 1988. An air-powered impulsive shear-wave source with repeatable signals: Bulletin of the Seismological Society of America 78, 355-369

Louie, J. N., 2001. Faster, Better: Shear-Wave Velocity to 100 Meters Depth From Refraction Microtremor Arrays, *Bulletin of the Seismological Society of America.*, (91), 347–364.

Luna, R. and Jadi, H.,2000. Determination of dynamic soil properties using geophysical methods', *First International Conference on the Application of Geophysical and NDT Methodologies to Transportation Facilities and Infrastructure*, (December), 1–15.

Lu, L. and Zhang, B., 2004. Analysis of dispersion curves of Rayleigh waves in the frequency wavenumber domain Analysis of dispersion curves of Rayleigh waves in the frequency – wavenumber domain', (January).

Mahajan, Slob, Siefko, Ranjan, Rajiv, Sporry, Rob, Champati ray, P.K., van Westen, Cees J., 2007. Seismic microzonation of Dehradun city using geophysical and geotechnical characteristics in the upper 30m of soil column. J. Seismol. 11, 355–370.

Martin, A. J. and Diehl, J. G., 2004. 13th World Conference on Earthquake Engineering practical experience using a simplified procedure to measure average shear-wave velocity to a depth of 30 meters (V_{S30})', in *13th World Conference on Earthquake Engineering*

McMechan, G. A., and Yedlin M. J., 1981. Analysis of dispersive waves by wave field transformation. *Geophysics* 46, 869–874.

McCall, G.J.H., 1967. Geology of the Nakuru-Thomson's Falls-Lake Hannington Area, Mines and Geological Department, Report Number 78. Nairobi.

Mohamed, A. M. E., Abu El Ata, A. S. A., Abdel Azim, F. and Taha, M. A.,2013. Site-specific shear wave velocity investigation for geotechnical engineering applications using seismic refraction and 2D multi-channel analysis of surface waves, *NRIAG Journal of Astronomy and Geophysics*. National Research Institute of Astronomy and Geophysics, 2(1), 88–101.

Moro, G. D., 2015. *Surface Wave Analysis for Near Surface Applications*. Amsterdam: Elsevier

Moro, G. D., 2015. Horizontal-to-Vertical Spectral Ratio', *Surface Wave Analysis for Near Surface Applications*, 65–85.

Mwangi, S. W., 2003. Challenges of urban environmental governance. Participation and partnership in Nakuru Municipality, Kenya. University of Amsterdam.

Nazarian, S., and Desai M. R.,1993. Automated surface wave method: Field testing: Journal of Geotechnical Engineering, **119**, 1094–1111.

Nazarian, S., and. Stokoe II K. H., 1984. In situ shear wave velocities from spectral analysis of surface waves: 8th Conference on Earthquake Engineering, vol. 3, 31–38.

Neducza, B., 2007. Stacking of surface waves: Geophysics, **72**, no. 2, V51–V58.

Building Seismic Safety Council (BSSC), 2015. NEHRP recommended provisions for seismic regulations for new buildings and other structures, Part 1: Provisions, FEMA 1050. Federal Emergency Management Agency, Washington, DC

Nighbor, R.L., and Imai T.,1994. The suspension P-S velocity logging method: Geophysical characterization of sites: International Science Publisher, New York, 57-61.
Ngecu, W. M. and Nyambok, I. O., 2000. Ground subsidence and its socio-economic implications on the population: a case study of the Nakuru area in Central Rift Valley, Kenya, *Environmental Geology*, 39(6), 567–574.

Nicholson, S. E., 2000. The nature of rainfall variability over Africa on time scales of decades to millenia, *Global and Planetary Change*, 26(1–3), 137–158.

Ohori, M., Nobata, A., Wakamatsu, K., 2002. A comparison of ESAC and FK methods of estimating phase velocity using arbitrarily shaped microtremor arrays. Bulletin of the Seismological Society of America 92, 2323-2332.

Ohya, S., Ogura, K., & Imai, T.,1984. The Suspension PS Velocity Logging System. Offshore Technology Conference.

Olago D., Opere A., & Barongo J., 2009. Holocene palaeohydrology, groundwater and climate change in the lake basins of the Central Kenya Rift,

O'Neill, A., 2003. Full-waveform reflectivity for modelling, inversion and appraisal of surface wave dispersion in shallow site investigations. PhD Thesis, University of Western Australia, Perth.

Park C.B, Miller R.D, Xia J., 1999. Multichannel analysis of surface waves. Geophysics 64:800–808

Park, C.B., Miller, R.D., Xia, J., and Ivanov, J., 2007. Multichannel analysis of surface waves (MASW) -active and passive methods: The Leading Edge, 26, 60–64.

Penumadu, D. & Park, C. B., 2005. Multichannel Analysis of Surface Wave (MASW) Method for Geotechnical Site Characterization. Earthquake Engineering and Soil Dynamics, 1–10.

Pérez-Santisteban I, García-Mayordomo J, Muñoz Martín A, Carbó A., 2011. Comparison among SASW, ReMi and PS-logging techniques: application to a railway embankment. J Appl Geophys 73: 59–64

Pei, D., 2007. Modeling and inversion of dispersion curves of surface waves in shallow site investigations PhD thesis. University of Nevada, Reno

Picozzi M, Milkereit C, Parolai S, Jaeckel K-H, Veit I, Fischer J, Zschau J., 2010a. GFZ wireless seismic array (GFZ-WISE), a wireless mesh network of seismic sensors: new perspectives for seismic noise array investigations and site monitoring. Sensors 10:3280–3304

Poggiagliolmi E, Berkhout AJ, Boone M.M., 1982. Phase unwrapping possibilities and limitations. Geophys Prospect 30:281–291

Poormirzaee, R., 2016. S-wave velocity profiling from refraction microtremor Rayleigh wave dispersion curves via PSO inversion algorithm, *Arabian Journal of Geosciences*. Arabian Journal of Geosciences, 1–10.

Pullammanappallil, S., Honjas, W and Louie, J. N., 2004. One-Dimensional Shear Wave Profiling for V_{s30} and Nehrp Soil Classification Using the Refraction Microtremor (Remi) Method, in *International Conference on Case Histories in Geotechnical Engineering*. New York.

Pullammanappallil, S., Honjas, W. and Louie, J. N., 2003. Determination of 1-D shear wave velocities using the refraction microtremor method, *Proceedings of the third international conference on the application of geophysical methodologies and NDT to transportation and infrastructure*, 89557, 1–8.

Raini J.A.,2005. Long term trends in water quality, water quantity and biodiversity at Lake Nakuru, In: Proceedings of the 11th world lakes conference, Volume II (Edited by Odada E.O., Olago D.O., Washington, W., Ntiba. M., Wandiga, S., Gichuki, N., Oyieke, H.), ILEC Nairobi, 57 - 62.

Rao, S., 2013. Assessing seismic risk in Kenya. GSDRC Helpdesk Research Report 964). Governance and Social Development Resource Centre, University of Birmingham, Birmingham, UK,10

Rayleigh, Lord, 1885. On waves propagated along the plane surface of an elastic solid, *Proceedings of the London Mathematical Society*, s1-17(1), 4–11.

Rosenblad, B.L. and Bertel, J. D., 2008. Potential Phase Unwrapping Errors Associated with SASW Measurements at Soft-Over-Stiff Sites, *Geotechnical Testing Journal*, Vol. 31, No. 5, 2008, 433-441

Rosenblad, B., Rathje, E. and Stokoe, K.,2002. Shear wave velocity profiling by SASW method at selected strong-motion stations in Turkey, *Lifelines projects topic*, 1–53.

Rošer, J. and Gosar, A., 2010. Determination of Vs30 for seismic ground classification in the ljubljana area, Slovenia, *Acta Geotechnica Slovenica*, 7(1), 61–76.

Rucker, M.,2003. Applying the refraction microtremor (ReMi) shear wave technique to geotechnical characterization, *Proceedings of the third international conference on Applied Geopyhsics*.

Scott, B. J. B., Rasmussen, T., Luke, B., Taylor, W. J., Wagoner, J. L., Smith, S. B. and Louie, J. N., 2006. Shallow Shear Velocity and Seismic Microzonation of the Urban Las Vegas , Nevada Basin, *BSSA, vol. 96, no. 3.*, 96(3).

Shearer, P. M., 2009. *Introduction to Seismology*. second. Cambridge, New York: Cambridge university press.

Simons N, Menzeis B, Matthews M., 2002. A short course in geotechnical site investigation. Thomas Telford, London , p3

Socco, L. V., Foti, S. and Boiero, D., 2010. Surface-wave analysis for building near-surface velocity models: Established approaches and new perspectives, *Geophysics*, 75(5), p. 75A83--75A102.

Steeples, D. W., 2001. Engineering and Environmental Geophysics at the Millenium. Geophysics p 31-35

Stephenson, W .J, Louie, J.N, Pullammanappallil, S, Williams, R.A, Odum, J. K., 2005. Blind shear-wave velocity comparison of ReMi and MASW results with boreholes to 200m in Santa Clara Valley: Implications for earthquake ground-motion assessment, Bulletin of the Seismological Society of America, 95(6), 2506–2516.

Stokoe, K. H., Wright, S. G. Bay J., and Roesset J. M., 1994. Characterization of geotechnical sites by SASW method. In: *Geophysical Characterization of Sites* (R. D. Woods, ed.). ISSMFE Technical Committee #10. Oxford: IBH,15–25.

Stokoe, K.H., II, Woods, R.D., 1972. In Situ Shear Wave Velocity by Cross-Hole Method, Journal of Soil Mechanics and Foundation Division, Proceedings of ASCE, Vol. 98, No. SM5, May, 1972, 443-460.

Strobbia, C., and Cassiani G., 2011. Refraction microtremors: Data analysis and diagnostics of key hypotheses. *Geophysics* 76(3), MA11–MA20

Tokimatsu, K., Tamura S.,Kojima H.,1992. Effects of multiple-modes on Rayleigh-wave dispersion characteristics. *J Geotech Eng* 118(10), 1529–1543.

Tokeshi, K., Harutoonian, P., Leo, C. J., & Liyanapathirana, S., 2013. Use of surface waves for geotechnical engineering applications in Western Sydney. Advances in Geosciences, 35(1), 37–44.

Tole, M. P.,1996. Geothermal energy research in Kenya: a review. J. Afr. Earth Sci.23 (4), 565–575.

UN-HABITAT., 2011. State of the World's Cities 2010/2011- Cities for All: Bridging the Urban Divide. UN-HABITAT

APPENDICES

1-D S-WAVE VELOCITY MODELS AND TABLES OF DERIVED GEOTEHNICAL PARAMETERS

On the curve, the plotted green dots connected by a line show the extent of depth control. This is an overlay of the one-third-wavelength approximation. A good control to a depth of about 30m allows for the Vs30 to be estimated with good levels of accuracy.

S1

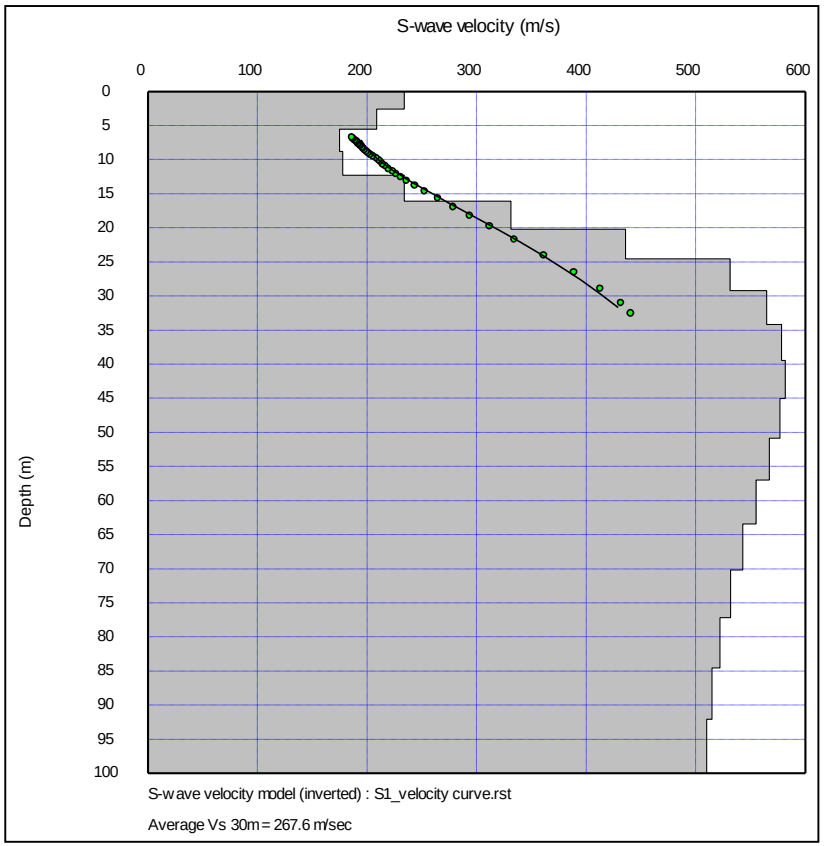

Depth(m)	S-wave velocity (m/s)	P-wave velocity (m/s)	Density (g/cc)	Poisson Ratio	Shear Modulus (Gpa)	Young Modulus (Mpa)
0.00	234.24	1546.54	1.79	0.49	0.10	292.72
2.63	208.99	1520.89	1.79	0.49	0.08	233.34
5.56	174.98	1485.99	1.79	0.49	0.05	164.04
8.77	178.04	1489.22	1.80	0.49	0.06	170.54
12.28	234.12	1549.36	1.81	0.49	0.10	296.11
16.08	331.48	1655.46	1.83	0.48	0.20	595.99
20.18	435.90	1770.21	1.85	0.47	0.35	1033.77
24.56	531.35	1875.71	1.87	0.46	0.53	1540.35
29.24	564.90	1913.00	1.88	0.45	0.60	1738.38
34.21	578.65	1928.56	1.88	0.45	0.63	1821.89
39.47	581.71	1932.40	1.88	0.45	0.63	1840.74
45.03	576.85	1927.47	1.88	0.45	0.62	1810.89
50.88	567.26	1917.26	1.88	0.45	0.60	1752.66
57.02	555.35	1904.41	1.88	0.45	0.58	1681.58
63.45	543.09	1891.11	1.88	0.46	0.55	1609.83
70.18	531.81	1878.83	1.88	0.46	0.53	1545.13
77.19	522.36	1868.53	1.88	0.46	0.51	1491.91
84.50	515.09	1860.59	1.88	0.46	0.50	1451.55
92.11	510.27	1855.32	1.88	0.46	0.49	1425.08
115.79	581.71	1932.40	1.88	0.45	0.63	1840.74

S2

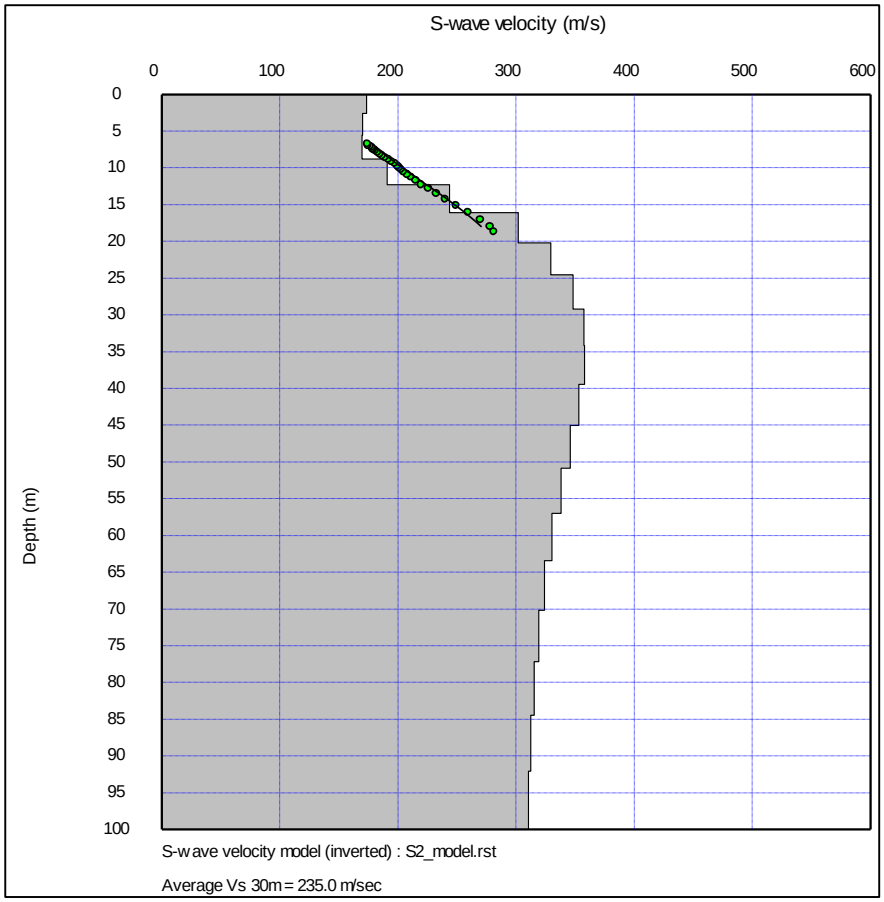

Depth(m)	S-wave velocity (m/s)	P-wave velocity (m/s)	Density (g/cc)	Poisson Ratio	Shear Modulus (Gpa)	Young Modulus (Mpa)
0.00	173.40	1482.92	1.79	0.49	0.05	160.43
2.63	169.96	1479.41	1.79	0.49	0.05	154.16
5.56	171.39	1481.42	1.79	0.49	0.05	157.02
8.77	191.77	1504.18	1.80	0.49	0.07	197.32
12.28	239.05	1555.70	1.81	0.49	0.10	308.06
16.08	307.99	1630.58	1.83	0.48	0.17	513.86
20.18	337.27	1661.57	1.83	0.48	0.21	615.78
24.56	354.44	1679.68	1.83	0.48	0.23	679.24
29.24	363.58	1689.49	1.83	0.48	0.24	714.26
34.21	365.59	1691.82	1.83	0.48	0.24	722.04
39.47	362.74	1689.03	1.83	0.48	0.24	710.98
45.03	357.48	1683.66	1.83	0.48	0.23	690.80
50.88	351.45	1677.41	1.83	0.48	0.23	667.97
57.02	345.71	1671.46	1.83	0.48	0.22	646.62
63.45	340.73	1666.28	1.83	0.48	0.21	628.34
70.18	336.64	1662.02	1.83	0.48	0.21	613.53
77.19	333.48	1658.70	1.83	0.48	0.20	602.17
84.50	331.18	1656.30	1.83	0.48	0.20	594.00
92.11	329.70	1654.75	1.83	0.48	0.20	588.76
115.79	365.59	1691.82	1.83	0.48	0.24	722.04

S3

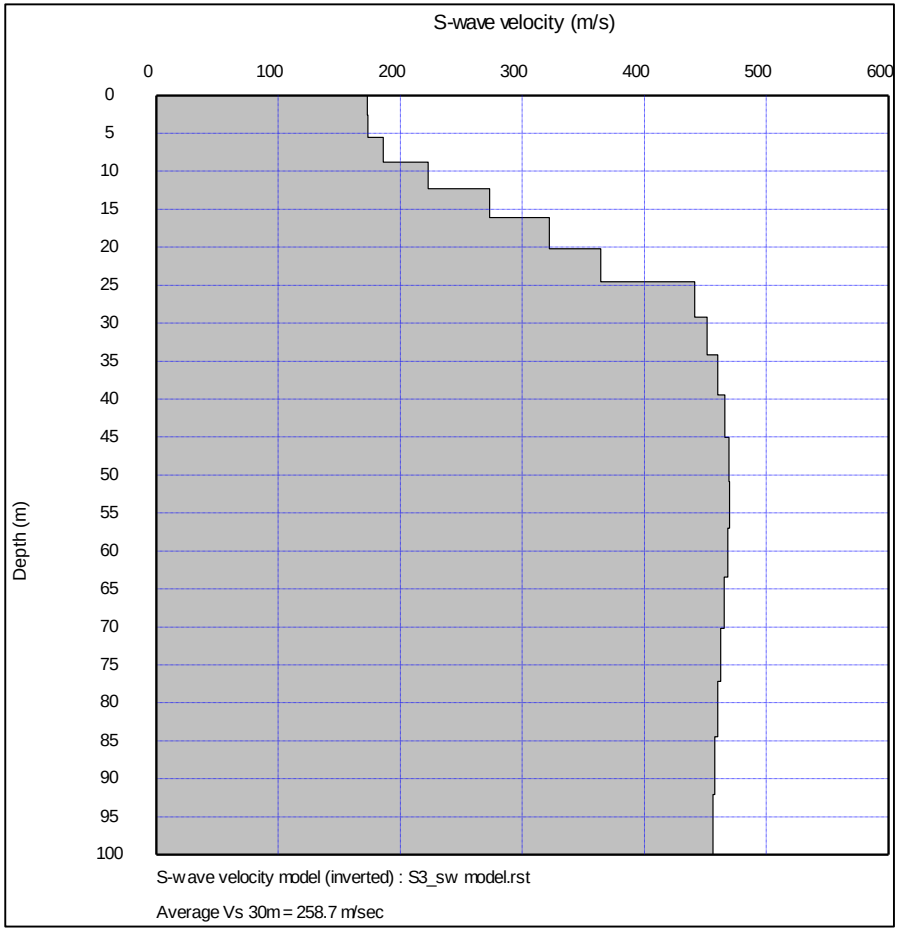

Depth(m)	S-wave velocity (m/s)	P-wave velocity (m/s)	Density (g/cc)	Poisson Ratio	Shear Modulus (Gpa)	Young Modulus (Mpa)
0.00	175.75	1487.05	1.79	0.49	0.06	165.36
2.63	175.23	1486.33	1.79	0.49	0.06	164.41
5.56	186.14	1497.78	1.80	0.49	0.06	185.74
8.77	220.80	1535.57	1.81	0.49	0.09	262.36
12.28	272.29	1592.52	1.82	0.48	0.14	401.19
16.08	325.68	1651.59	1.84	0.48	0.19	576.71
20.18	374.29	1704.90	1.85	0.47	0.26	764.18
24.56	423.97	1758.98	1.86	0.47	0.33	983.18
29.24	437.93	1773.35	1.86	0.47	0.36	1047.85
34.21	448.39	1784.02	1.86	0.47	0.37	1097.58
39.47	454.37	1790.08	1.86	0.47	0.38	1126.50
45.03	455.92	1791.53	1.86	0.47	0.39	1134.01
50.88	454.10	1789.56	1.86	0.47	0.38	1125.13
57.02	450.43	1785.74	1.86	0.47	0.38	1107.37
63.45	445.91	1781.10	1.86	0.47	0.37	1085.67
70.18	441.62	1776.72	1.86	0.47	0.36	1065.22
77.19	437.85	1772.86	1.86	0.47	0.36	1047.46
84.50	434.84	1769.71	1.86	0.47	0.35	1033.34
92.11	432.81	1767.61	1.86	0.47	0.35	1023.90
115.79	455.92	1791.53	1.86	0.47	0.39	1134.01

S4

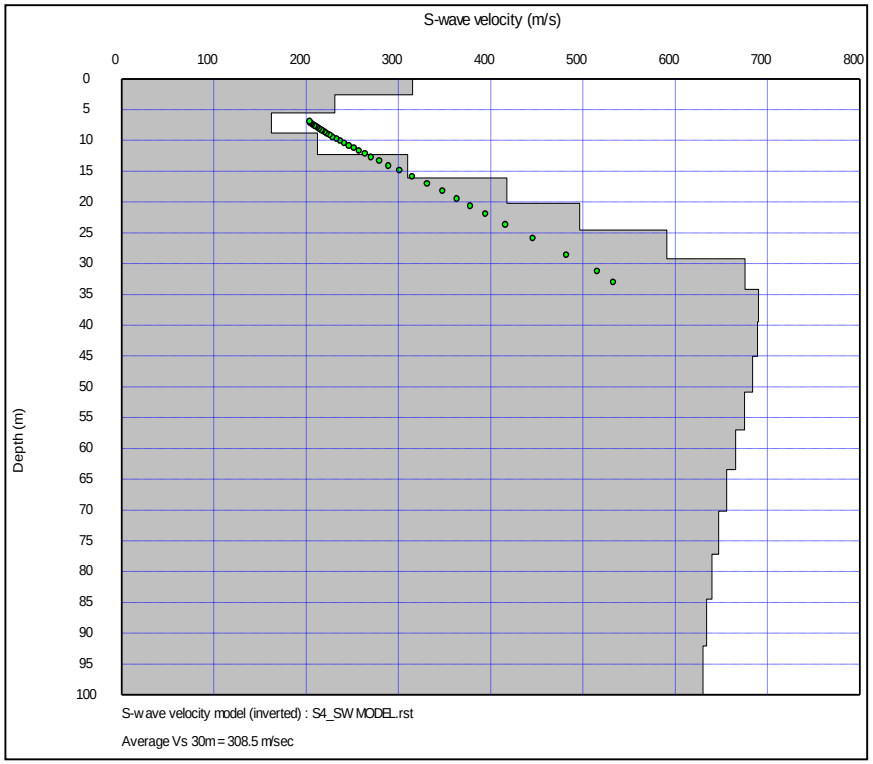

Depth(m)	S-wave velocity (m/s)	P-wave velocity (m/s)	Density (g/cc)	Poisson Ratio	Shear Modulus (Gpa)	Young Modulus (Mpa)
0.00	315.33	1634.96	1.80	0.48	0.18	529.67
2.63	231.01	1547.18	1.80	0.49	0.10	285.80
5.56	162.58	1472.97	1.80	0.49	0.05	142.27
8.77	212.38	1525.15	1.81	0.49	0.08	243.70
12.28	310.07	1633.23	1.83	0.48	0.18	521.63
16.08	417.82	1753.28	1.85	0.47	0.32	951.56
20.18	496.81	1841.04	1.87	0.46	0.46	1348.10
24.56	590.84	1945.14	1.89	0.45	0.66	1916.09
29.24	675.76	2039.17	1.92	0.44	0.88	2519.43
34.21	690.12	2054.85	1.92	0.44	0.91	2628.36
39.47	689.14	2053.51	1.92	0.44	0.91	2621.08
45.03	683.82	2047.45	1.92	0.44	0.90	2581.99
50.88	675.41	2038.06	1.92	0.44	0.88	2520.80
57.02	665.79	2027.43	1.92	0.44	0.85	2451.65
63.45	655.90	2016.70	1.92	0.44	0.83	2381.49
70.18	647.06	2007.07	1.92	0.44	0.80	2319.52
77.19	639.79	1999.14	1.92	0.44	0.79	2269.19
84.50	634.21	1993.05	1.92	0.44	0.77	2230.89
92.11	630.49	1988.99	1.92	0.44	0.76	2205.55
115.79	690.12	2054.85	1.92	0.44	0.91	2628.36

S5

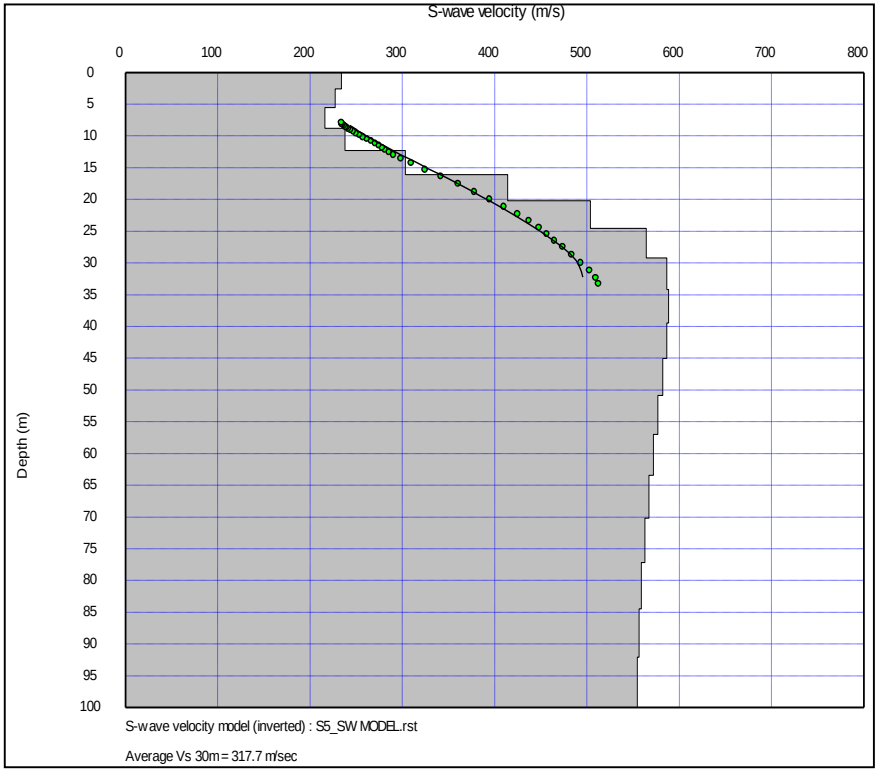

Depth(m)	S-wave velocity (m/s)	P-wave velocity (m/s)	Density (g/cc)	Poisson Ratio	Shear Modulus (Gpa)	Young Modulus (Mpa)
0.00	233.94	1548.71	1.81	0.49	0.10	294.83
2.63	227.58	1542.72	1.81	0.49	0.09	279.14
5.56	216.45	1533.02	1.81	0.49	0.08	252.85
8.77	237.79	1556.51	1.82	0.49	0.10	306.37
12.28	303.30	1625.59	1.84	0.48	0.17	500.32
16.08	414.48	1746.04	1.86	0.47	0.32	940.26
20.18	503.70	1844.11	1.88	0.46	0.48	1394.08
24.56	564.32	1911.82	1.90	0.45	0.60	1754.34
29.24	586.59	1937.56	1.90	0.45	0.65	1896.61
34.21	588.57	1940.75	1.90	0.45	0.66	1909.18
39.47	586.45	1939.11	1.90	0.45	0.65	1895.86
45.03	582.20	1934.79	1.90	0.45	0.64	1869.19
50.88	577.19	1929.37	1.90	0.45	0.63	1837.96
57.02	572.02	1923.63	1.90	0.45	0.62	1805.98
63.45	567.21	1918.22	1.90	0.45	0.61	1776.46
70.18	562.85	1913.29	1.90	0.45	0.60	1749.91
77.19	559.24	1909.18	1.90	0.45	0.59	1728.03
84.50	556.51	1906.08	1.90	0.45	0.59	1711.58
92.11	554.75	1904.08	1.90	0.45	0.59	1701.08
115.79	588.57	1940.75	1.90	0.45	0.66	1909.18

S6

Depth(m)	S-wave velocity (m/s)	P-wave velocity (m/s)	Density (g/cc)	Poisson Ratio	Shear Modulus (Gpa)	Young Modulus (Mpa)
0.00	249.10	1562.57	1.81	0.49	0.11	333.73
2.63	234.24	1548.83	1.81	0.49	0.10	295.34
5.56	226.39	1542.92	1.81	0.49	0.09	276.28
8.77	242.36	1561.16	1.82	0.49	0.11	317.93
12.28	274.79	1596.22	1.83	0.48	0.14	410.98
16.08	329.37	1654.88	1.85	0.48	0.20	593.21
20.18	426.20	1759.87	1.87	0.47	0.34	997.49
24.56	534.54	1877.89	1.89	0.46	0.54	1572.24
29.24	626.25	1978.31	1.90	0.44	0.75	2157.85
34.21	663.90	2019.54	1.90	0.44	0.84	2416.93
39.47	687.86	2046.18	1.90	0.44	0.90	2588.86
45.03	698.33	2058.22	1.90	0.43	0.93	2665.79
50.88	697.75	2058.24	1.90	0.44	0.93	2661.58
57.02	689.80	2050.10	1.90	0.44	0.91	2603.26
63.45	677.81	2037.45	1.90	0.44	0.88	2516.36
70.18	664.75	2023.50	1.90	0.44	0.84	2423.24
77.19	652.56	2010.42	1.90	0.44	0.81	2337.83
84.50	642.81	1999.92	1.90	0.44	0.79	2270.51
92.11	636.13	1992.72	1.90	0.44	0.77	2224.88
115.79	698.33	2058.24	1.90	0.43	0.93	2665.79

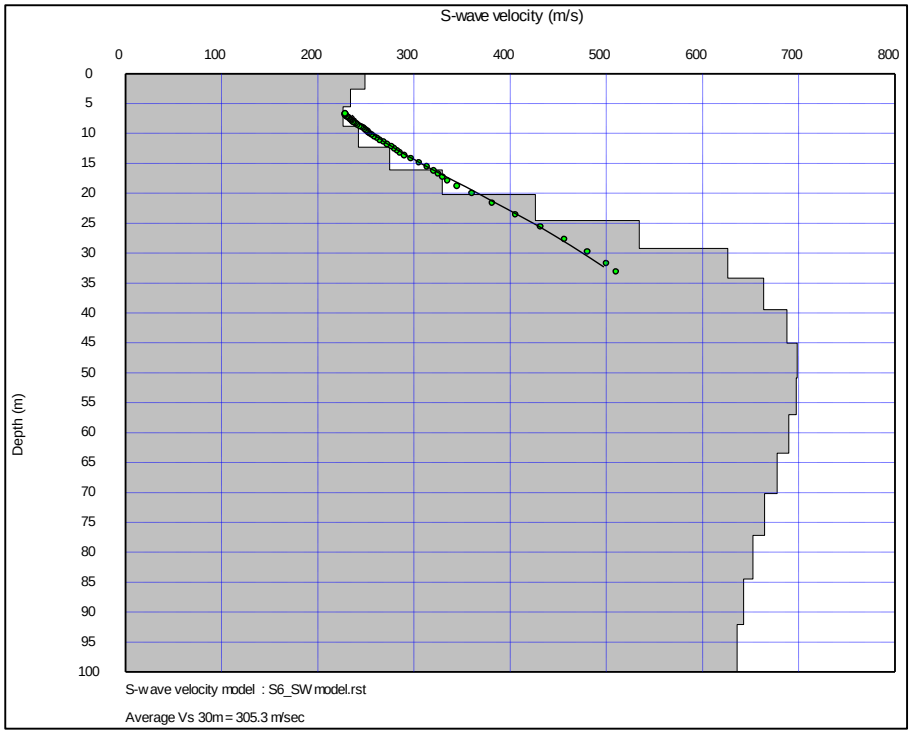
S-wave velocity (m/s)
0
100
200
300
400
500
600
700
800
Depth (m)
0
5
10
15
20
25
30
35
40
45
50
55
60
65
70
75
80
85
90
95
100
S-wave velocity model : S6_SW model.rst
Average Vs 30m = 305.3 m/sec

S7

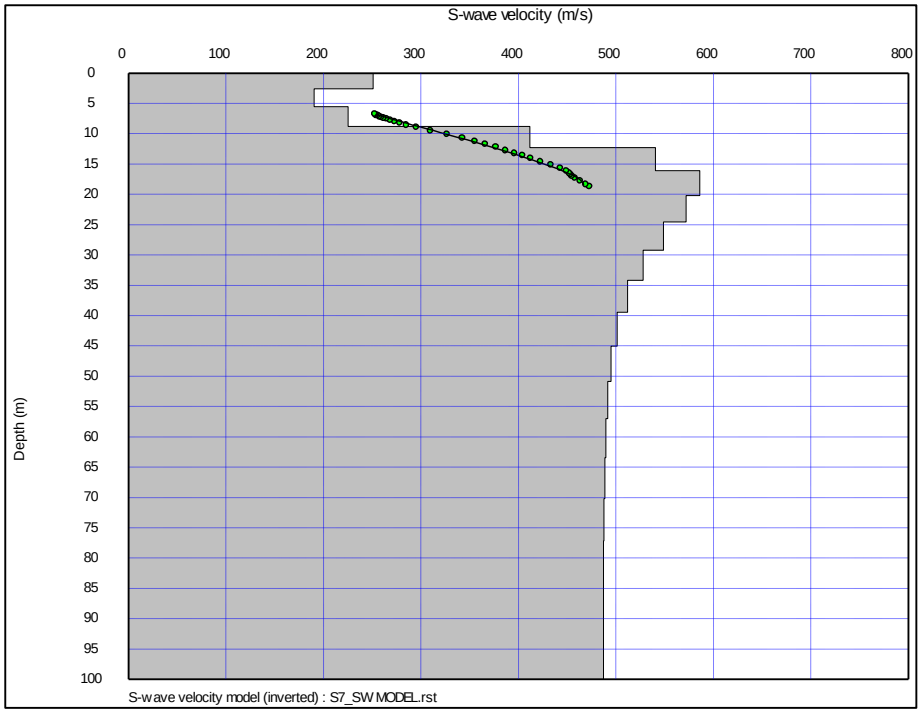

Depth(m)	S-wave velocity (m/s)	P-wave velocity (m/s)	Density (g/cc)	Poisson Ratio	Shear Modulus (Gpa)	Young Modulus (Mpa)
0.00	250.97	1563.66	1.82	0.49	0.11	340.39
2.63	190.77	1502.70	1.82	0.49	0.07	197.35
5.56	225.65	1541.93	1.82	0.49	0.09	276.32
8.77	411.65	1743.53	1.85	0.47	0.31	923.39
12.28	540.59	1885.88	1.88	0.46	0.55	1597.66
16.08	586.34	1938.06	1.89	0.45	0.65	1884.29
20.18	571.93	1923.91	1.89	0.45	0.62	1795.21
24.56	549.08	1899.95	1.89	0.45	0.57	1657.90
29.24	527.94	1877.27	1.89	0.46	0.53	1535.50
34.21	512.11	1859.95	1.89	0.46	0.50	1446.69
39.47	501.63	1848.26	1.89	0.46	0.48	1389.26
45.03	495.37	1841.09	1.89	0.46	0.46	1355.51
50.88	491.87	1836.94	1.89	0.46	0.46	1336.78
57.02	489.90	1834.51	1.89	0.46	0.45	1326.28
63.45	488.74	1833.01	1.89	0.46	0.45	1320.14
70.18	488.06	1832.08	1.89	0.46	0.45	1316.55
77.19	487.62	1831.48	1.89	0.46	0.45	1314.19
84.50	487.38	1831.14	1.89	0.46	0.45	1312.93
92.11	487.23	1830.93	1.89	0.46	0.45	1312.15
115.79	586.34	1938.06	1.89	0.45	0.65	1884.29

S8

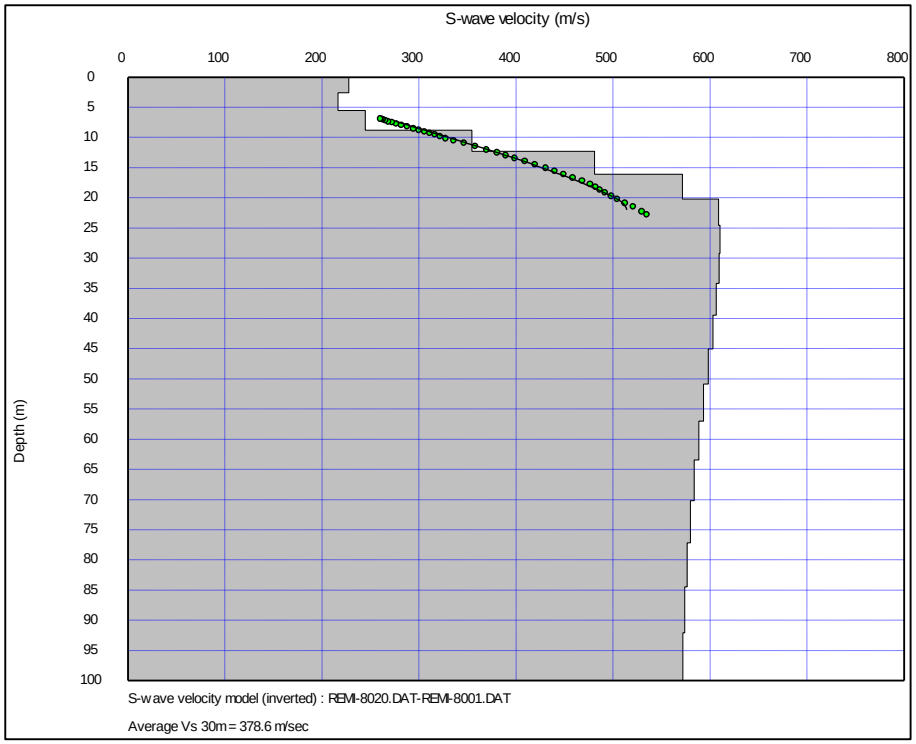

Depth(m)	S-wave velocity (m/s)	P-wave velocity (m/s)	Density (g/cc)	Poisson Ratio	Shear Modulus (Gpa)	Young Modulus (Mpa)
0.00	227.95	1541.30	1.82	0.49	0.09	281.63
2.63	216.89	1533.17	1.82	0.49	0.09	255.14
5.56	244.84	1564.56	1.83	0.49	0.11	325.68
8.77	354.59	1680.86	1.85	0.48	0.23	686.15
12.28	481.07	1818.79	1.88	0.46	0.43	1271.26
16.08	571.46	1919.65	1.90	0.45	0.62	1803.37
20.18	608.86	1962.61	1.91	0.45	0.71	2051.47
24.56	610.33	1965.55	1.91	0.45	0.71	2061.28
29.24	609.22	1965.02	1.91	0.45	0.71	2054.02
34.21	606.65	1962.40	1.91	0.45	0.70	2037.18
39.47	602.94	1958.36	1.91	0.45	0.70	2013.02
45.03	598.50	1953.38	1.91	0.45	0.69	1984.27
50.88	593.50	1947.73	1.91	0.45	0.67	1952.07
57.02	588.50	1942.07	1.91	0.45	0.66	1920.15
63.45	583.83	1936.84	1.91	0.45	0.65	1890.55
70.18	579.76	1932.31	1.91	0.45	0.64	1864.96
77.19	576.46	1928.64	1.91	0.45	0.64	1844.32
84.50	573.94	1925.77	1.91	0.45	0.63	1828.61
92.11	572.38	1923.95	1.91	0.45	0.63	1818.90
115.79	610.33	1965.55	1.91	0.45	0.71	2061.28

S9

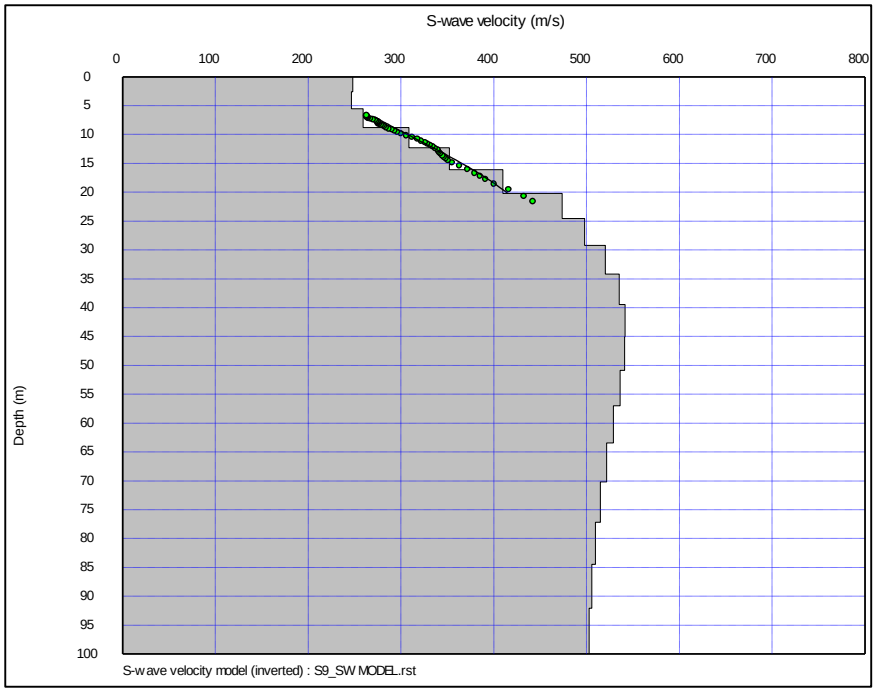

Depth(m)	S-wave velocity (m/s)	P-wave velocity (m/s)	Density (g/cc)	Poisson Ratio	Shear Modulus (Gpa)	Young Modulus (Mpa)
0.00	246.36	1565.83	1.82	0.49	0.11	328.84
2.63	245.98	1565.32	1.82	0.49	0.11	327.85
5.56	259.67	1579.55	1.82	0.49	0.12	365.64
8.77	308.80	1633.35	1.84	0.48	0.18	519.57
12.28	354.66	1684.47	1.85	0.48	0.23	688.39
16.08	410.59	1746.67	1.87	0.47	0.32	927.00
20.18	475.32	1817.66	1.89	0.46	0.43	1247.30
24.56	499.15	1842.55	1.89	0.46	0.47	1374.10
29.24	517.10	1860.77	1.89	0.46	0.50	1472.41
34.21	529.84	1873.64	1.89	0.46	0.53	1544.17
39.47	535.99	1879.76	1.89	0.46	0.54	1579.33
45.03	536.61	1880.30	1.89	0.46	0.54	1582.89
50.88	533.40	1876.98	1.89	0.46	0.54	1564.45
57.02	528.33	1871.77	1.89	0.46	0.53	1535.52
63.45	522.86	1866.16	1.89	0.46	0.52	1504.63
70.18	517.68	1860.88	1.89	0.46	0.51	1475.61
77.19	513.24	1856.35	1.89	0.46	0.50	1451.00
84.50	509.95	1853.03	1.89	0.46	0.49	1432.81
92.11	507.74	1850.80	1.89	0.46	0.49	1420.72
115.79	536.61	1880.30	1.89	0.46	0.54	1582.89

S10

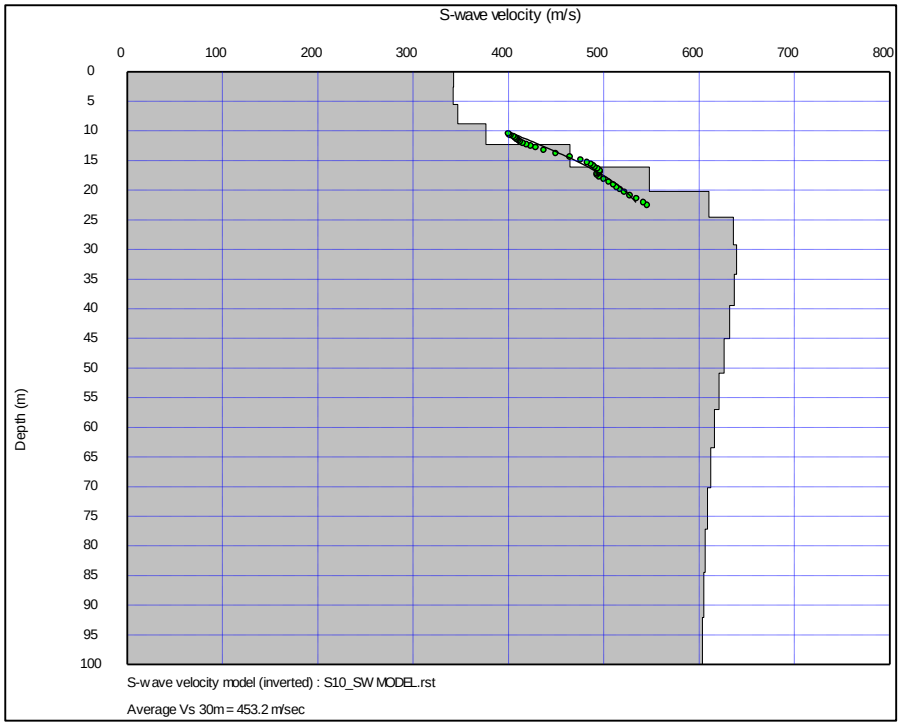

Depth(m)	S-wave velocity (m/s)	P-wave velocity (m/s)	Density (g/cc)	Poisson Ratio	Shear Modulus (Gpa)	Young Modulus (Mpa)
0.00	340.87	1672.76	1.87	0.48	0.22	643.34
2.63	340.20	1671.88	1.87	0.48	0.22	640.81
5.56	344.04	1675.52	1.87	0.48	0.22	655.19
8.77	373.77	1706.69	1.88	0.47	0.26	772.75
12.28	466.35	1807.02	1.89	0.46	0.41	1205.87
16.08	555.59	1904.42	1.91	0.45	0.59	1713.14
20.18	604.19	1957.84	1.91	0.45	0.70	2022.79
24.56	625.16	1981.35	1.91	0.44	0.75	2161.65
29.24	634.17	1991.88	1.91	0.44	0.77	2222.71
34.21	634.78	1992.95	1.91	0.44	0.77	2226.92
39.47	630.35	1988.29	1.91	0.44	0.76	2196.82
45.03	623.71	1980.96	1.91	0.44	0.74	2152.04
50.88	616.33	1972.72	1.91	0.45	0.73	2102.75
57.02	609.14	1964.64	1.91	0.45	0.71	2055.28
63.45	602.65	1957.35	1.91	0.45	0.70	2012.86
70.18	597.14	1951.21	1.91	0.45	0.68	1977.17
77.19	592.68	1946.32	1.91	0.45	0.67	1948.52
84.50	589.34	1942.68	1.91	0.45	0.66	1927.19
92.11	587.15	1940.31	1.91	0.45	0.66	1913.24
115.79	634.78	1992.95	1.91	0.44	0.77	2226.92

S11

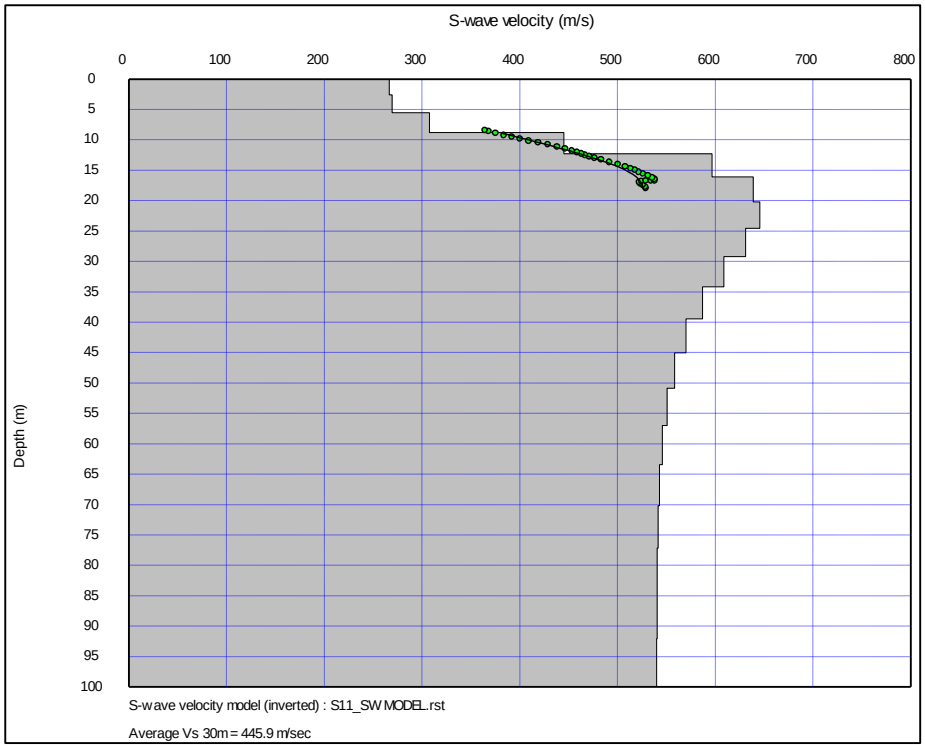

Depth(m)	S-wave velocity (m/s)	P-wave velocity (m/s)	Density (g/cc)	Poisson Ratio	Shear Modulus (Gpa)	Young Modulus (Mpa)
0.00	266.69	1592.27	1.86	0.49	0.13	392.45
2.63	269.26	1594.22	1.86	0.49	0.13	399.97
5.56	307.69	1632.99	1.86	0.48	0.18	521.31
8.77	445.33	1780.82	1.88	0.47	0.37	1093.56
12.28	597.02	1946.97	1.91	0.45	0.68	1970.10
16.08	638.87	1993.66	1.91	0.44	0.78	2248.98
20.18	645.61	2002.90	1.91	0.44	0.80	2295.50
24.56	631.28	1989.17	1.91	0.44	0.76	2197.74
29.24	608.89	1966.13	1.91	0.45	0.71	2048.79
34.21	587.38	1943.51	1.91	0.45	0.66	1910.27
39.47	570.37	1925.33	1.91	0.45	0.62	1803.90
45.03	558.59	1912.54	1.91	0.45	0.60	1731.92
50.88	550.98	1904.10	1.91	0.45	0.58	1686.15
57.02	546.16	1898.57	1.91	0.45	0.57	1657.43
63.45	543.32	1895.19	1.91	0.46	0.56	1640.63
70.18	541.70	1893.09	1.91	0.46	0.56	1631.02
77.19	540.84	1891.93	1.91	0.46	0.56	1625.97
84.50	540.51	1891.42	1.91	0.46	0.56	1624.05
92.11	540.41	1891.21	1.91	0.46	0.56	1623.41
115.79	645.61	2002.90	1.91	0.44	0.80	2295.50

S12

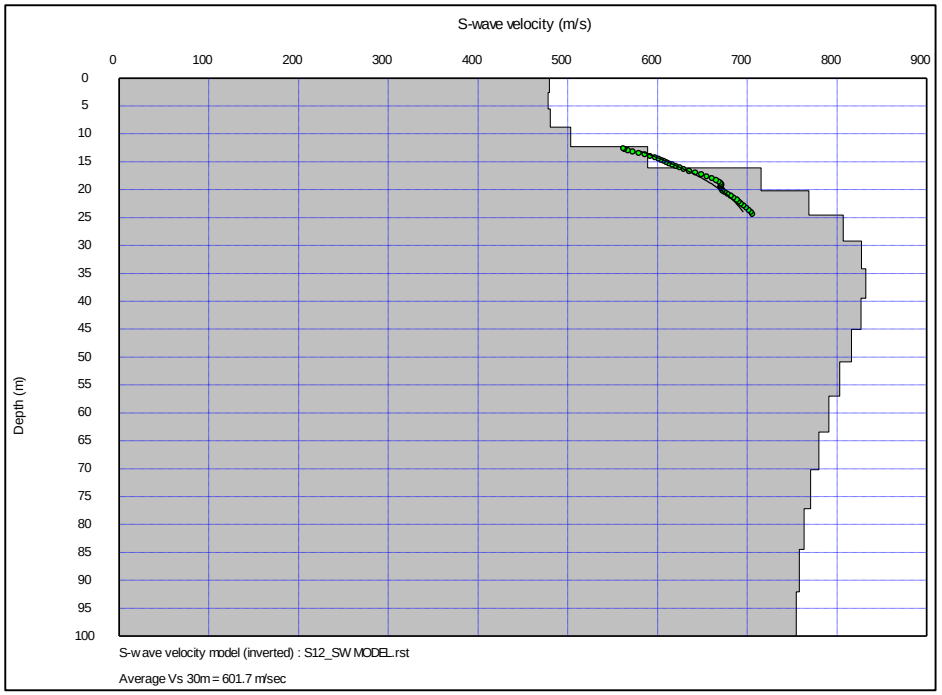

Depth(m)	S-wave velocity (m/s)	P-wave velocity (m/s)	Density (g/cc)	Poisson Ratio	Shear Modulus (Gpa)	Young Modulus (Mpa)
0.00	479.80	1829.77	1.93	0.46	0.44	1300.23
2.63	478.10	1827.90	1.93	0.46	0.44	1291.23
5.56	480.69	1830.04	1.93	0.46	0.45	1304.94
8.77	503.38	1852.79	1.93	0.46	0.49	1428.32
12.28	589.12	1944.24	1.94	0.45	0.67	1954.79
16.08	715.35	2081.04	1.97	0.43	1.01	2882.32
20.18	768.71	2138.31	1.97	0.43	1.16	3311.62
24.56	806.95	2180.29	1.97	0.42	1.28	3636.08
29.24	827.16	2203.46	1.97	0.42	1.34	3813.40
34.21	832.16	2210.23	1.97	0.42	1.36	3858.03
39.47	826.82	2205.56	1.97	0.42	1.34	3810.92
45.03	816.08	2194.69	1.97	0.42	1.31	3716.55
50.88	803.35	2181.29	1.97	0.42	1.27	3605.99
57.02	791.03	2168.01	1.97	0.42	1.23	3500.39
63.45	779.84	2155.86	1.97	0.42	1.20	3405.70
70.18	770.52	2145.60	1.97	0.43	1.17	3327.68
77.19	763.35	2137.57	1.97	0.43	1.15	3268.20
84.50	758.23	2131.84	1.97	0.43	1.13	3226.00
92.11	754.92	2128.14	1.97	0.43	1.12	3198.85
115.79	832.16	2210.23	1.97	0.42	1.36	3858.03

S13

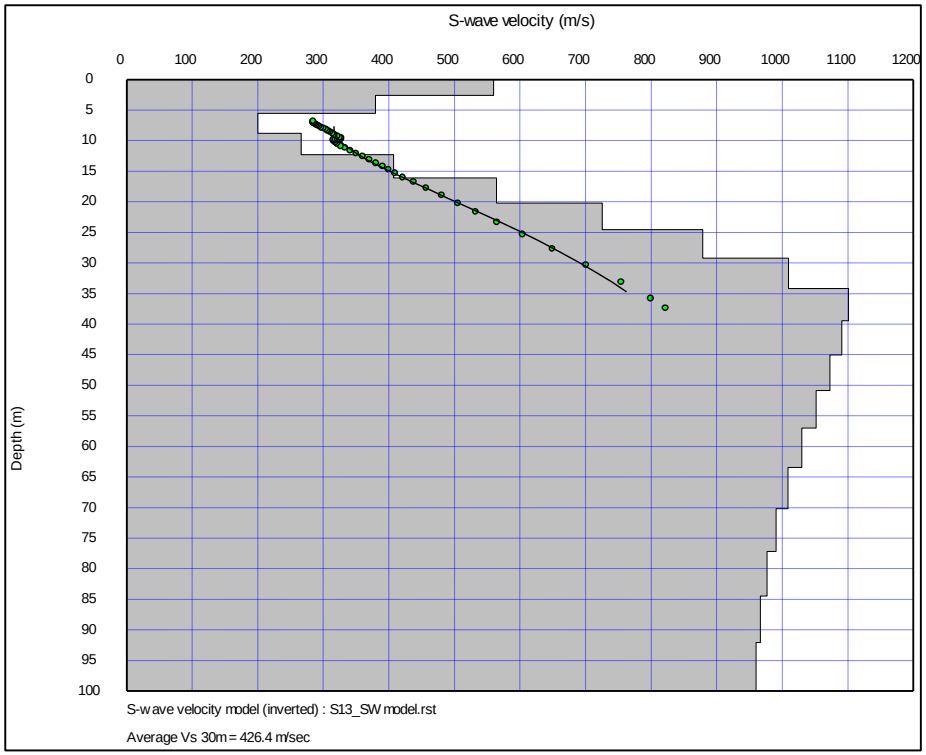

Depth(m)	S-wave velocity (m/s)	P-wave velocity (m/s)	Density (g/cc)	Poisson Ratio	Shear Modulus (Gpa)	Young Modulus (Mpa)
0.00	559.95	1900.65	1.83	0.45	0.57	1666.59
2.63	379.58	1712.67	1.83	0.47	0.26	777.26
5.56	200.20	1518.27	1.83	0.49	0.07	219.16
8.77	266.57	1583.19	1.84	0.49	0.13	389.44
12.28	407.20	1741.30	1.87	0.47	0.31	911.61
16.08	563.98	1917.27	1.89	0.45	0.60	1748.83
20.18	725.44	2096.14	1.92	0.43	1.01	2894.04
24.56	878.26	2264.86	1.95	0.41	1.51	4252.98
29.24	1009.44	2409.68	1.99	0.39	2.03	5644.34
34.21	1100.63	2510.35	2.02	0.38	2.44	6742.95
39.47	1090.83	2499.48	2.02	0.38	2.40	6629.85
45.03	1072.76	2479.51	2.02	0.38	2.32	6423.51
50.88	1051.53	2456.03	2.02	0.39	2.23	6184.86
57.02	1029.32	2431.64	2.02	0.39	2.14	5939.48
63.45	1008.41	2408.57	2.02	0.39	2.05	5712.38
70.18	990.75	2389.08	2.02	0.40	1.98	5523.71
77.19	976.79	2373.67	2.02	0.40	1.92	5376.52
84.50	966.60	2362.41	2.02	0.40	1.88	5270.15
92.11	960.04	2355.16	2.02	0.40	1.86	5202.17
115.79	1100.63	2510.39	2.02	0.38	2.44	6742.97

S14

Depth(m)	S-wave velocity (m/s)	P-wave velocity (m/s)	Density (g/cc)	Poisson Ratio	Shear Modulus (Gpa)	Young Modulus (Mpa)
0.00	284.44	1604.66	1.82	0.48	0.15	437.28
2.63	277.05	1597.16	1.82	0.48	0.14	415.05
5.56	257.86	1578.05	1.82	0.49	0.12	360.32
8.77	250.68	1570.94	1.83	0.49	0.11	341.19
12.28	321.41	1647.49	1.84	0.48	0.19	564.07
16.08	378.24	1707.31	1.85	0.47	0.26	780.28
20.18	421.00	1752.21	1.85	0.47	0.33	963.51
24.56	450.33	1783.53	1.85	0.47	0.38	1099.89
29.24	463.17	1797.59	1.85	0.46	0.40	1162.29
34.21	463.10	1797.93	1.85	0.46	0.40	1161.96
39.47	455.22	1789.86	1.85	0.47	0.38	1123.50
45.03	444.14	1778.29	1.85	0.47	0.36	1070.42
50.88	432.48	1766.07	1.85	0.47	0.35	1015.91
57.02	421.60	1754.61	1.85	0.47	0.33	966.26
63.45	412.11	1744.58	1.85	0.47	0.31	923.93
70.18	405.81	1738.00	1.85	0.47	0.30	896.35
77.19	400.90	1732.85	1.85	0.47	0.30	875.13
84.50	397.37	1729.15	1.85	0.47	0.29	860.00
92.11	395.09	1726.76	1.85	0.47	0.29	850.30
115.79	463.17	1797.93	1.85	0.46	0.40	1162.30

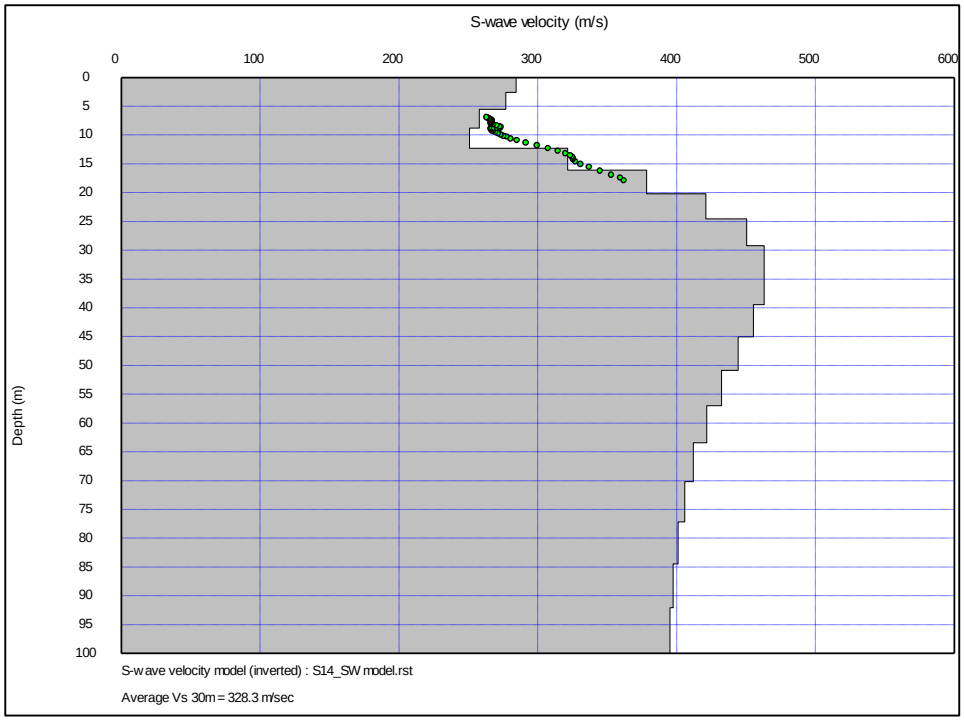
S-wave velocity (m/s)
0
100
200
300
400
500
600
Depth (m)
0
5
10
15
20
25
30
35
40
45
50
55
60
65
70
75
80
85
90
95
100
S-wave velocity model (inverted) : S14_SW model.rst
Average Vs 30m = 328.3 m/sec

S15

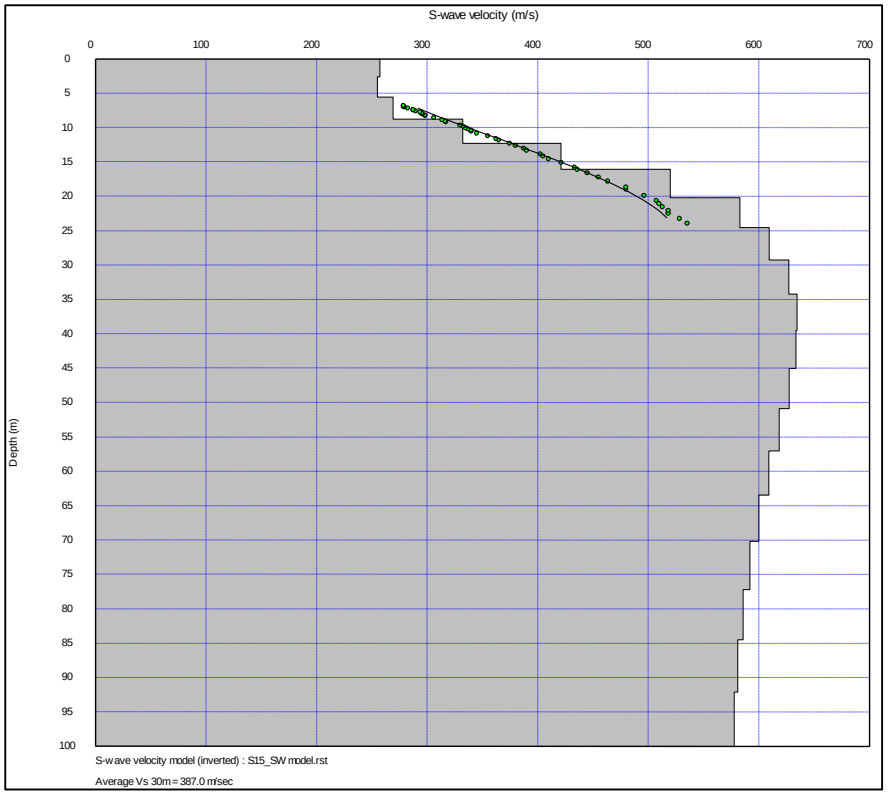

Depth(m)	S-wave velocity (m/s)	P-wave velocity (m/s)	Density (g/cc)	Poisson Ratio	Shear Modulus (Gpa)	Young Modulus (Mpa)
0.00	257.17	1578.61	1.83	0.49	0.12	359.27
2.63	254.92	1575.90	1.83	0.49	0.12	353.07
5.56	269.30	1590.76	1.83	0.49	0.13	394.58
8.77	332.22	1659.13	1.85	0.48	0.20	603.86
12.28	421.14	1756.71	1.87	0.47	0.33	976.26
16.08	519.73	1865.17	1.90	0.46	0.51	1493.72
20.18	582.94	1934.39	1.91	0.45	0.65	1879.70
24.56	609.46	1963.08	1.91	0.45	0.71	2049.83
29.24	626.95	1982.05	1.91	0.44	0.75	2165.79
34.21	634.37	1990.18	1.91	0.44	0.77	2215.91
39.47	633.60	1989.47	1.91	0.44	0.77	2210.71
45.03	627.44	1982.92	1.91	0.44	0.75	2169.10
50.88	618.48	1973.33	1.91	0.45	0.73	2109.29
57.02	608.87	1963.03	1.91	0.45	0.71	2046.02
63.45	599.84	1953.34	1.91	0.45	0.69	1987.40
70.18	591.96	1944.88	1.91	0.45	0.67	1936.86
77.19	585.60	1938.05	1.91	0.45	0.65	1896.52
84.50	580.81	1932.91	1.91	0.45	0.64	1866.44
92.11	577.65	1929.51	1.91	0.45	0.64	1846.65
115.79	634.37	1990.18	1.91	0.44	0.77	2215.91

S16

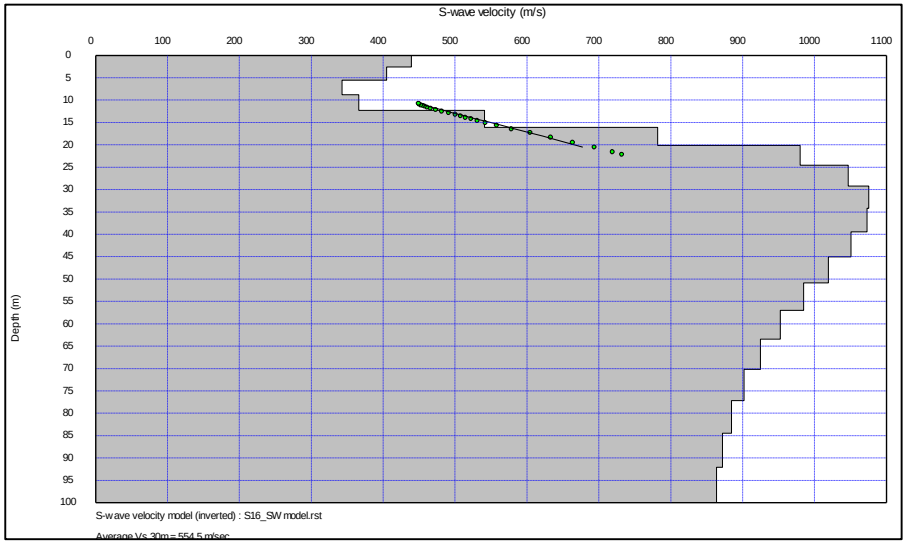

Depth(m)	S-wave velocity (m/s)	P-wave velocity (m/s)	Density (g/cc)	Poisson Ratio	Shear Modulus (Gpa)	Young Modulus (Mpa)
0.00	439.33	1767.14	1.89	0.47	0.36	1070.23
2.63	404.61	1732.68	1.89	0.47	0.31	910.31
5.56	342.83	1672.34	1.89	0.48	0.22	656.59
8.77	365.92	1699.98	1.89	0.48	0.25	748.31
12.28	540.74	1888.72	1.91	0.46	0.56	1629.69
16.08	781.74	2151.08	1.95	0.42	1.19	3395.09
20.18	980.04	2368.38	1.98	0.40	1.90	5315.35
24.56	1046.74	2441.44	1.98	0.39	2.17	6023.12
29.24	1075.12	2473.18	1.98	0.38	2.29	6336.32
34.21	1072.81	2471.48	1.98	0.38	2.28	6311.01
39.47	1050.54	2447.85	1.98	0.39	2.19	6065.66
45.03	1019.23	2414.29	1.98	0.39	2.06	5727.80
50.88	984.56	2376.83	1.98	0.40	1.92	5363.52
57.02	952.05	2341.55	1.98	0.40	1.80	5031.45
63.45	924.56	2311.75	1.98	0.40	1.69	4758.05
70.18	901.81	2287.12	1.98	0.41	1.61	4536.90
77.19	884.26	2268.13	1.98	0.41	1.55	4369.59
84.50	871.75	2254.59	1.98	0.41	1.51	4252.02
92.11	863.68	2245.85	1.98	0.41	1.48	4176.93
115.79	1075.12	2473.18	1.98	0.38	2.29	6336.32

S17

Depth(m)	S-wave velocity (m/s)	P-wave velocity (m/s)	Density (g/cc)	Poisson Ratio	Shear Modulus (Gpa)	Young Modulus (Mpa)
0.00	713.87	2080.23	1.95	0.43	0.99	2851.98
2.63	716.12	2082.19	1.95	0.43	1.00	2869.30
5.56	718.09	2083.86	1.95	0.43	1.01	2884.50
8.77	714.53	2079.94	1.95	0.43	1.00	2856.95
12.28	703.43	2068.53	1.95	0.43	0.97	2771.77
16.08	685.93	2050.62	1.95	0.44	0.92	2639.96
20.18	659.80	2023.32	1.95	0.44	0.85	2446.17
24.56	645.17	2008.26	1.95	0.44	0.81	2343.43
29.24	631.54	1993.66	1.95	0.44	0.78	2248.21
34.21	623.50	1984.75	1.95	0.45	0.76	2192.88
39.47	620.80	1981.33	1.95	0.45	0.75	2174.45
45.03	622.04	1981.98	1.95	0.45	0.76	2182.83
50.88	625.89	1985.64	1.95	0.44	0.76	2209.11
57.02	630.99	1990.78	1.95	0.44	0.78	2244.22
63.45	635.99	1996.08	1.95	0.44	0.79	2278.91
70.18	639.89	2000.38	1.95	0.44	0.80	2306.09
77.19	642.72	2003.62	1.95	0.44	0.81	2325.97
84.50	644.61	2006.01	1.95	0.44	0.81	2339.29
92.11	645.32	2007.16	1.95	0.44	0.81	2344.39
115.79	718.09	2083.86	1.95	0.43	1.01	2884.50

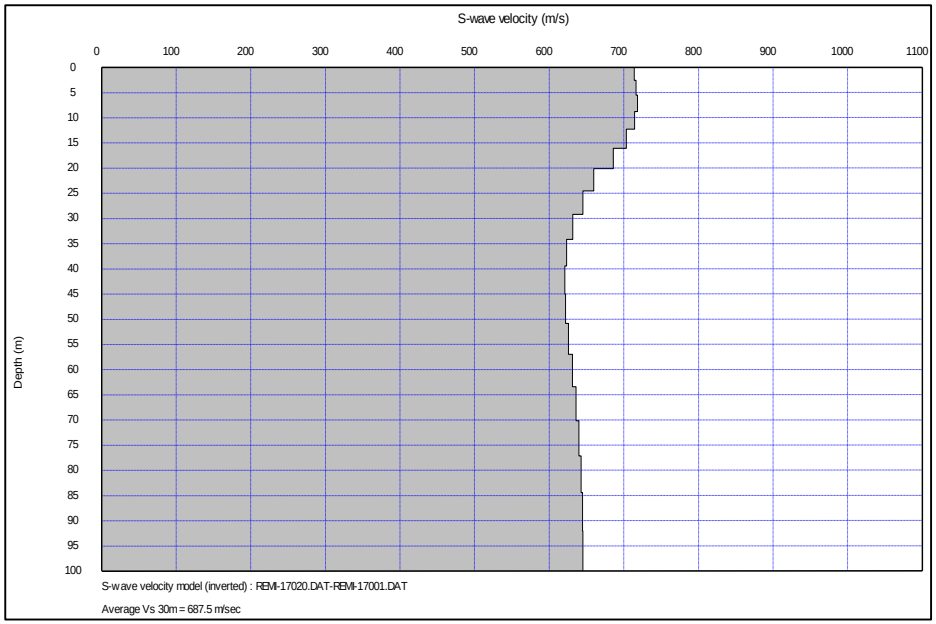
S-wave velocity (m/s)
0
100
200
300
400
500
600
700
800
900
1000
1100
Depth (m)
0
5
10
15
20
25
30
35
40
45
50
55
60
65
70
75
80
85
90
95
100
S-wave velocity model (inverted) : REMI-17020.DAT-REMI-17001.DAT
Average Vs 30m = 687.5 m/sec

S18

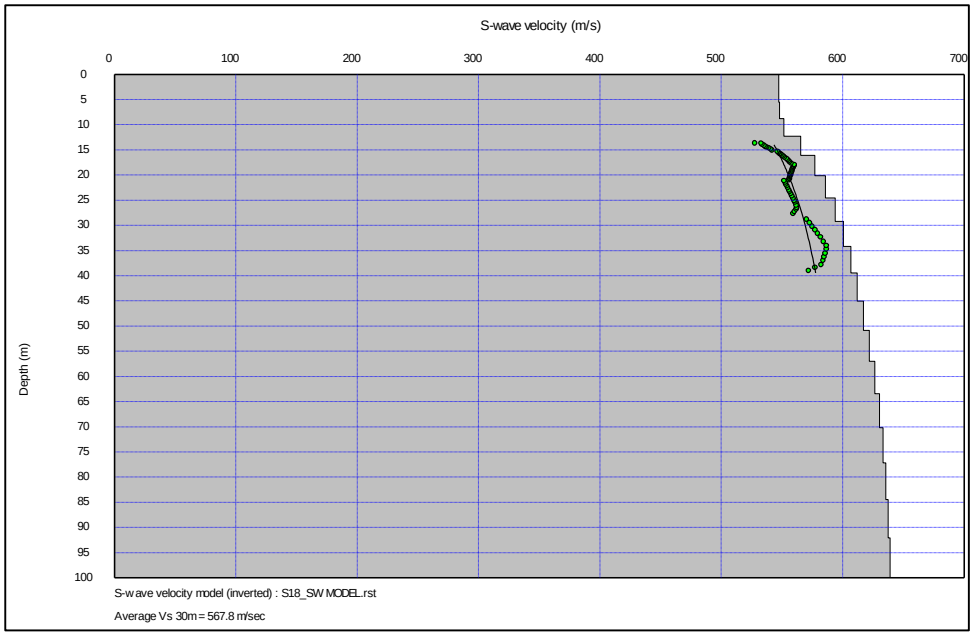

Depth(m)	S-wave velocity (m/s)	P-wave velocity (m/s)	Density (g/cc)	Poisson Ratio	Shear Modulus (Gpa)	Young Modulus (Mpa)
0.00	547.23	1898.98	1.92	0.45	0.58	1673.74
2.63	547.25	1899.02	1.92	0.45	0.58	1673.85
5.56	547.90	1899.72	1.92	0.45	0.58	1677.79
8.77	551.41	1903.25	1.92	0.45	0.58	1698.77
12.28	565.30	1918.12	1.92	0.45	0.61	1785.58
16.08	576.89	1930.45	1.92	0.45	0.64	1858.57
20.18	585.88	1940.02	1.92	0.45	0.66	1915.43
24.56	593.88	1948.70	1.92	0.45	0.68	1966.75
29.24	600.65	1956.14	1.92	0.45	0.69	2010.65
34.21	606.64	1962.70	1.92	0.45	0.71	2049.87
39.47	611.96	1968.52	1.92	0.45	0.72	2085.00
45.03	617.14	1973.98	1.92	0.45	0.73	2119.46
50.88	622.06	1978.97	1.92	0.45	0.74	2152.37
57.02	626.44	1983.35	1.92	0.44	0.76	2181.91
63.45	630.18	1987.00	1.92	0.44	0.76	2207.28
70.18	633.32	1990.01	1.92	0.44	0.77	2228.63
77.19	635.56	1992.20	1.92	0.44	0.78	2243.97
84.50	637.44	1994.07	1.92	0.44	0.78	2256.89
92.11	639.12	1995.88	1.92	0.44	0.79	2268.47
115.79	639.12	1995.88	1.92	0.44	0.79	2268.47

S19

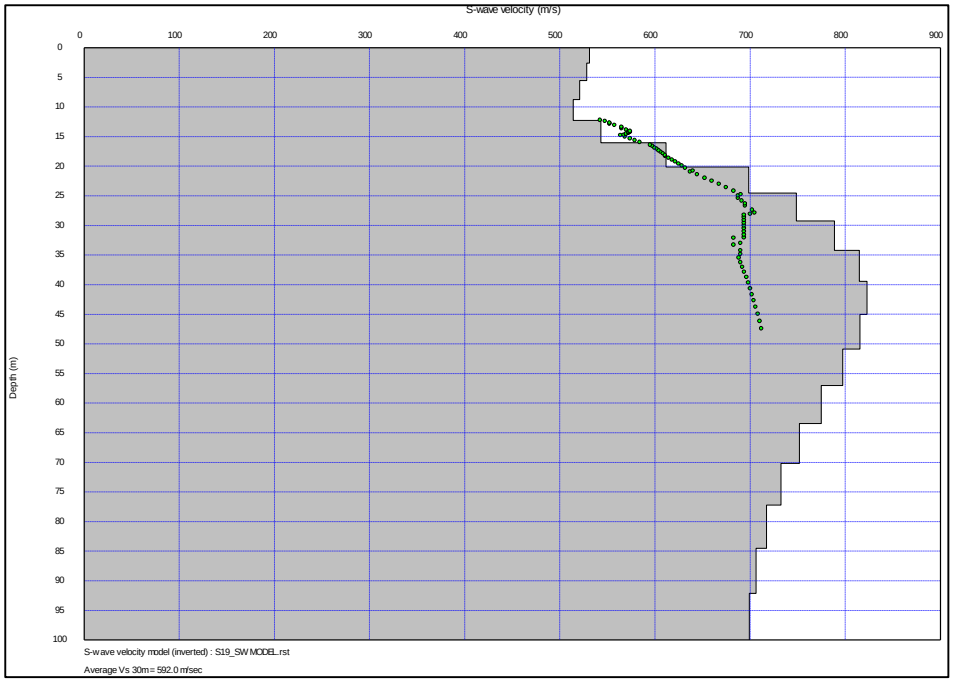

Depth(m)	S-wave velocity (m/s)	P-wave velocity (m/s)	Density (g/cc)	Poisson Ratio	Shear Modulus (Gpa)	Young Modulus (Mpa)
0.00	531.19	1879.66	1.92	0.46	0.54	1581.87
2.63	528.26	1876.68	1.92	0.46	0.54	1564.84
5.56	520.79	1869.13	1.92	0.46	0.52	1521.90
8.77	514.12	1862.66	1.92	0.46	0.51	1483.99
12.28	542.98	1896.15	1.93	0.46	0.57	1658.78
16.08	611.61	1972.00	1.95	0.45	0.73	2108.93
20.18	698.36	2066.03	1.96	0.44	0.96	2750.03
24.56	748.60	2118.76	1.97	0.43	1.10	3147.19
29.24	788.69	2160.52	1.97	0.42	1.22	3479.74
34.21	814.70	2187.77	1.97	0.42	1.30	3703.55
39.47	822.74	2196.62	1.97	0.42	1.33	3774.12
45.03	815.31	2189.45	1.97	0.42	1.31	3709.17
50.88	797.28	2171.25	1.97	0.42	1.25	3553.33
57.02	774.61	2148.06	1.97	0.43	1.18	3361.67
63.45	751.94	2124.66	1.97	0.43	1.11	3174.70
70.18	732.28	2104.29	1.97	0.43	1.05	3016.58
77.19	717.20	2088.39	1.97	0.43	1.01	2897.78
84.50	706.13	2076.49	1.97	0.43	0.98	2811.84
92.11	699.07	2068.74	1.97	0.44	0.96	2757.67
115.79	822.74	2196.62	1.97	0.42	1.33	3774.12

S20

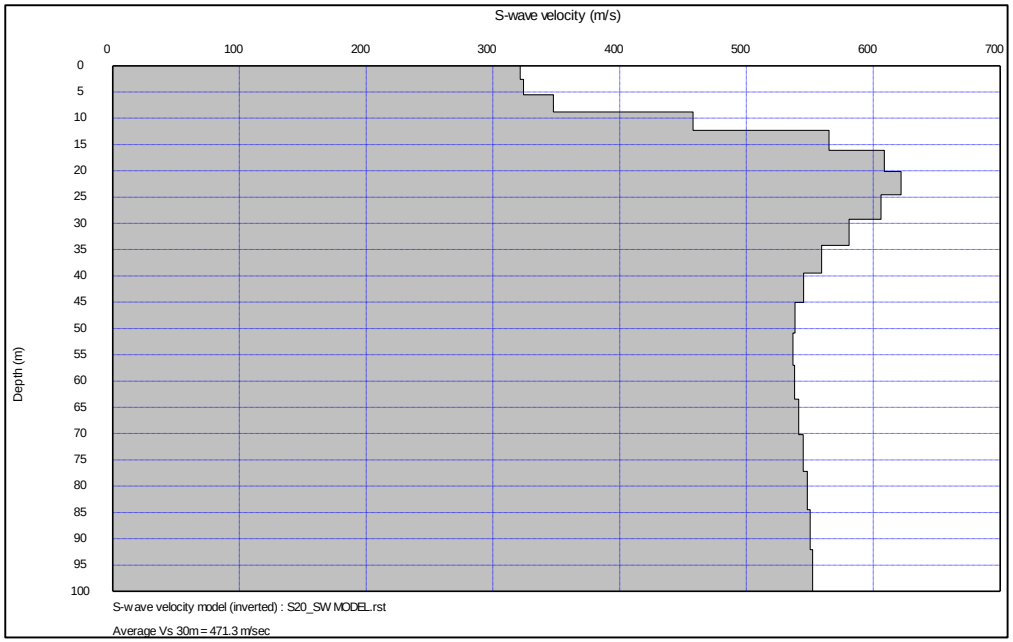

Depth(m)	S-wave velocity (m/s)	P-wave velocity (m/s)	Density (g/cc)	Poisson Ratio	Shear Modulus (Gpa)	Young Modulus (Mpa)
0.00	324.73	1656.93	1.87	0.48	0.20	583.37
2.63	324.23	1656.00	1.87	0.48	0.20	581.58
5.56	346.12	1677.76	1.87	0.48	0.22	661.76
8.77	458.82	1798.33	1.89	0.47	0.40	1165.18
12.28	565.21	1913.20	1.91	0.45	0.61	1767.65
16.08	602.68	1954.00	1.91	0.45	0.69	2003.26
20.18	611.71	1965.03	1.91	0.45	0.71	2062.16
24.56	599.86	1953.59	1.91	0.45	0.69	1985.23
29.24	578.83	1931.83	1.91	0.45	0.64	1851.95
34.21	557.74	1909.52	1.91	0.45	0.59	1722.65
39.47	540.98	1891.51	1.91	0.46	0.56	1623.03
45.03	529.68	1879.12	1.91	0.46	0.53	1557.41
50.88	522.99	1871.62	1.91	0.46	0.52	1519.17
57.02	519.46	1867.54	1.91	0.46	0.51	1499.12
63.45	518.10	1865.89	1.91	0.46	0.51	1491.48
70.18	517.89	1865.51	1.91	0.46	0.51	1490.26
77.19	518.33	1865.83	1.91	0.46	0.51	1492.74
84.50	519.00	1866.45	1.91	0.46	0.51	1496.53
92.11	519.59	1866.98	1.91	0.46	0.51	1499.85
115.79	611.71	1965.03	1.91	0.45	0.71	2062.16

S21

Depth(m)	S-wave velocity (m/s)	P-wave velocity (m/s)	Density (g/cc)	Poisson Ratio	Shear Modulus (Gpa)	Young Modulus (Mpa)
0.00	527.97	1884.54	1.93	0.46	0.54	1567.92
2.63	527.33	1883.68	1.93	0.46	0.54	1564.15
5.56	533.11	1889.07	1.93	0.46	0.55	1597.82
8.77	554.64	1910.14	1.93	0.45	0.59	1726.19
12.28	590.35	1945.89	1.93	0.45	0.67	1949.37
16.08	629.73	1985.78	1.93	0.44	0.77	2210.18
20.18	660.03	2016.95	1.93	0.44	0.84	2421.12
24.56	673.74	2031.54	1.93	0.44	0.88	2519.53
29.24	670.76	2029.28	1.93	0.44	0.87	2498.12
34.21	655.96	2014.77	1.93	0.44	0.83	2392.48
39.47	635.13	1993.87	1.93	0.44	0.78	2247.35
45.03	614.06	1972.16	1.93	0.45	0.73	2104.77
50.88	595.93	1952.95	1.93	0.45	0.69	1985.49
57.02	582.23	1937.93	1.93	0.45	0.65	1897.52
63.45	573.03	1927.37	1.93	0.45	0.63	1839.49
70.18	566.34	1919.53	1.93	0.45	0.62	1797.76
77.19	560.93	1913.00	1.93	0.45	0.61	1764.37
84.50	556.35	1907.73	1.93	0.45	0.60	1736.32
92.11	552.10	1903.11	1.93	0.45	0.59	1710.56
115.79	673.74	2031.54	1.93	0.44	0.88	2519.53

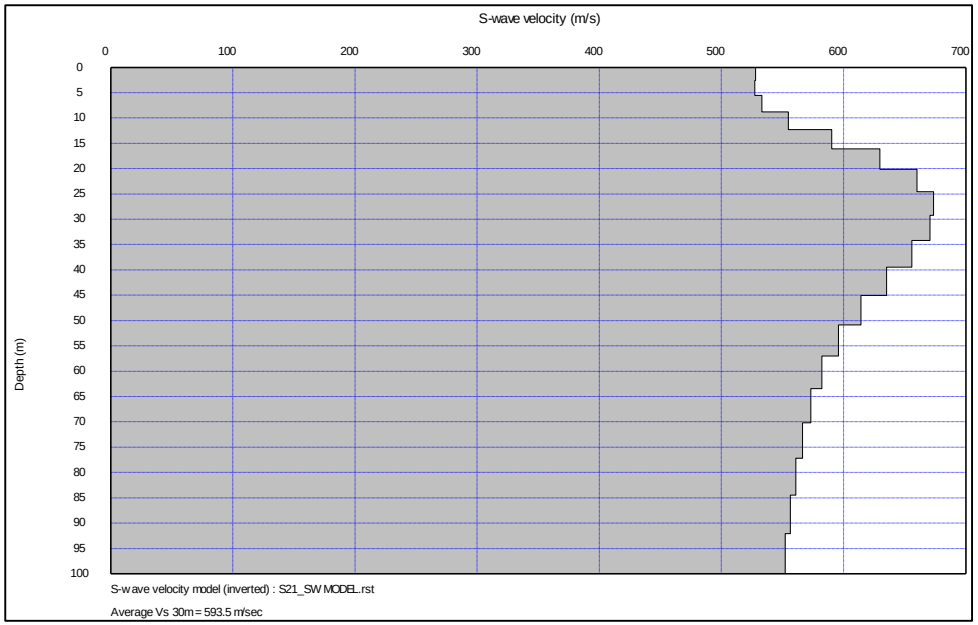
S-wave velocity (m/s)
0
100
200
300
400
500
600
700
Depth (m)
0
5
10
15
20
25
30
35
40
45
50
55
60
65
70
75
80
85
90
95
100
S-wave velocity model (inverted) : S21_SW MODEL.rst
Average Vs 30m = 593.5 m/sec

S22

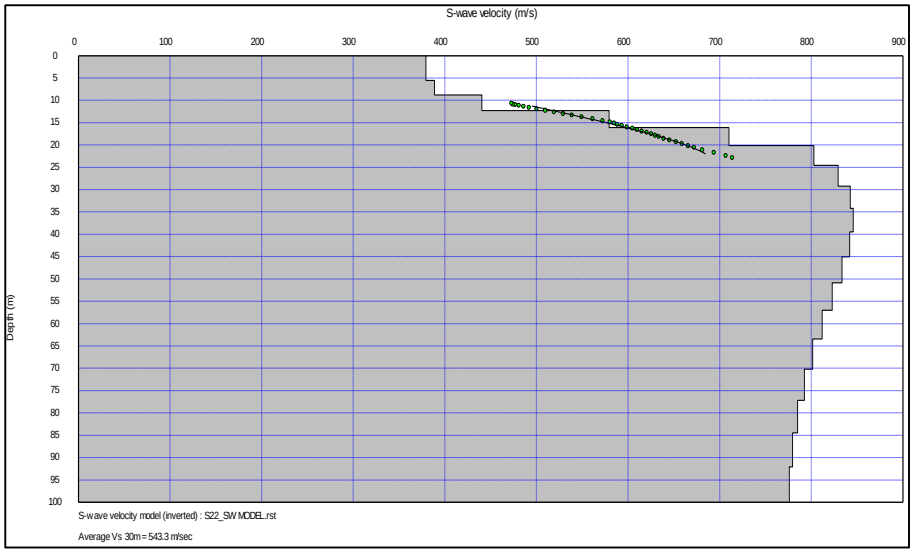

Depth(m)	S-wave velocity (m/s)	P-wave velocity (m/s)	Density (g/cc)	Poisson Ratio	Shear Modulus (Gpa)	Young Modulus (Mpa)
0.00	379.42	1717.34	1.90	0.47	0.27	805.76
2.63	379.50	1717.14	1.90	0.47	0.27	806.09
5.56	388.83	1726.14	1.90	0.47	0.29	845.61
8.77	440.45	1779.95	1.90	0.47	0.37	1083.22
12.28	579.16	1930.72	1.93	0.45	0.65	1877.73
16.08	709.98	2074.75	1.95	0.43	0.99	2825.38
20.18	802.83	2177.87	1.97	0.42	1.27	3612.61
24.56	829.20	2207.58	1.97	0.42	1.36	3844.33
29.24	842.57	2222.69	1.97	0.42	1.40	3964.31
34.21	845.81	2226.30	1.97	0.42	1.41	3993.62
39.47	841.78	2221.71	1.97	0.42	1.40	3957.12
45.03	833.53	2212.43	1.97	0.42	1.37	3882.95
50.88	822.96	2200.90	1.97	0.42	1.34	3788.99
57.02	811.87	2188.91	1.97	0.42	1.30	3691.47
63.45	801.54	2177.77	1.97	0.42	1.27	3601.76
70.18	792.37	2167.83	1.97	0.42	1.24	3522.84
77.19	785.00	2159.83	1.97	0.42	1.21	3460.06
84.50	779.61	2153.88	1.97	0.42	1.20	3414.40
92.11	776.15	2150.06	1.97	0.43	1.19	3385.32
115.79	845.81	2226.30	1.97	0.42	1.41	3993.62

S23

Depth(m)	S-wave velocity (m/s)	P-wave velocity (m/s)	Density (g/cc)	Poisson Ratio	Shear Modulus (Gpa)	Young Modulus (Mpa)
0.00	337.84	1659.15	1.83	0.48	0.21	618.13
2.63	295.83	1616.95	1.83	0.48	0.16	475.33
5.56	248.29	1569.06	1.84	0.49	0.11	336.79
8.77	320.62	1646.13	1.85	0.48	0.19	564.22
12.28	505.85	1846.59	1.88	0.46	0.48	1406.42
16.08	718.34	2079.56	1.92	0.43	0.99	2838.84
20.18	792.15	2160.39	1.92	0.42	1.21	3428.28
24.56	828.83	2201.14	1.92	0.42	1.32	3740.11
29.24	833.58	2207.14	1.92	0.42	1.33	3781.54
34.21	817.38	2190.05	1.92	0.42	1.28	3641.80
39.47	790.65	2161.39	1.92	0.42	1.20	3416.35
45.03	760.95	2129.38	1.92	0.43	1.11	3173.49
50.88	732.63	2098.83	1.92	0.43	1.03	2949.57
57.02	708.08	2072.29	1.92	0.43	0.96	2761.56
63.45	687.85	2050.39	1.92	0.44	0.91	2610.85
70.18	671.95	2033.19	1.92	0.44	0.87	2495.19
77.19	659.94	2020.19	1.92	0.44	0.84	2409.47
84.50	651.34	2010.88	1.92	0.44	0.81	2348.86
92.11	645.78	2004.86	1.92	0.44	0.80	2310.14
115.79	833.58	2207.14	1.92	0.42	1.33	3781.54

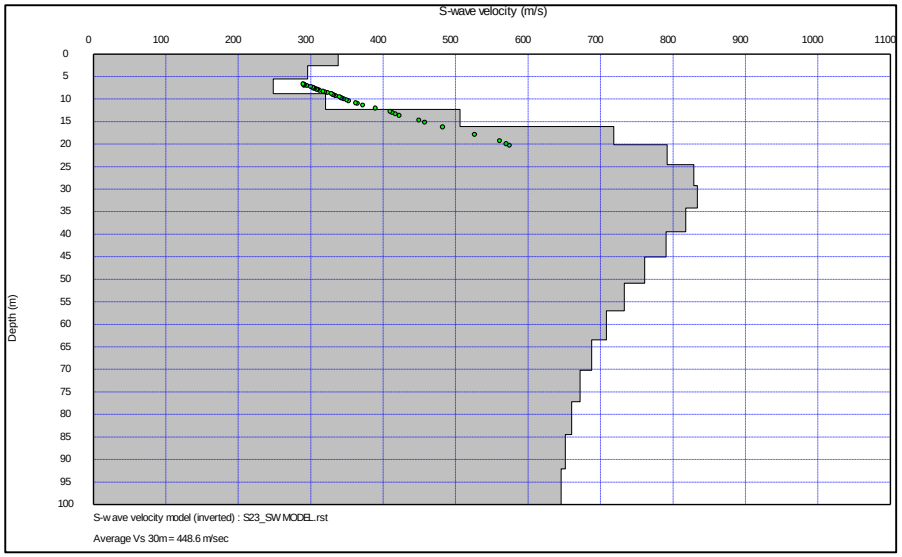
S-wave velocity (m/s)
0
100
200
300
400
500
600
700
800
900
1000
1100
Depth (m)
0
5
10
15
20
25
30
35
40
45
50
55
60
65
70
75
80
85
90
95
100
S-wave velocity model (inverted) : S23_SW MODEL.rst
Average Vs 30m = 448.6 m/sec

S24

Depth(m)	S-wave velocity (m/s)	P-wave velocity (m/s)	Density (g/cc)	Poisson Ratio	Shear Modulus (Gpa)	Young Modulus (Mpa)
0.00	506.51	1845.55	1.83	0.46	0.47	1368.36
2.63	336.39	1665.17	1.83	0.48	0.21	611.58
5.56	187.96	1500.96	1.83	0.49	0.06	193.08
8.77	313.25	1636.34	1.85	0.48	0.18	537.79
12.28	527.42	1873.45	1.88	0.46	0.52	1522.30
16.08	743.17	2112.04	1.91	0.43	1.06	3022.59
20.18	912.99	2299.39	1.95	0.41	1.63	4571.12
24.56	1030.06	2428.62	1.98	0.39	2.10	5840.17
29.24	1029.49	2427.75	1.98	0.39	2.10	5833.94
34.21	1011.95	2408.41	1.98	0.39	2.03	5646.65
39.47	984.94	2378.84	1.98	0.40	1.92	5363.72
45.03	955.45	2346.64	1.98	0.40	1.81	5062.10
50.88	926.46	2315.12	1.98	0.40	1.70	4773.25
57.02	900.80	2287.16	1.98	0.41	1.61	4523.88
63.45	879.25	2263.66	1.98	0.41	1.53	4319.10
70.18	862.31	2245.18	1.98	0.41	1.47	4161.08
77.19	849.26	2230.94	1.98	0.42	1.43	4041.15
84.50	839.78	2220.60	1.98	0.42	1.40	3955.06
92.11	833.67	2213.92	1.98	0.42	1.38	3899.97
115.79	1030.06	2428.62	1.98	0.39	2.10	5840.17

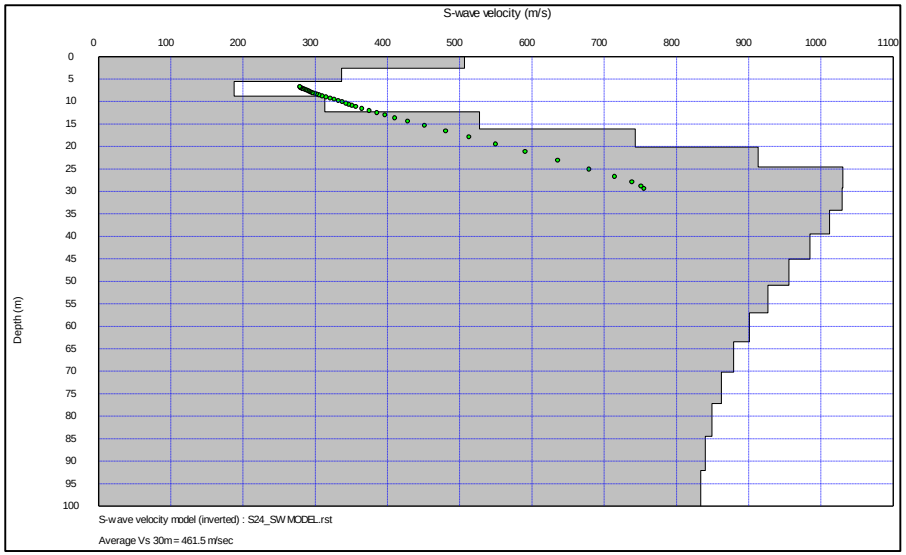
S-wave velocity (m/s)
0
100
200
300
400
500
600
700
800
900
1000
1100
Depth (m)
0
5
10
15
20
25
30
35
40
45
50
55
60
65
70
75
80
85
90
95
100
S-wave velocity model (inverted) : S24_SW MODEL.rst
Average Vs 30m = 461.5 m/sec

S25

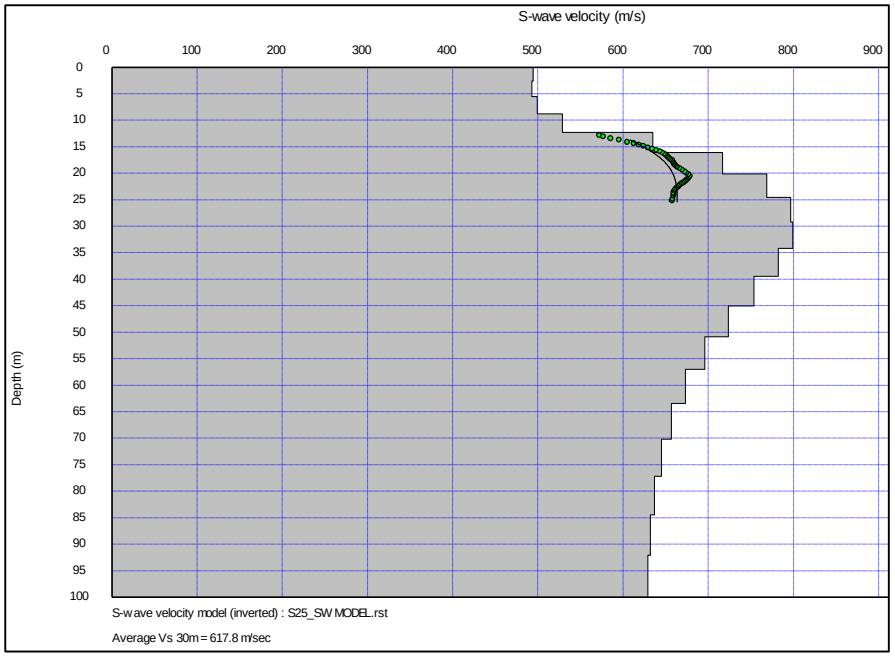

Depth(m)	S-wave velocity (m/s)	P-wave velocity (m/s)	Density (g/cc)	Poisson Ratio	Shear Modulus (Gpa)	Young Modulus (Mpa)
0.00	494.28	1849.86	1.93	0.46	0.47	1379.48
2.63	493.06	1848.51	1.93	0.46	0.47	1372.82
5.56	499.15	1854.50	1.93	0.46	0.48	1406.23
8.77	528.73	1883.87	1.93	0.46	0.54	1573.84
12.28	635.12	1996.16	1.95	0.44	0.79	2269.77
16.08	716.97	2081.01	1.96	0.43	1.01	2879.77
20.18	768.84	2134.29	1.96	0.43	1.16	3294.83
24.56	796.77	2163.84	1.96	0.42	1.24	3529.00
29.24	799.34	2167.75	1.96	0.42	1.25	3551.16
34.21	782.11	2151.33	1.96	0.42	1.20	3405.74
39.47	753.80	2123.33	1.96	0.43	1.11	3172.62
45.03	723.42	2092.98	1.96	0.43	1.02	2930.80
50.88	695.84	2065.28	1.96	0.44	0.95	2718.79
57.02	673.32	2042.45	1.96	0.44	0.89	2551.12
63.45	656.53	2025.34	1.96	0.44	0.84	2429.23
70.18	644.98	2013.50	1.96	0.44	0.81	2347.04
77.19	637.11	2005.50	1.96	0.44	0.79	2291.77
84.50	632.14	2000.53	1.96	0.44	0.78	2257.22
92.11	628.97	1997.41	1.96	0.44	0.77	2235.25
115.79	799.34	2167.75	1.96	0.42	1.25	3551.16

S26

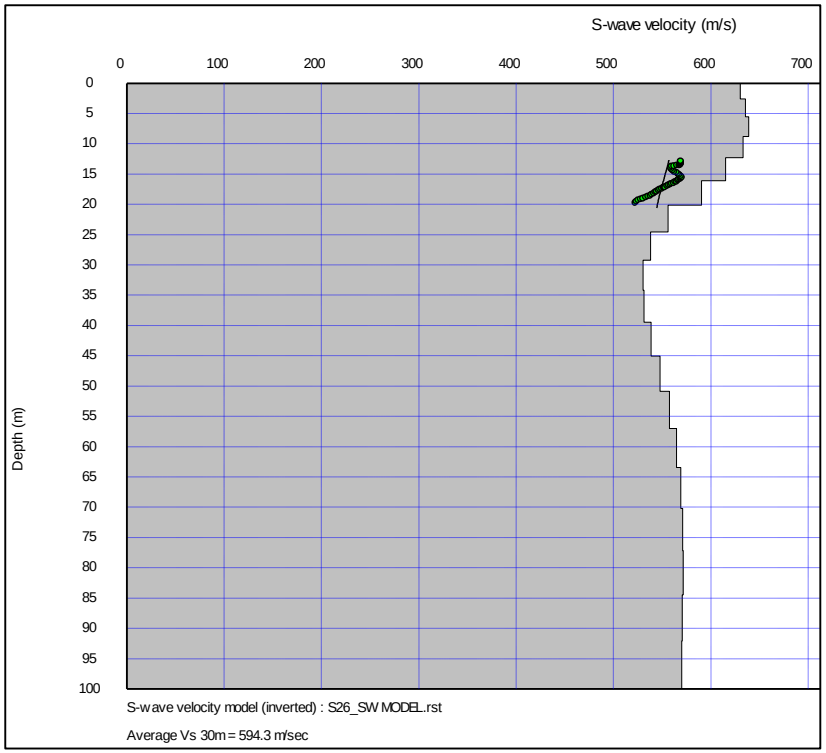

Depth(m)	S-wave velocity (m/s)	P-wave velocity (m/s)	Density (g/cc)	Poisson Ratio	Shear Modulus (Gpa)	Young Modulus (Mpa)
0.00	644.45	2004.36	1.92	0.44	0.80	2299.63
2.63	657.31	2017.74	1.92	0.44	0.83	2389.50
5.56	668.38	2029.19	1.92	0.44	0.86	2468.16
8.77	660.25	2020.36	1.92	0.44	0.84	2410.23
12.28	629.28	1987.40	1.92	0.44	0.76	2195.61
16.08	586.02	1941.35	1.92	0.45	0.66	1911.45
20.18	536.81	1888.35	1.92	0.46	0.55	1608.13
24.56	513.19	1862.66	1.92	0.46	0.50	1472.66
29.24	510.09	1858.46	1.92	0.46	0.50	1455.24
34.21	523.21	1871.53	1.92	0.46	0.52	1529.36
39.47	544.01	1892.93	1.92	0.45	0.57	1650.38
45.03	564.09	1914.02	1.92	0.45	0.61	1771.35
50.88	578.68	1929.73	1.92	0.45	0.64	1861.78
57.02	585.88	1937.76	1.92	0.45	0.66	1907.22
63.45	587.06	1939.46	1.92	0.45	0.66	1914.77
70.18	584.47	1937.05	1.92	0.45	0.65	1898.39
77.19	580.44	1932.96	1.92	0.45	0.65	1872.92
84.50	576.32	1928.58	1.92	0.45	0.64	1847.12
92.11	572.95	1925.01	1.92	0.45	0.63	1826.15
115.79	668.38	2029.19	1.92	0.44	0.86	2468.16

S27

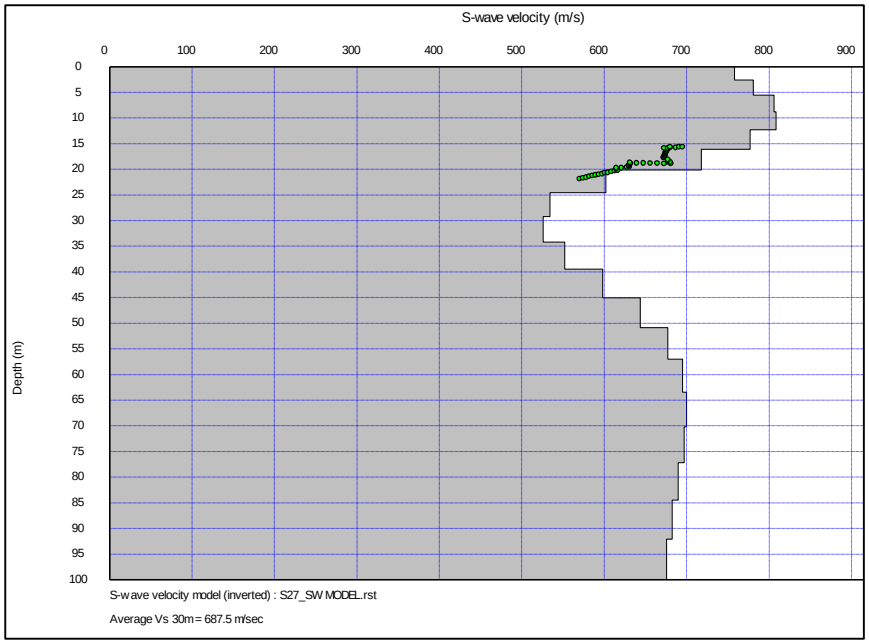

Depth(m)	S-wave velocity (m/s)	P-wave velocity (m/s)	Density (g/cc)	Poisson Ratio	Shear Modulus (Gpa)	Young Modulus (Mpa)
0.00	784.71	2159.51	1.98	0.42	1.22	3468.89
2.63	808.18	2182.25	1.98	0.42	1.29	3670.64
5.56	832.65	2206.11	1.98	0.42	1.37	3886.44
8.77	832.09	2205.11	1.98	0.42	1.37	3881.33
12.28	785.60	2157.21	1.97	0.42	1.22	3468.72
16.08	700.90	2069.61	1.97	0.44	0.97	2771.37
20.18	573.81	1934.06	1.94	0.45	0.64	1857.05
24.56	516.35	1871.71	1.93	0.46	0.52	1504.70
29.24	519.32	1875.13	1.93	0.46	0.52	1521.69
34.21	558.91	1912.56	1.93	0.45	0.60	1756.34
39.47	614.82	1965.73	1.93	0.45	0.73	2114.25
45.03	665.80	2015.01	1.93	0.44	0.86	2467.30
50.88	700.46	2049.64	1.93	0.43	0.95	2721.73
57.02	717.57	2067.92	1.93	0.43	1.00	2851.67
63.45	721.21	2072.93	1.93	0.43	1.01	2879.84
70.18	717.03	2069.64	1.93	0.43	0.99	2847.84
77.19	709.40	2062.58	1.93	0.43	0.97	2789.74
84.50	701.49	2055.17	1.93	0.43	0.95	2730.06
92.11	695.67	2049.73	1.93	0.43	0.94	2686.56
115.79	836.05	2206.11	1.98	0.42	1.38	3916.12

S28

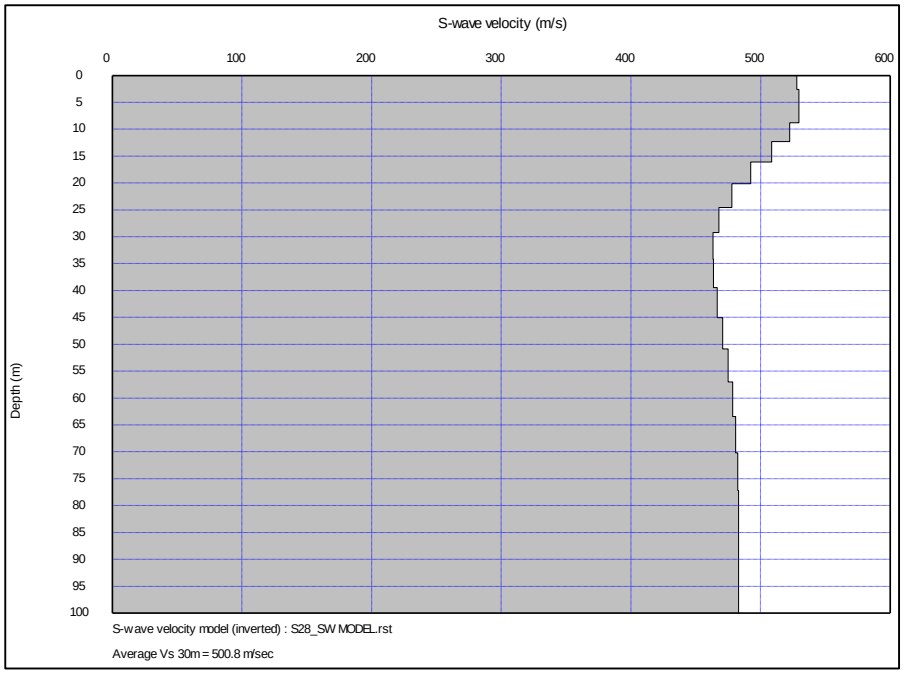

Depth(m)	S-wave velocity (m/s)	P-wave velocity (m/s)	Density (g/cc)	Poisson Ratio	Shear Modulus (Gpa)	Young Modulus (Mpa)
0.00	527.79	1873.38	1.89	0.46	0.53	1534.44
2.63	529.62	1875.07	1.89	0.46	0.53	1544.84
5.56	529.45	1874.77	1.89	0.46	0.53	1543.87
8.77	522.42	1867.64	1.89	0.46	0.52	1504.05
12.28	508.71	1853.76	1.89	0.46	0.49	1427.86
16.08	492.30	1836.95	1.89	0.46	0.46	1339.06
20.18	477.72	1821.74	1.89	0.46	0.43	1262.45
24.56	467.81	1810.98	1.89	0.46	0.41	1211.59
29.24	463.40	1805.70	1.89	0.46	0.41	1189.24
34.21	463.60	1805.16	1.89	0.46	0.41	1190.23
39.47	466.68	1807.62	1.89	0.46	0.41	1205.76
45.03	470.80	1811.34	1.89	0.46	0.42	1226.73
50.88	474.96	1815.38	1.89	0.46	0.43	1248.05
57.02	478.41	1818.95	1.89	0.46	0.43	1265.88
63.45	480.81	1821.58	1.89	0.46	0.44	1278.37
70.18	482.27	1823.30	1.89	0.46	0.44	1285.98
77.19	482.88	1824.13	1.89	0.46	0.44	1289.22
84.50	483.08	1824.52	1.89	0.46	0.44	1290.25
92.11	482.97	1824.55	1.89	0.46	0.44	1289.71
115.79	529.62	1875.07	1.89	0.46	0.53	1544.84

S29

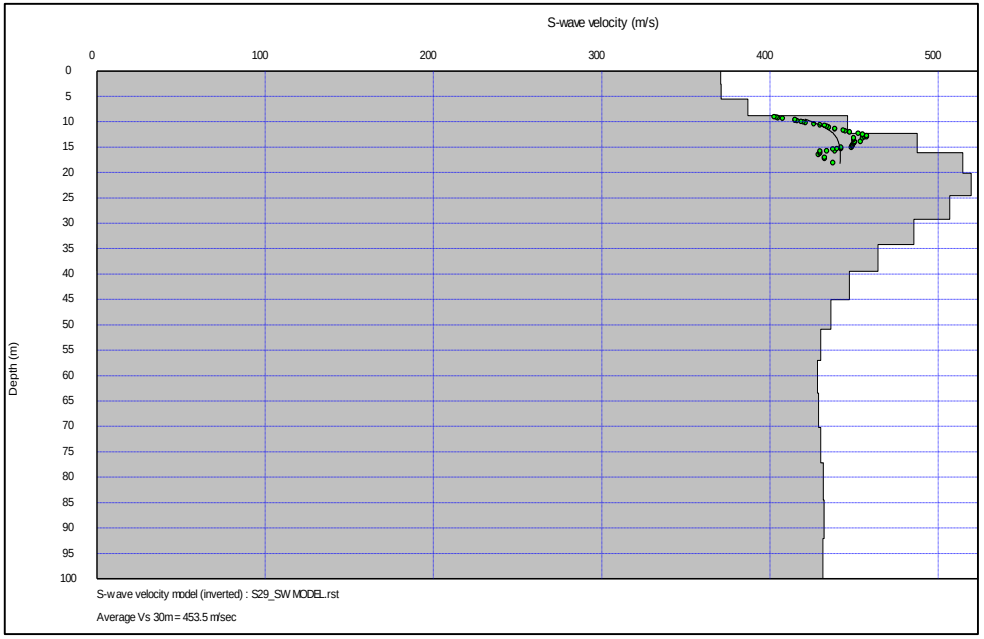

Depth (m)	S-wave velocity (m/s)	P-wave velocity (m/s)	Density (g/cc)	Poisson Ratio	Shear Modulus (Gpa)	Young Modulus (Mpa)
0.00	370.71	1707.31	1.87	0.48	0.26	759.69
2.63	371.01	1707.87	1.87	0.48	0.26	760.89
5.56	386.90	1723.98	1.87	0.47	0.28	826.50
8.77	446.05	1785.87	1.88	0.47	0.37	1097.92
12.28	487.36	1827.81	1.88	0.46	0.45	1306.26
16.08	514.44	1855.83	1.88	0.46	0.50	1452.11
20.18	519.48	1861.74	1.88	0.46	0.51	1480.10
24.56	506.69	1849.39	1.88	0.46	0.48	1409.66
29.24	485.54	1828.16	1.88	0.46	0.44	1296.79
34.21	464.14	1806.12	1.88	0.46	0.41	1187.10
39.47	447.18	1788.16	1.88	0.47	0.38	1103.42
45.03	436.17	1775.95	1.88	0.47	0.36	1050.67
50.88	430.23	1768.78	1.88	0.47	0.35	1022.69
57.02	428.28	1765.64	1.88	0.47	0.35	1013.56
63.45	428.73	1765.14	1.88	0.47	0.35	1015.64
70.18	430.23	1766.02	1.88	0.47	0.35	1022.63
77.19	431.63	1767.19	1.88	0.47	0.35	1029.18
84.50	432.07	1767.75	1.88	0.47	0.35	1031.24
92.11	431.52	1767.52	1.88	0.47	0.35	1028.66
115.79	519.48	1861.74	1.88	0.46	0.51	1480.10

S30

Depth (m)	S-wave velocity (m/s)	P-wave velocity (m/s)	Density (g/cc)	Poisson Ratio	Shear Modulus (Gpa)	Young Modulus (Mpa)
0.00	383.97	1726.35	1.88	0.47	0.28	818.70
2.63	384.53	1727.02	1.88	0.47	0.28	821.06
5.56	400.68	1743.01	1.88	0.47	0.30	890.36
8.77	476.10	1821.20	1.89	0.46	0.43	1256.90
12.28	539.75	1885.05	1.90	0.46	0.55	1609.71
16.08	579.61	1924.44	1.90	0.45	0.64	1849.61
20.18	594.71	1939.70	1.90	0.45	0.67	1944.54
24.56	587.12	1932.69	1.90	0.45	0.65	1896.54
29.24	566.25	1912.61	1.90	0.45	0.61	1767.54
34.21	541.65	1888.89	1.90	0.46	0.56	1620.91
39.47	519.50	1867.76	1.90	0.46	0.51	1494.02
45.03	502.08	1851.36	1.90	0.46	0.48	1397.64
50.88	489.85	1840.19	1.90	0.46	0.46	1331.80
57.02	481.80	1833.17	1.90	0.46	0.44	1289.26
63.45	477.02	1829.26	1.90	0.46	0.43	1264.35
70.18	474.69	1827.66	1.90	0.46	0.43	1252.29
77.19	473.95	1827.51	1.90	0.46	0.43	1248.49
84.50	473.86	1827.86	1.90	0.46	0.43	1248.07
92.11	473.99	1828.31	1.90	0.46	0.43	1248.71
115.79	594.71	1939.70	1.90	0.45	0.67	1944.54

S31

Depth (m)	S-wave velocity (m/s)	P-wave velocity (m/s)	Density (g/cc)	Poisson Ratio	Shear Modulus (Gpa)	Young Modulus (Mpa)
0.00	526.61	1865.68	1.91	0.46	0.53	1542.63
2.63	566.18	1907.42	1.91	0.45	0.61	1777.05
5.56	613.68	1957.53	1.91	0.45	0.72	2078.85
8.77	633.45	1979.05	1.91	0.44	0.77	2211.00
12.28	611.77	1958.23	1.91	0.45	0.71	2066.49
16.08	547.18	1893.25	1.91	0.45	0.57	1659.62
20.18	466.86	1812.57	1.90	0.46	0.41	1212.32
24.56	410.84	1757.72	1.89	0.47	0.32	940.71
29.24	392.43	1740.53	1.89	0.47	0.29	857.10
34.21	428.84	1779.23	1.89	0.47	0.35	1020.06
39.47	486.50	1838.86	1.89	0.46	0.45	1306.75
45.03	529.89	1882.49	1.89	0.46	0.53	1544.50
50.88	546.12	1896.69	1.89	0.45	0.56	1638.11
57.02	541.13	1887.82	1.89	0.46	0.55	1608.80
63.45	527.02	1868.81	1.89	0.46	0.52	1527.62
70.18	512.01	1848.67	1.89	0.46	0.49	1443.52
77.19	499.54	1831.64	1.89	0.46	0.47	1375.31
84.50	489.19	1817.55	1.89	0.46	0.45	1319.97
92.11	479.91	1805.33	1.89	0.46	0.43	1271.22
115.79	635.69	1979.05	1.91	0.44	0.77	2225.96

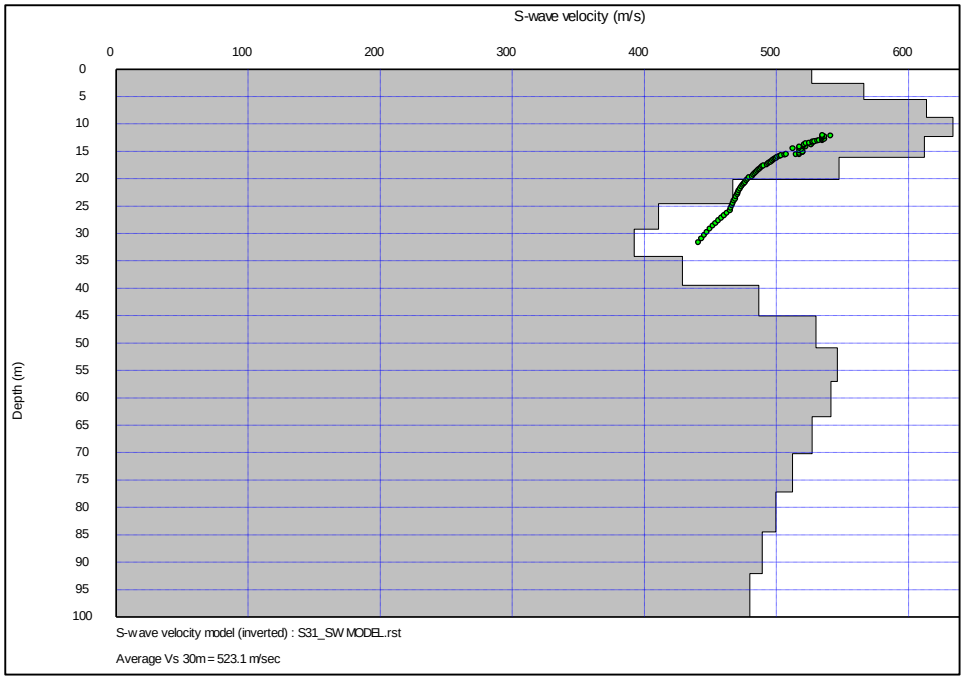
S-wave velocity (m/s)
0
100
200
300
400
500
600
Depth (m)
0
5
10
15
20
25
30
35
40
45
50
55
60
65
70
75
80
85
90
95
100
S-wave velocity model (inverted) : S31_SW MODEL.rst
Average Vs 30m = 523.1 m/sec

S32

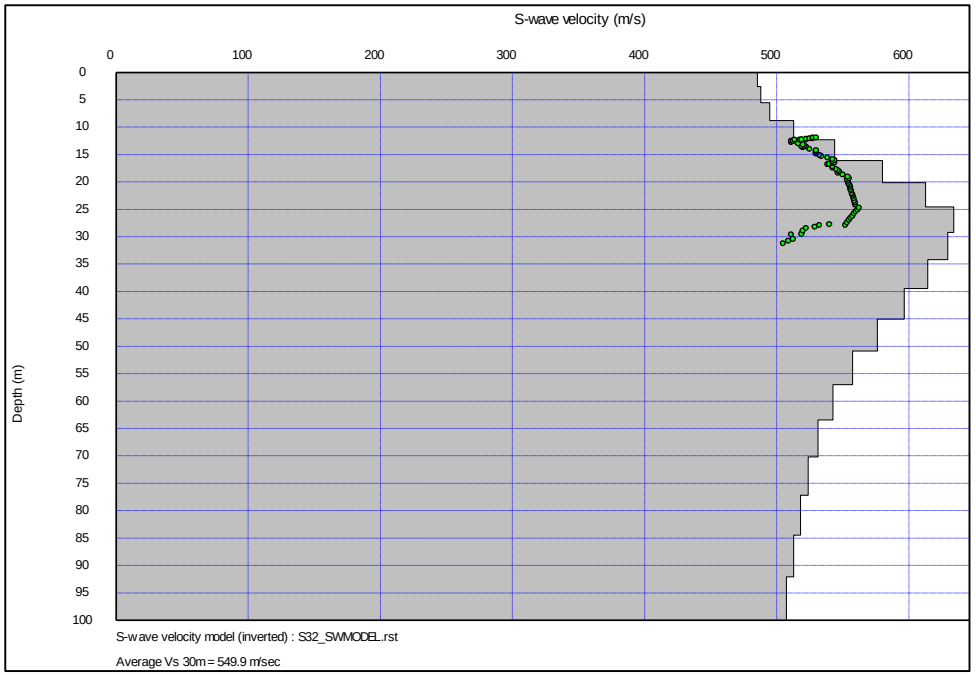

Depth (m)	S-wave velocity (m/s)	P-wave velocity (m/s)	Density (g/cc)	Poisson Ratio	Shear Modulus (Gpa)	Young Modulus (Mpa)
0.00	485.26	1833.47	1.92	0.46	0.45	1319.87
2.63	487.82	1835.70	1.92	0.46	0.46	1333.54
5.56	494.79	1842.60	1.92	0.46	0.47	1371.13
8.77	512.92	1861.45	1.92	0.46	0.50	1471.16
12.28	543.77	1894.04	1.92	0.46	0.57	1649.10
16.08	580.08	1932.51	1.92	0.45	0.64	1870.79
20.18	612.67	1967.25	1.92	0.45	0.72	2080.87
24.56	633.76	1989.87	1.92	0.44	0.77	2222.39
29.24	629.43	1985.31	1.91	0.44	0.76	2189.17
34.21	614.07	1969.42	1.91	0.45	0.72	2084.10
39.47	596.44	1951.55	1.91	0.45	0.68	1969.35
45.03	576.15	1930.38	1.91	0.45	0.63	1840.96
50.88	557.40	1910.25	1.91	0.45	0.59	1725.88
57.02	542.32	1893.39	1.91	0.46	0.56	1635.83
63.45	531.32	1880.39	1.91	0.46	0.54	1571.55
70.18	523.80	1870.83	1.91	0.46	0.52	1528.26
77.19	518.07	1863.35	1.91	0.46	0.51	1495.70
84.50	512.76	1856.73	1.91	0.46	0.50	1465.77
92.11	507.28	1850.11	1.91	0.46	0.49	1435.27
115.79	633.76	1989.87	1.92	0.44	0.77	2222.39

S33

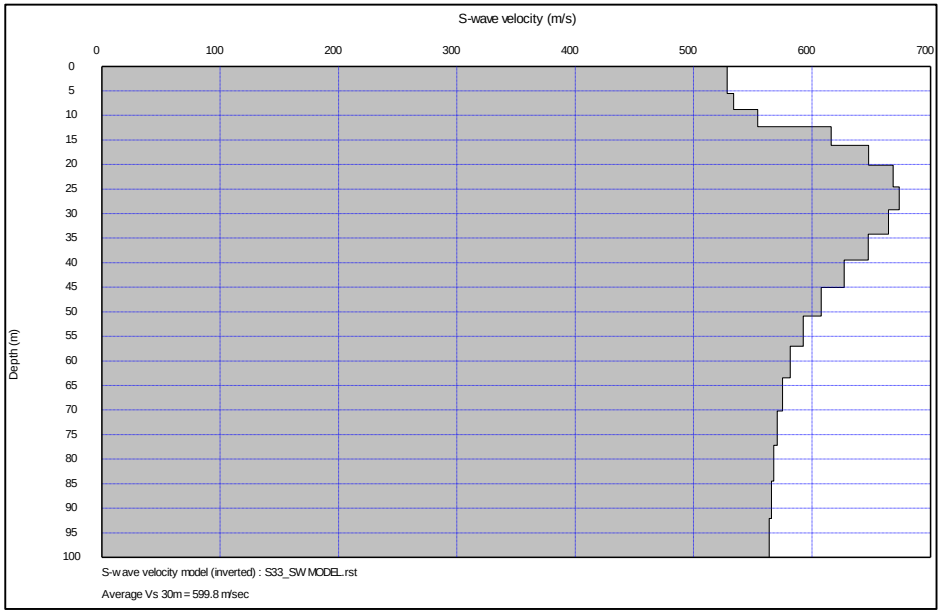

Depth (m)	S-wave velocity (m/s)	P-wave velocity (m/s)	Density (g/cc)	Poisson Ratio	Shear Modulus (Gpa)	Young Modulus (Mpa)
0.00	528.36	1876.48	1.91	0.46	0.53	1549.68
2.63	528.22	1876.33	1.90	0.46	0.53	1548.85
5.56	533.79	1882.51	1.91	0.46	0.54	1582.49
8.77	554.08	1905.03	1.91	0.45	0.59	1708.17
12.28	616.15	1973.93	1.93	0.45	0.73	2123.63
16.08	647.78	2009.03	1.94	0.44	0.82	2353.23
20.18	668.54	2032.08	1.95	0.44	0.87	2510.56
24.56	673.52	2037.60	1.95	0.44	0.89	2549.08
29.24	664.56	2027.66	1.95	0.44	0.86	2480.02
34.21	647.35	2008.56	1.94	0.44	0.81	2350.04
39.47	627.25	1986.25	1.94	0.44	0.76	2202.83
45.03	607.88	1964.74	1.93	0.45	0.71	2065.57
50.88	592.55	1947.73	1.93	0.45	0.68	1960.15
57.02	581.52	1935.48	1.92	0.45	0.65	1886.07
63.45	574.96	1928.21	1.92	0.45	0.63	1842.76
70.18	570.63	1923.40	1.92	0.45	0.62	1814.39
77.19	567.72	1920.16	1.92	0.45	0.62	1795.46
84.50	565.75	1917.98	1.92	0.45	0.61	1782.72
92.11	563.79	1915.80	1.92	0.45	0.61	1770.09
115.79	673.52	2037.60	1.95	0.44	0.89	2549.08

S34

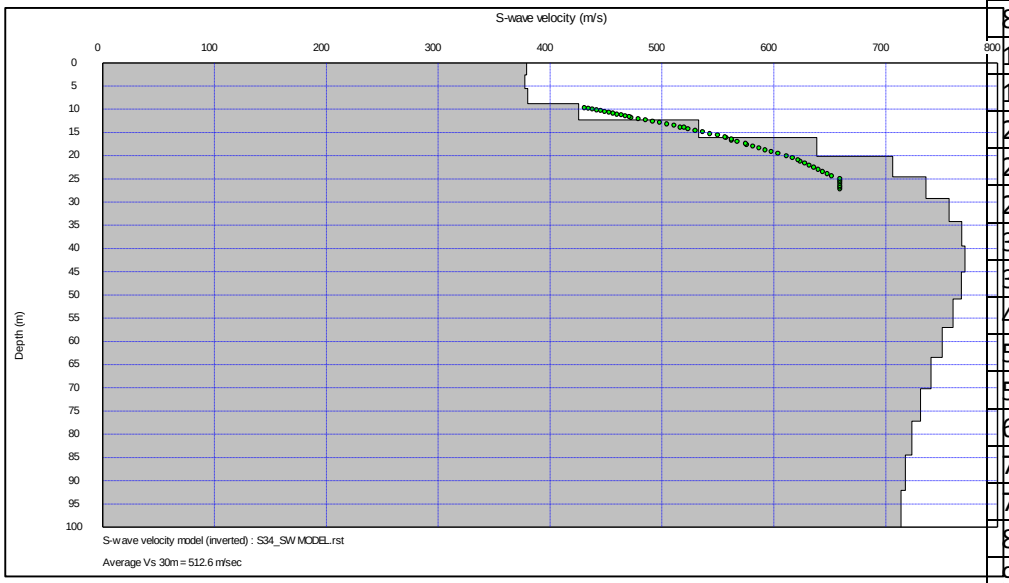

Depth (m)	S-wave velocity (m/s)	P-wave velocity (m/s)	Density (g/cc)	Poisson Ratio	Shear Modulus (Gpa)	Young Modulus (Mpa)
0.00	379.10	1714.79	1.88	0.47	0.27	798.37
2.63	377.28	1712.70	1.88	0.47	0.27	790.81
5.56	379.87	1714.96	1.88	0.47	0.27	801.56
8.77	425.61	1763.88	1.89	0.47	0.34	1007.33
12.28	532.90	1881.12	1.92	0.46	0.54	1585.33
16.08	638.36	1997.13	1.94	0.44	0.79	2279.63
20.18	706.19	2071.80	1.95	0.43	0.97	2787.28
24.56	736.01	2104.36	1.95	0.43	1.06	3019.26
29.24	756.69	2126.67	1.95	0.43	1.12	3185.09
34.21	767.96	2138.54	1.95	0.43	1.15	3277.11
39.47	770.93	2141.37	1.95	0.43	1.16	3301.51
45.03	767.52	2137.37	1.95	0.43	1.15	3273.35
50.88	760.04	2129.12	1.95	0.43	1.13	3212.12
57.02	750.41	2118.71	1.95	0.43	1.10	3134.12
63.45	740.36	2107.96	1.95	0.43	1.07	3053.67
70.18	731.16	2098.18	1.95	0.43	1.04	2980.84
77.19	723.41	2089.98	1.95	0.43	1.02	2920.10
84.50	717.46	2083.69	1.95	0.43	1.00	2873.88
92.11	713.53	2079.54	1.95	0.43	0.99	2843.52
115.79	770.93	2141.37	1.95	0.43	1.16	3301.51

S35

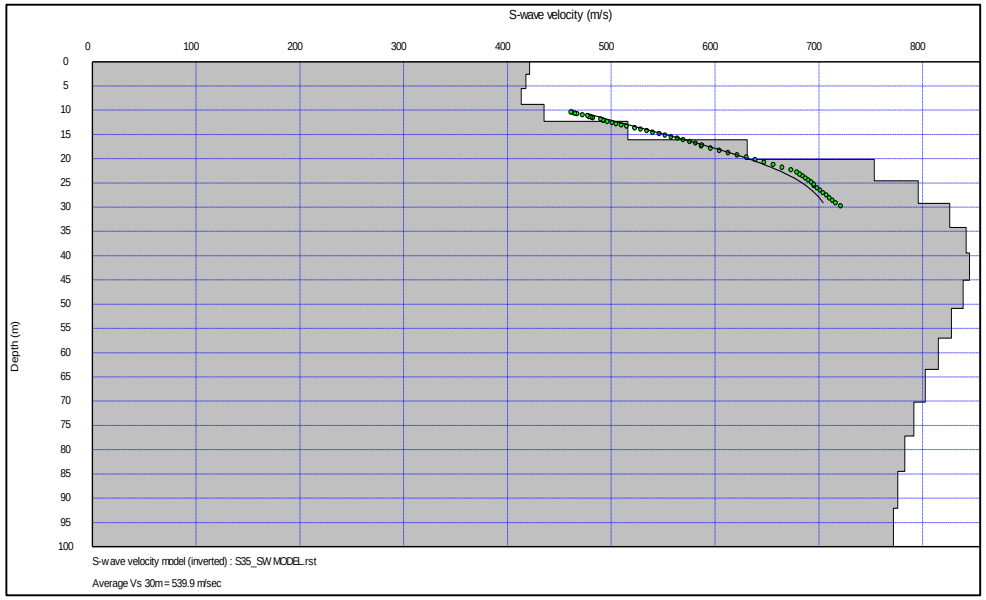

Depth (m)	S-wave velocity (m/s)	P-wave velocity (m/s)	Density (g/cc)	Poisson Ratio	Shear Modulus (Gpa)	Young Modulus (Mpa)
0.00	421.41	1761.15	1.90	0.47	0.34	989.16
2.63	417.86	1757.29	1.90	0.47	0.33	972.83
5.56	413.13	1752.00	1.90	0.47	0.32	951.26
8.77	435.31	1775.93	1.90	0.47	0.36	1057.52
12.28	516.10	1863.97	1.92	0.46	0.51	1491.33
16.08	630.91	1989.28	1.94	0.44	0.77	2234.48
20.18	753.52	2123.49	1.97	0.43	1.12	3191.97
24.56	795.68	2168.93	1.97	0.42	1.25	3544.84
29.24	825.99	2201.96	1.97	0.42	1.34	3809.06
34.21	841.91	2219.67	1.97	0.42	1.40	3951.28
39.47	845.02	2223.59	1.97	0.42	1.41	3979.43
45.03	838.88	2217.47	1.97	0.42	1.39	3924.27
50.88	827.79	2205.85	1.97	0.42	1.35	3825.44
57.02	814.97	2192.20	1.97	0.42	1.31	3712.46
63.45	802.46	2178.79	1.97	0.42	1.27	3603.75
70.18	791.44	2166.94	1.97	0.42	1.23	3509.18
77.19	782.63	2157.37	1.97	0.42	1.21	3434.31
84.50	776.16	2150.34	1.97	0.43	1.19	3379.81
92.11	771.92	2145.72	1.97	0.43	1.17	3344.39
115.79	845.02	2223.59	1.97	0.42	1.41	3979.43

S36

Depth (m)	S-wave velocity (m/s)	P-wave velocity (m/s)	Density (g/cc)	Poisson Ratio	Shear Modulus (Gpa)	Young Modulus (Mpa)
0.00	472.75	1817.08	1.90	0.46	0.43	1244.26

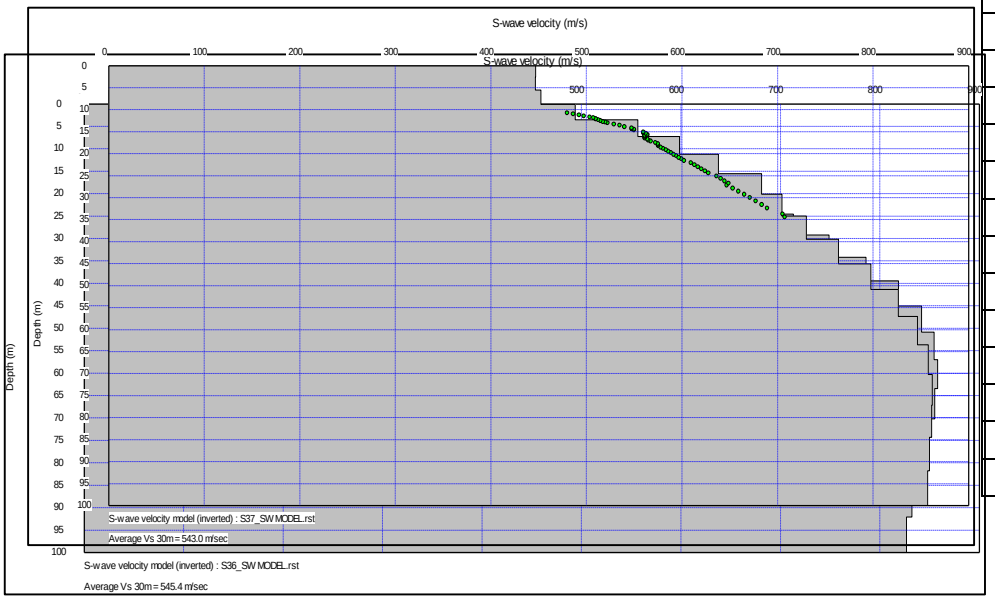

2.63	470.44	1814.71	1.90	0.46	0.42	1232.33
5.56	466.80	1810.60	1.90	0.46	0.41	1213.71
8.77	475.72	1820.11	1.91	0.46	0.43	1262.29
12.28	514.25	1862.54	1.92	0.46	0.51	1480.23
16.08	572.56	1927.16	1.94	0.45	0.63	1842.03
20.18	640.94	2002.78	1.95	0.44	0.80	2314.39
24.56	712.86	2081.51	1.97	0.43	1.00	2864.73
29.24	748.81	2119.48	1.97	0.43	1.10	3150.26
34.21	786.15	2158.67	1.97	0.42	1.22	3459.72
39.47	818.55	2192.49	1.97	0.42	1.32	3738.85
45.03	841.81	2216.68	1.97	0.42	1.39	3945.25
50.88	854.45	2229.76	1.97	0.41	1.44	4059.47
57.02	858.19	2233.60	1.97	0.41	1.45	4093.47
63.45	855.12	2230.46	1.97	0.41	1.44	4065.55
70.18	848.30	2223.41	1.97	0.41	1.41	4003.73
77.19	840.02	2214.83	1.97	0.42	1.39	3929.20
84.50	832.22	2206.67	1.97	0.42	1.36	3859.53
92.11	826.75	2200.94	1.97	0.42	1.34	3810.99
115.79	858.19	2233.60	1.97	0.41	1.45	4093.47

S37

Depth (m)	S-wave velocity (m/s)	P-wave velocity (m/s)	Density (g/cc)	Poisson Ratio	Shear Modulus (Gpa)	Young Modulus (Mpa)

0.00	446.76	1790.51	1.90	0.47	0.38	1113.61
2.63	446.67	1790.27	1.90	0.47	0.38	1113.16
5.56	452.22	1795.40	1.90	0.47	0.39	1140.47
8.77	488.15	1833.09	1.91	0.46	0.45	1329.66
12.28	553.85	1904.07	1.92	0.45	0.59	1716.22
16.08	597.32	1952.05	1.94	0.45	0.69	2000.11
20.18	638.13	1998.58	1.95	0.44	0.79	2289.63
24.56	683.38	2050.08	1.96	0.44	0.92	2633.59
29.24	704.50	2073.74	1.96	0.43	0.97	2797.31
34.21	730.21	2101.09	1.96	0.43	1.05	2997.97
39.47	763.62	2135.99	1.96	0.43	1.15	3268.05
45.03	797.64	2171.41	1.96	0.42	1.25	3553.93
50.88	826.23	2201.06	1.96	0.42	1.34	3802.50
57.02	846.40	2222.03	1.96	0.42	1.41	3982.41
63.45	857.79	2233.93	1.96	0.41	1.45	4085.66
70.18	861.85	2238.20	1.96	0.41	1.46	4122.72
77.19	861.23	2237.61	1.96	0.41	1.46	4117.30
84.50	858.89	2235.18	1.96	0.41	1.45	4095.74
92.11	857.16	2233.41	1.96	0.41	1.44	4079.92
115.79	861.85	2238.20	1.96	0.41	1.46	4122.72

S38

Depth (m)	S-wave velocity (m/s)	P-wave velocity (m/s)	Density (g/cc)	Poisson Ratio	Shear Modulus (Gpa)	Young Modulus (Mpa)
0.00	413.06	1753.84	1.89	0.47	0.32	947.26
2.63	412.86	1753.58	1.89	0.47	0.32	946.36
5.56	413.92	1753.91	1.89	0.47	0.32	951.14
8.77	453.03	1794.71	1.90	0.47	0.39	1141.13
12.28	523.32	1870.70	1.92	0.46	0.52	1529.04
16.08	585.50	1939.86	1.93	0.45	0.66	1923.41
20.18	641.81	2003.86	1.95	0.44	0.81	2323.16
24.56	701.62	2071.28	1.97	0.44	0.97	2787.29
29.24	777.99	2155.41	1.99	0.43	1.20	3434.13
34.21	822.22	2202.25	1.99	0.42	1.35	3824.91
39.47	865.49	2247.16	1.99	0.41	1.49	4219.86
45.03	908.28	2291.50	1.99	0.41	1.64	4627.37
50.88	943.10	2327.55	1.99	0.40	1.77	4971.12
57.02	967.38	2352.75	1.99	0.40	1.87	5217.25

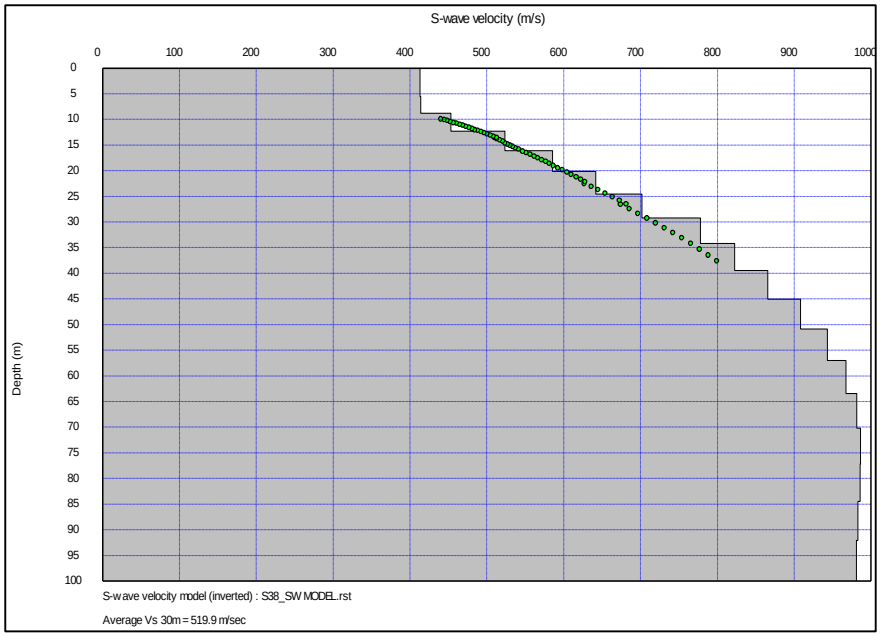

63.45	981.20	2367.07	1.99	0.40	1.92	5359.71
70.18	986.33	2372.30	1.99	0.40	1.94	5412.90
77.19	985.88	2371.81	1.99	0.40	1.94	5408.22
84.50	983.02	2368.88	1.99	0.40	1.93	5378.50
92.11	980.78	2366.57	1.99	0.40	1.92	5355.30
115.79	986.33	2372.30	1.99	0.40	1.94	5412.90

S39

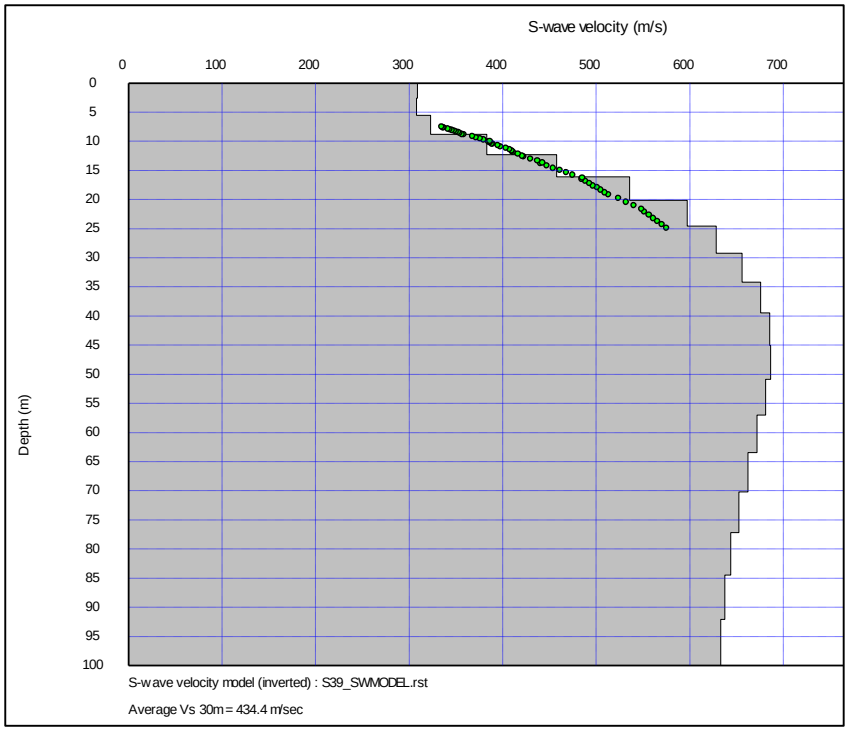

Depth (m)	S-wave velocity (m/s)	P-wave velocity (m/s)	Density (g/cc)	Poisson Ratio	Shear Modulus (Gpa)	Young Modulus (Mpa)
0.00	308.81	1636.39	1.85	0.48	0.18	522.34
2.63	307.67	1634.81	1.85	0.48	0.17	518.51
5.56	322.83	1650.47	1.85	0.48	0.19	571.41
8.77	382.87	1715.53	1.87	0.47	0.27	807.43
12.28	457.39	1797.79	1.89	0.47	0.40	1158.45
16.08	535.37	1884.29	1.91	0.46	0.55	1593.58
20.18	597.05	1952.10	1.92	0.45	0.68	1983.39
24.56	627.98	1985.08	1.92	0.44	0.76	2188.08
29.24	655.97	2014.58	1.92	0.44	0.83	2381.43
34.21	675.76	2035.20	1.92	0.44	0.88	2522.60
39.47	685.55	2045.22	1.92	0.44	0.90	2593.84
45.03	686.36	2045.80	1.92	0.44	0.90	2599.69
50.88	680.87	2039.85	1.92	0.44	0.89	2559.59
57.02	671.95	2030.37	1.92	0.44	0.87	2495.06
63.45	661.98	2019.81	1.92	0.44	0.84	2423.78
70.18	652.22	2009.50	1.92	0.44	0.82	2354.93
77.19	643.78	2000.61	1.92	0.44	0.80	2296.18
84.50	637.35	1993.83	1.92	0.44	0.78	2251.85
92.11	633.09	1989.34	1.92	0.44	0.77	2222.72
115.79	686.36	2045.80	1.92	0.44	0.90	2599.69

S40

Depth (m)	S-wave velocity (m/s)	P-wave velocity (m/s)	Density (g/cc)	Poisson Ratio	Shear Modulus (Gpa)	Young Modulus (Mpa)
0.00	383.84	1716.48	1.87	0.47	0.27	810.37

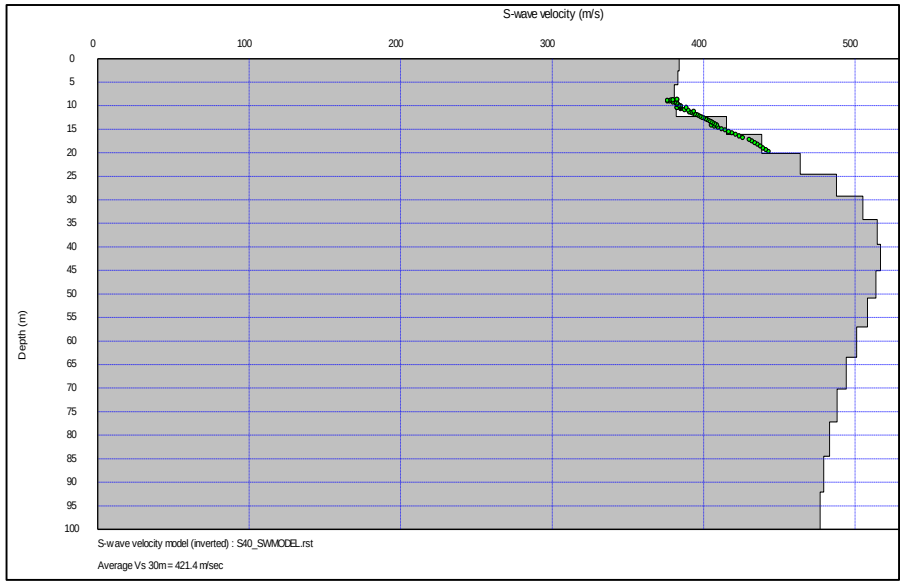

2.63	383.04	1715.72	1.87	0.47	0.27	807.03
5.56	380.60	1713.55	1.87	0.47	0.27	796.95
8.77	381.80	1715.45	1.87	0.47	0.27	802.34
12.28	414.96	1752.11	1.88	0.47	0.32	949.49
16.08	438.20	1776.88	1.88	0.47	0.36	1057.50
20.18	463.77	1803.67	1.88	0.46	0.40	1182.10
24.56	487.72	1828.65	1.88	0.46	0.45	1304.75
29.24	505.13	1846.82	1.88	0.46	0.48	1397.52
34.21	514.49	1856.61	1.88	0.46	0.50	1448.60
39.47	516.62	1858.89	1.88	0.46	0.50	1460.40
45.03	513.75	1855.94	1.88	0.46	0.50	1444.52
50.88	507.98	1849.96	1.88	0.46	0.48	1412.95
57.02	501.06	1842.77	1.88	0.46	0.47	1375.54
63.45	494.19	1835.60	1.88	0.46	0.46	1338.84
70.18	488.07	1829.20	1.88	0.46	0.45	1306.56
77.19	483.01	1823.90	1.88	0.46	0.44	1280.18
84.50	479.26	1819.96	1.88	0.46	0.43	1260.73
92.11	476.79	1817.36	1.88	0.46	0.43	1248.02
115.79	516.62	1858.89	1.88	0.46	0.50	1460.40

S41

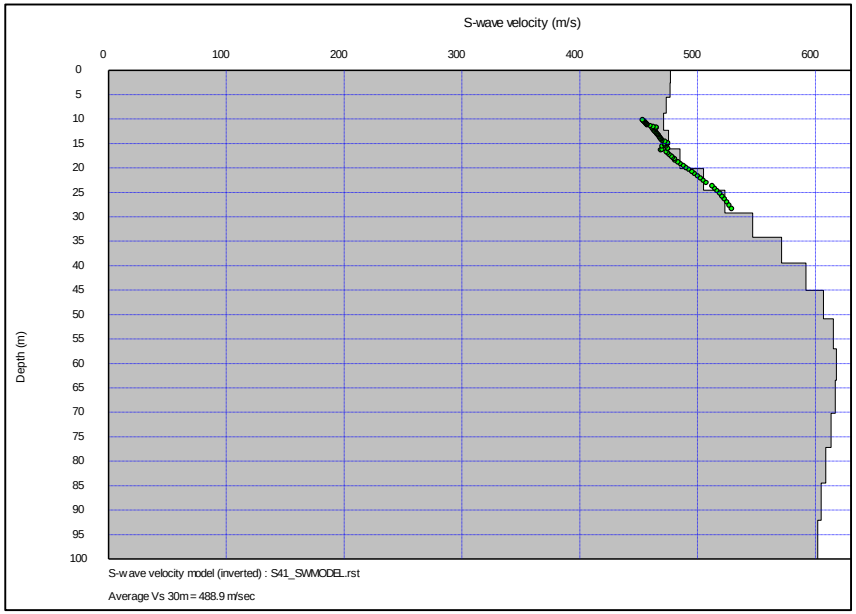

Depth (m)	S-wave velocity (m/s)	P-wave velocity (m/s)	Density (g/cc)	Poisson Ratio	Shear Modulus (Gpa)	Young Modulus (Mpa)
0.00	477.00	1819.42	1.89	0.46	0.43	1259.81
2.63	476.60	1819.01	1.89	0.46	0.43	1257.74
5.56	473.38	1815.64	1.89	0.46	0.42	1241.14
8.77	470.93	1813.42	1.89	0.46	0.42	1229.83
12.28	475.23	1819.10	1.90	0.46	0.43	1254.52
16.08	484.86	1830.27	1.90	0.46	0.45	1307.33
20.18	505.09	1852.37	1.91	0.46	0.49	1419.14
24.56	523.10	1871.21	1.91	0.46	0.52	1519.84
29.24	546.73	1895.76	1.91	0.45	0.57	1656.87
34.21	571.14	1921.10	1.91	0.45	0.62	1804.24
39.47	591.94	1942.73	1.91	0.45	0.67	1934.46
45.03	606.74	1958.21	1.91	0.45	0.70	2029.73
50.88	615.08	1967.00	1.91	0.45	0.72	2084.33
57.02	617.83	1969.93	1.91	0.45	0.73	2102.47
63.45	616.65	1968.77	1.91	0.45	0.72	2094.68
70.18	613.17	1965.22	1.91	0.45	0.72	2071.79
77.19	608.83	1960.75	1.91	0.45	0.71	2043.33
84.50	604.82	1956.63	1.91	0.45	0.70	2017.29
92.11	601.86	1953.59	1.91	0.45	0.69	1998.13
115.79	617.83	1969.93	1.91	0.45	0.73	2102.47

S42

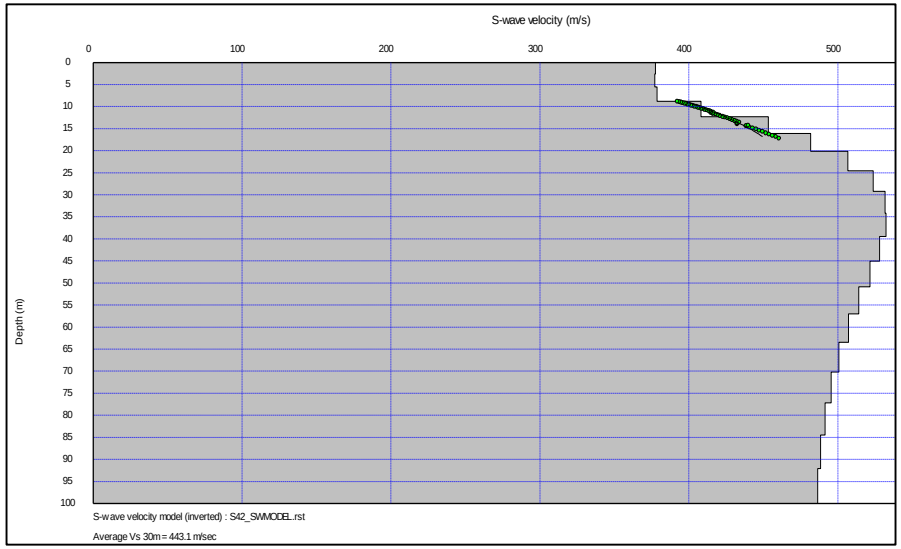

Depth (m)	S-wave velocity (m/s)	P-wave velocity (m/s)	Density (g/cc)	Poisson Ratio	Shear Modulus (Gpa)	Young Modulus (Mpa)
0.00	377.67	1710.44	1.87	0.47	0.27	786.44
2.63	377.12	1709.77	1.87	0.47	0.27	784.21
5.56	378.76	1712.14	1.87	0.47	0.27	790.96
8.77	408.06	1744.44	1.88	0.47	0.31	918.66
12.28	453.32	1793.66	1.88	0.47	0.39	1134.01
16.08	481.88	1823.92	1.88	0.46	0.44	1278.42
20.18	506.86	1850.29	1.88	0.46	0.48	1411.47
24.56	523.73	1868.05	1.88	0.46	0.52	1504.82
29.24	531.66	1876.37	1.88	0.46	0.53	1549.65
34.21	532.31	1877.04	1.88	0.46	0.53	1553.39
39.47	528.18	1872.67	1.88	0.46	0.53	1529.89
45.03	521.56	1865.70	1.88	0.46	0.51	1492.66
50.88	514.18	1857.91	1.88	0.46	0.50	1451.62
57.02	507.11	1850.45	1.88	0.46	0.48	1412.79
63.45	500.85	1843.84	1.88	0.46	0.47	1378.87
70.18	495.64	1838.35	1.88	0.46	0.46	1350.95
77.19	491.57	1834.05	1.88	0.46	0.45	1329.28
84.50	488.56	1830.87	1.88	0.46	0.45	1313.38
92.11	486.58	1828.78	1.88	0.46	0.45	1302.97
115.79	532.31	1877.04	1.88	0.46	0.53	1553.39

S43

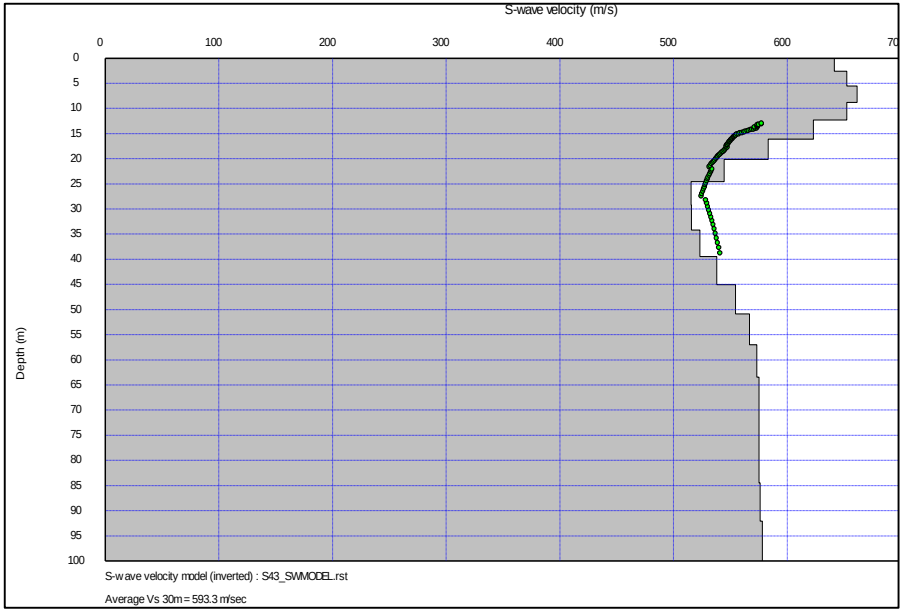

Depth (m)	S-wave velocity (m/s)	P-wave velocity (m/s)	Density (g/cc)	Poisson Ratio	Shear Modulus (Gpa)	Young Modulus (Mpa)
0.00	641.18	2001.46	1.92	0.44	0.79	2279.41
2.63	652.17	2011.65	1.92	0.44	0.82	2355.69
5.56	661.19	2019.59	1.92	0.44	0.84	2419.12
8.77	652.19	2009.57	1.92	0.44	0.82	2355.59
12.28	623.03	1979.45	1.92	0.45	0.75	2155.50
16.08	583.06	1938.50	1.92	0.45	0.65	1894.66
20.18	544.46	1898.46	1.92	0.46	0.57	1657.20
24.56	515.31	1866.79	1.92	0.46	0.51	1486.60
29.24	515.71	1865.42	1.92	0.46	0.51	1490.45
34.21	523.05	1871.69	1.92	0.46	0.53	1532.44
39.47	538.07	1885.80	1.92	0.46	0.56	1619.53
45.03	554.49	1902.15	1.92	0.45	0.59	1717.40
50.88	566.70	1915.17	1.92	0.45	0.62	1791.96
57.02	573.16	1923.20	1.92	0.45	0.63	1832.11
63.45	575.10	1927.11	1.92	0.45	0.64	1844.36
70.18	574.94	1928.75	1.92	0.45	0.64	1843.46
77.19	575.15	1930.43	1.92	0.45	0.64	1844.85
84.50	576.12	1932.57	1.92	0.45	0.64	1851.05
92.11	577.94	1935.41	1.92	0.45	0.64	1862.54
115.79	661.19	2019.59	1.92	0.44	0.84	2419.12

S44

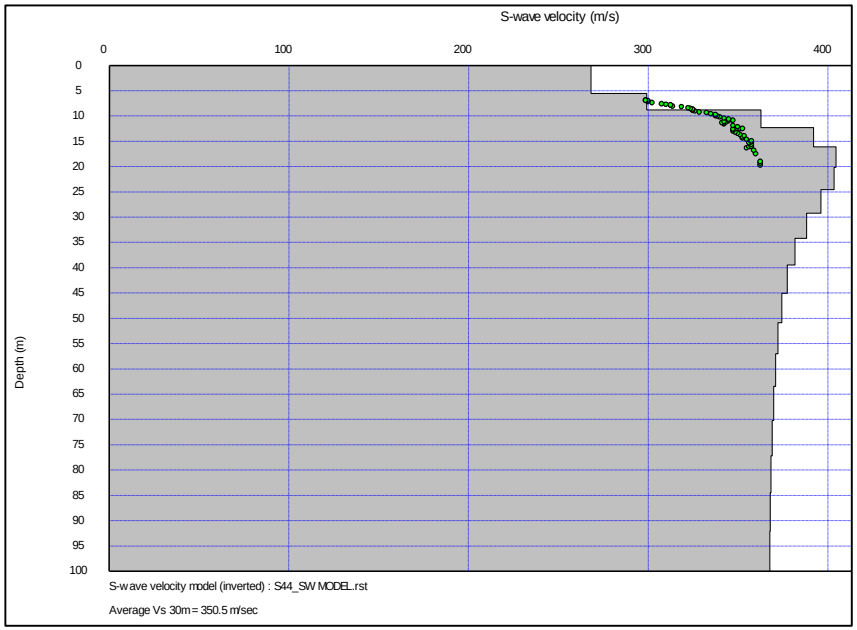

Depth (m)	S-wave velocity (m/s)	P-wave velocity (m/s)	Density (g/cc)	Poisson Ratio	Shear Modulus (Gpa)	Young Modulus (Mpa)
0.00	268.15	1591.29	1.83	0.49	0.13	391.97
2.63	268.16	1590.96	1.83	0.49	0.13	391.99
5.56	299.16	1623.38	1.84	0.48	0.16	487.92
8.77	362.70	1691.46	1.85	0.48	0.24	717.84
12.28	392.07	1722.90	1.85	0.47	0.28	836.99
16.08	404.60	1737.04	1.85	0.47	0.30	890.51
20.18	403.42	1736.54	1.85	0.47	0.30	885.44
24.56	396.12	1729.09	1.85	0.47	0.29	854.15
29.24	388.17	1720.55	1.85	0.47	0.28	820.69
34.21	381.78	1713.46	1.85	0.47	0.27	794.27
39.47	377.35	1708.43	1.85	0.47	0.26	776.19
45.03	374.30	1704.92	1.85	0.47	0.26	763.89
50.88	372.25	1702.52	1.85	0.47	0.26	755.62
57.02	370.83	1700.88	1.85	0.48	0.25	749.96
63.45	369.74	1699.63	1.85	0.48	0.25	745.63
70.18	368.93	1698.72	1.85	0.48	0.25	742.41
77.19	368.35	1698.09	1.85	0.48	0.25	740.10
84.50	367.94	1697.65	1.85	0.48	0.25	738.48
92.11	367.68	1697.36	1.85	0.48	0.25	737.42
115.79	404.60	1737.04	1.85	0.47	0.30	890.51

S45

Depth (m)	S-wave velocity (m/s)	P-wave velocity (m/s)	Density (g/cc)	Poisson Ratio	Shear Modulus (Gpa)	Young Modulus (Mpa)
0.00	365.73	1697.87	1.86	0.48	0.25	734.31
2.63	365.64	1697.63	1.86	0.48	0.25	733.97
5.56	374.78	1707.36	1.86	0.47	0.26	771.06
8.77	391.35	1724.83	1.86	0.47	0.29	840.04
12.28	409.28	1743.63	1.86	0.47	0.31	917.51
16.08	424.09	1759.24	1.86	0.47	0.33	983.99
20.18	431.44	1767.08	1.86	0.47	0.35	1017.79
24.56	430.94	1766.72	1.86	0.47	0.35	1015.46
29.24	424.55	1760.16	1.86	0.47	0.34	986.07
34.21	415.18	1750.41	1.86	0.47	0.32	943.72
39.47	405.31	1740.00	1.86	0.47	0.31	900.07
45.03	396.61	1730.73	1.86	0.47	0.29	862.42
50.88	389.90	1723.44	1.86	0.47	0.28	833.91

57.02	385.11	1718.15	1.86	0.47	0.28	813.83
63.45	382.13	1714.76	1.86	0.47	0.27	801.48
70.18	380.24	1712.56	1.86	0.47	0.27	793.68
77.19	379.11	1711.22	1.86	0.47	0.27	789.04
84.50	378.32	1710.31	1.86	0.47	0.27	785.78
92.11	377.48	1709.40	1.86	0.47	0.27	782.33
115.79	431.44	1767.08	1.86	0.47	0.35	1017.79

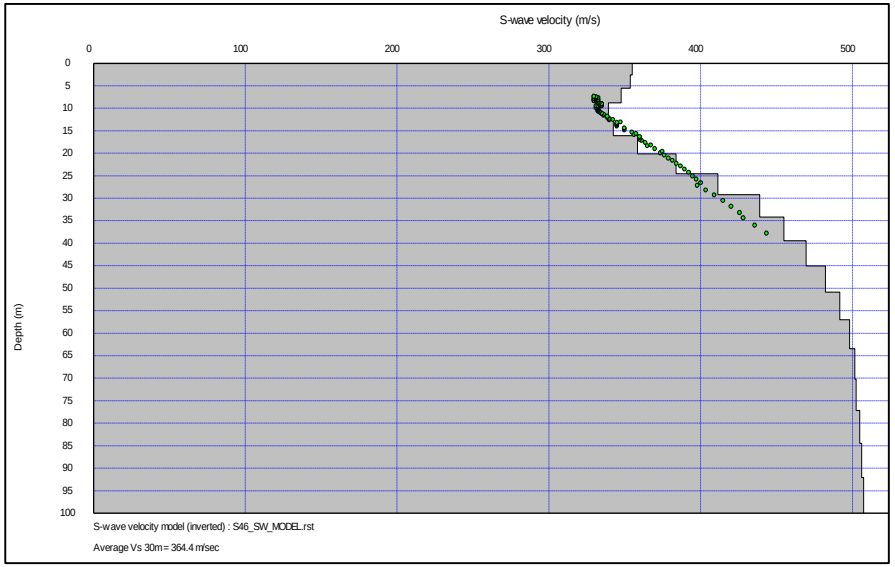

S46

Depth (m)	S-wave velocity (m/s)	P-wave velocity (m/s)	Density (g/cc)	Poisson Ratio	Shear Modulus (Gpa)	Young Modulus (Mpa)
0.00	355.02	1684.07	1.85	0.48	0.23	687.44
2.63	353.71	1682.69	1.85	0.48	0.23	682.41
5.56	347.70	1676.53	1.85	0.48	0.22	659.86

8.77	339.18	1667.81	1.85	0.48	0.21	628.69
12.28	342.38	1671.78	1.85	0.48	0.22	642.22
16.08	358.39	1689.42	1.86	0.48	0.24	705.41
20.18	383.85	1717.21	1.87	0.47	0.28	810.72
24.56	411.34	1747.10	1.87	0.47	0.32	931.73
29.24	438.98	1777.16	1.88	0.47	0.36	1061.30
34.21	454.84	1794.16	1.88	0.47	0.39	1137.97
39.47	469.60	1809.93	1.88	0.46	0.41	1211.53
45.03	482.15	1823.26	1.88	0.46	0.44	1275.88
50.88	491.77	1833.37	1.88	0.46	0.45	1326.23
57.02	498.19	1840.02	1.88	0.46	0.47	1360.35
63.45	501.59	1843.45	1.88	0.46	0.47	1378.55
70.18	502.48	1844.22	1.88	0.46	0.47	1383.38
77.19	504.84	1846.70	1.88	0.46	0.48	1396.09
84.50	506.22	1848.14	1.88	0.46	0.48	1403.57
92.11	507.41	1849.39	1.88	0.46	0.48	1410.03
115.79	507.41	1849.39	1.88	0.46	0.48	1410.03

S47

Depth (m)	S-wave velocity (m/s)	P-wave velocity (m/s)	Density (g/cc)	Poisson Ratio	Shear Modulus (Gpa)	Young Modulus (Mpa)
0.00	512.75	1856.05	1.88	0.46	0.49	1444.09
2.63	512.27	1855.24	1.88	0.46	0.49	1441.44
5.56	495.97	1838.42	1.88	0.46	0.46	1353.02
8.77	454.32	1795.45	1.88	0.47	0.39	1138.74
12.28	394.75	1732.64	1.88	0.47	0.29	861.88

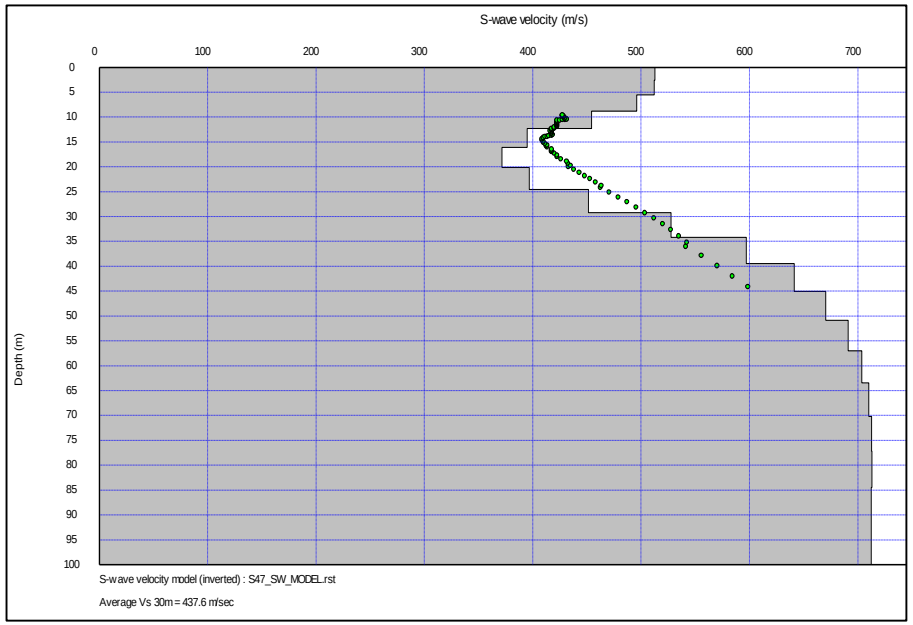

16.08	371.51	1707.98	1.88	0.48	0.26	766.17
20.18	396.73	1734.34	1.89	0.47	0.30	876.85
24.56	451.30	1791.83	1.90	0.47	0.39	1136.53
29.24	527.59	1873.56	1.92	0.46	0.53	1554.25
34.21	597.02	1948.60	1.93	0.45	0.69	1988.20
39.47	641.43	1996.85	1.93	0.44	0.79	2288.98
45.03	670.48	2028.84	1.93	0.44	0.87	2494.48
50.88	690.94	2051.81	1.93	0.44	0.92	2644.16
57.02	703.52	2066.29	1.93	0.43	0.95	2738.24
63.45	710.11	2074.15	1.93	0.43	0.97	2788.15
70.18	712.61	2077.44	1.93	0.43	0.98	2807.23
77.19	712.87	2078.15	1.93	0.43	0.98	2809.28
84.50	712.30	2077.85	1.93	0.43	0.98	2805.04
92.11	712.48	2078.23	1.93	0.43	0.98	2806.38
115.79	712.87	2078.23	1.93	0.43	0.98	2809.29

S48

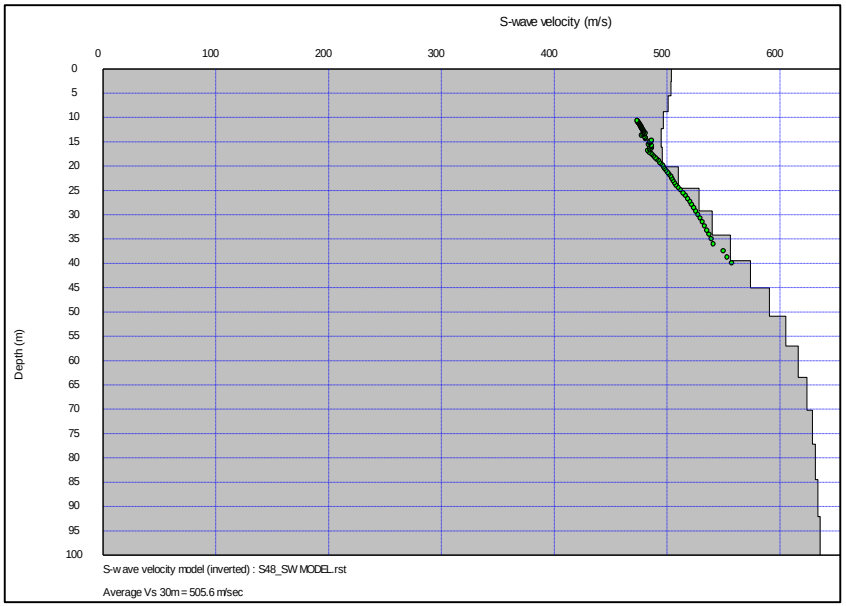

Depth (m)	S-wave velocity (m/s)	P-wave velocity (m/s)	Density (g/cc)	Poisson Ratio	Shear Modulus (Gpa)	Young Modulus (Mpa)
0.00	503.84	1849.47	1.90	0.46	0.48	1407.97
2.63	503.35	1848.95	1.90	0.46	0.48	1405.30
5.56	500.73	1846.18	1.90	0.46	0.48	1390.98
8.77	496.60	1841.96	1.90	0.46	0.47	1369.16
12.28	494.68	1840.35	1.90	0.46	0.47	1360.37
16.08	495.53	1841.70	1.90	0.46	0.47	1366.79
20.18	509.89	1857.75	1.91	0.46	0.50	1449.49
24.56	528.13	1877.69	1.91	0.46	0.53	1556.26
29.24	539.76	1889.90	1.91	0.46	0.56	1623.93
34.21	555.88	1906.84	1.91	0.45	0.59	1719.97
39.47	573.69	1925.56	1.91	0.45	0.63	1829.07
45.03	590.68	1943.49	1.91	0.45	0.67	1936.14
50.88	605.13	1958.79	1.91	0.45	0.70	2029.38
57.02	616.11	1970.46	1.91	0.45	0.73	2101.60
63.45	623.75	1978.62	1.91	0.44	0.74	2152.55
70.18	628.57	1983.82	1.91	0.44	0.76	2185.00
77.19	631.45	1986.98	1.91	0.44	0.76	2204.54
84.50	633.44	1989.17	1.91	0.44	0.77	2218.03
92.11	635.45	1991.38	1.91	0.44	0.77	2231.77
115.79	635.45	1991.38	1.91	0.44	0.77	2231.77

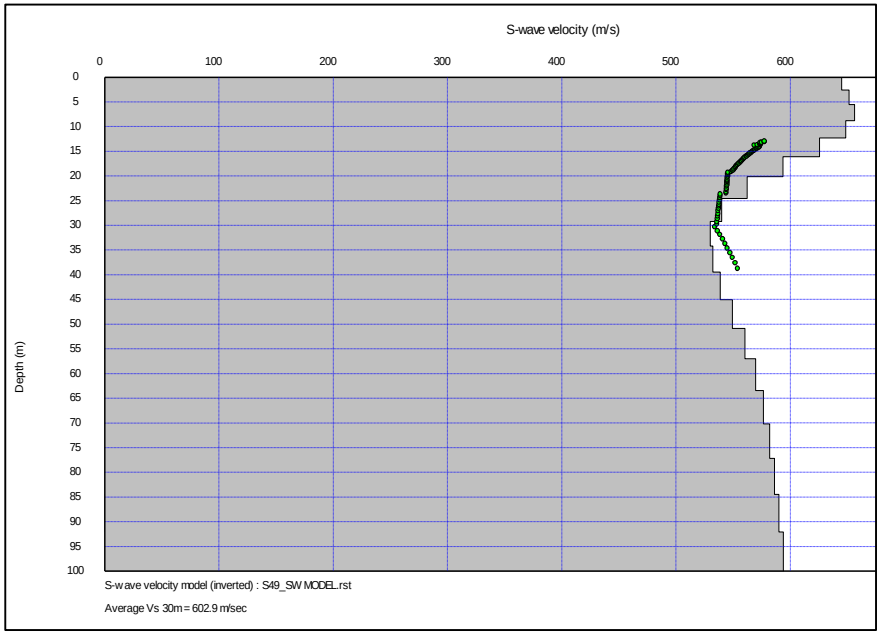

S49

Depth (m)	S-wave velocity (m/s)	P-wave velocity (m/s)	Density (g/cc)	Poisson Ratio	Shear Modulus (Gpa)	Young Modulus (Mpa)
0.00	644.96	2003.75	1.92	0.44	0.80	2305.37
2.63	651.23	2009.42	1.92	0.44	0.81	2349.00
5.56	656.17	2013.57	1.92	0.44	0.83	2383.59
8.77	648.43	2005.16	1.92	0.44	0.81	2329.31
12.28	625.43	1981.54	1.92	0.44	0.75	2171.58
16.08	593.56	1949.15	1.92	0.45	0.68	1961.65
20.18	562.32	1917.17	1.92	0.45	0.61	1765.46

24.56	539.85	1893.57	1.92	0.46	0.56	1630.38
29.24	529.95	1882.29	1.92	0.46	0.54	1572.39
34.21	532.01	1882.88	1.92	0.46	0.54	1584.27
39.47	538.57	1887.93	1.92	0.46	0.56	1622.60
45.03	549.35	1897.86	1.92	0.45	0.58	1686.55
50.88	560.37	1908.88	1.92	0.45	0.60	1753.16
57.02	569.48	1918.80	1.92	0.45	0.62	1809.21
63.45	576.48	1927.11	1.92	0.45	0.64	1852.86
70.18	581.74	1933.87	1.92	0.45	0.65	1886.06
77.19	585.99	1939.58	1.92	0.45	0.66	1913.08
84.50	589.89	1944.65	1.92	0.45	0.67	1938.06
92.11	593.97	1949.66	1.92	0.45	0.68	1964.27
115.79	656.17	2013.57	1.92	0.44	0.83	2383.59

S50

Depth (m)	S-wave velocity (m/s)	P-wave velocity (m/s)	Density (g/cc)	Poisson Ratio	Shear Modulus (Gpa)	Young Modulus (Mpa)
0.00	649.76	2006.85	1.92	0.44	0.81	2341.31
2.63	651.91	2008.89	1.92	0.44	0.82	2356.35
5.56	650.19	2007.00	1.92	0.44	0.81	2344.30
8.77	636.82	1993.26	1.92	0.44	0.78	2251.65
12.28	611.95	1967.70	1.92	0.45	0.72	2084.00
16.08	582.52	1937.36	1.92	0.45	0.65	1893.41
20.18	557.00	1910.84	1.92	0.45	0.60	1735.05
24.56	541.30	1894.26	1.92	0.46	0.56	1640.80
29.24	537.73	1890.11	1.92	0.46	0.56	1619.69

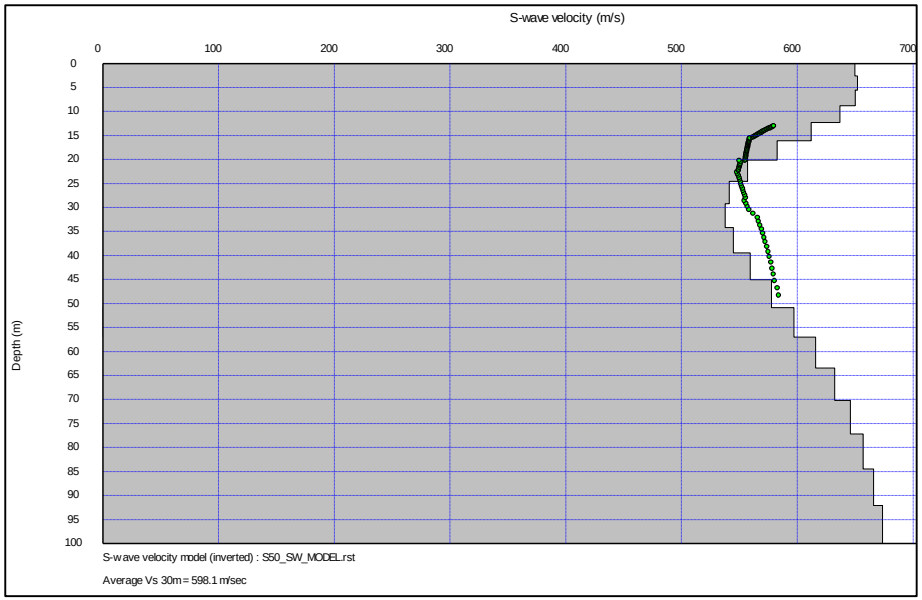

34.21	544.74	1896.93	1.92	0.46	0.57	1661.19
39.47	559.20	1911.58	1.92	0.45	0.60	1748.32
45.03	577.64	1930.60	1.92	0.45	0.64	1862.50
50.88	597.05	1950.85	1.92	0.45	0.69	1986.28
57.02	615.66	1970.44	1.92	0.45	0.73	2108.52
63.45	632.15	1987.94	1.92	0.44	0.77	2219.69
70.18	645.84	2002.63	1.92	0.44	0.80	2314.00
77.19	656.74	2014.41	1.92	0.44	0.83	2390.35
84.50	665.70	2024.20	1.92	0.44	0.85	2454.09
92.11	673.63	2032.90	1.92	0.44	0.87	2511.05
115.79	676.01	2035.65	1.92	0.44	0.88	2528.29

THE SHORT PROFILE

R1

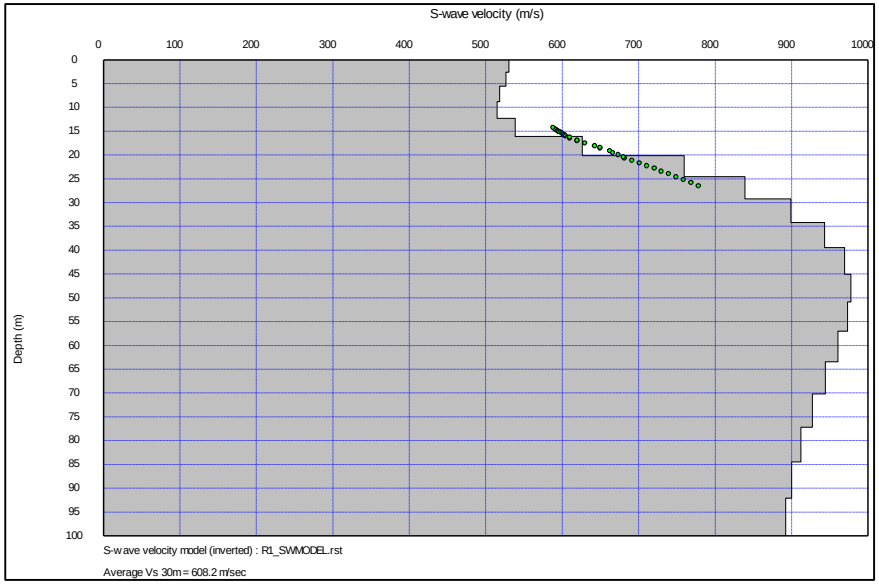

Depth (m)	S-wave velocity (m/s)	P-wave velocity (m/s)	Density (g/cc)	Poisson Ratio	Shear Modulus (Gpa)	Young Modulus (Mpa)
0.00	530.45	1879.94	1.94	0.46	0.55	1590.98
2.63	526.44	1875.90	1.94	0.46	0.54	1567.56
5.56	518.19	1867.61	1.94	0.46	0.52	1519.92
8.77	514.67	1864.74	1.94	0.46	0.51	1499.82
12.28	538.74	1891.72	1.94	0.46	0.56	1642.56
16.08	626.19	1987.46	1.96	0.44	0.77	2219.56
20.18	759.34	2132.42	1.98	0.43	1.14	3263.01
24.56	839.08	2217.46	1.99	0.42	1.40	3962.48
29.24	898.82	2280.50	1.99	0.41	1.60	4519.80
34.21	943.17	2327.30	1.99	0.40	1.77	4954.58
39.47	969.04	2354.63	1.99	0.40	1.87	5216.32
45.03	977.62	2363.69	1.99	0.40	1.90	5304.45
50.88	973.16	2359.03	1.99	0.40	1.88	5258.53
57.02	960.47	2345.71	1.99	0.40	1.83	5128.98
63.45	944.15	2328.54	1.99	0.40	1.77	4964.46
70.18	927.21	2310.67	1.99	0.40	1.71	4796.15
77.19	912.12	2294.77	1.99	0.41	1.65	4648.40
84.50	900.07	2282.08	1.99	0.41	1.61	4531.93
92.11	892.22	2273.83	1.99	0.41	1.58	4456.71
115.79	977.62	2363.69	1.99	0.40	1.90	5304.45

R2

Depth (m)	S-wave velocity (m/s)	P-wave velocity (m/s)	Density (g/cc)	Poisson Ratio	Shear Modulus (Gpa)	Young Modulus (Mpa)
0.00	231.99	1550.49	1.83	0.49	0.10	292.45
2.63	231.71	1549.90	1.83	0.49	0.10	291.75
5.56	267.57	1588.15	1.83	0.49	0.13	389.83
8.77	374.38	1704.41	1.86	0.47	0.26	767.29
12.28	494.26	1835.45	1.88	0.46	0.46	1342.89
16.08	541.95	1886.93	1.88	0.46	0.55	1610.79
20.18	564.46	1911.17	1.88	0.45	0.60	1743.94
24.56	571.22	1918.56	1.88	0.45	0.61	1784.94
29.24	566.75	1913.95	1.88	0.45	0.61	1757.79
34.21	556.34	1902.98	1.88	0.45	0.58	1695.39
39.47	544.09	1890.03	1.88	0.45	0.56	1623.26
45.03	532.21	1877.46	1.88	0.46	0.53	1554.72
50.88	521.72	1866.35	1.88	0.46	0.51	1495.37
57.02	513.07	1857.19	1.88	0.46	0.50	1447.27
63.45	506.11	1849.83	1.88	0.46	0.48	1409.13
70.18	500.68	1844.07	1.88	0.46	0.47	1379.65
77.19	496.57	1839.72	1.88	0.46	0.46	1357.57
84.50	493.62	1836.60	1.88	0.46	0.46	1341.84
92.11	491.72	1834.58	1.88	0.46	0.46	1331.73
115.79	571.22	1918.56	1.88	0.45	0.61	1784.94

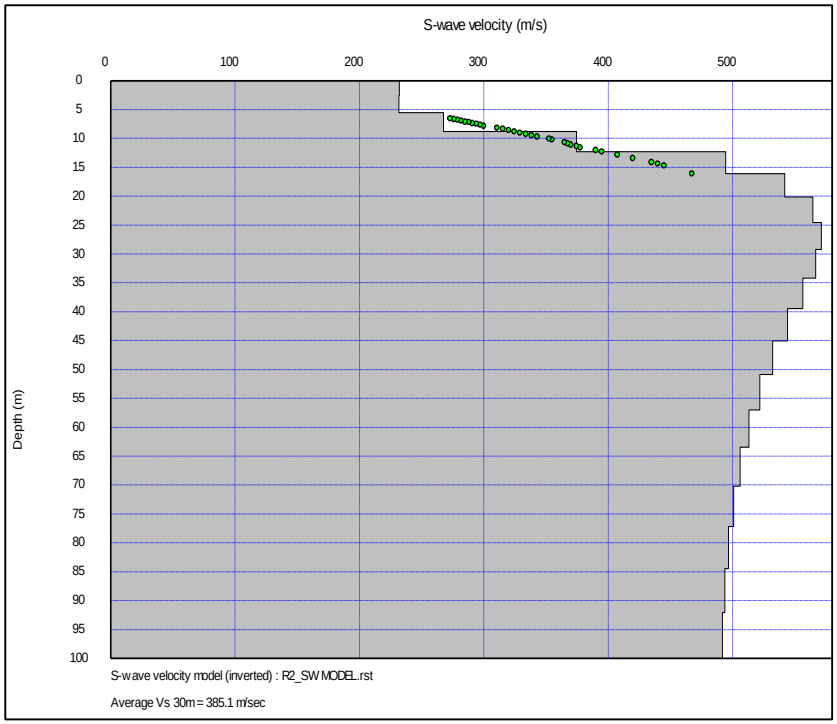

R3

Depth (m)	S-wave velocity (m/s)	P-wave velocity (m/s)	Density (g/cc)	Poisson Ratio	Shear Modulus (Gpa)	Young Modulus (Mpa)
0.00	319.82	1647.93	1.85	0.48	0.19	560.69
2.63	318.60	1646.59	1.85	0.48	0.19	556.47

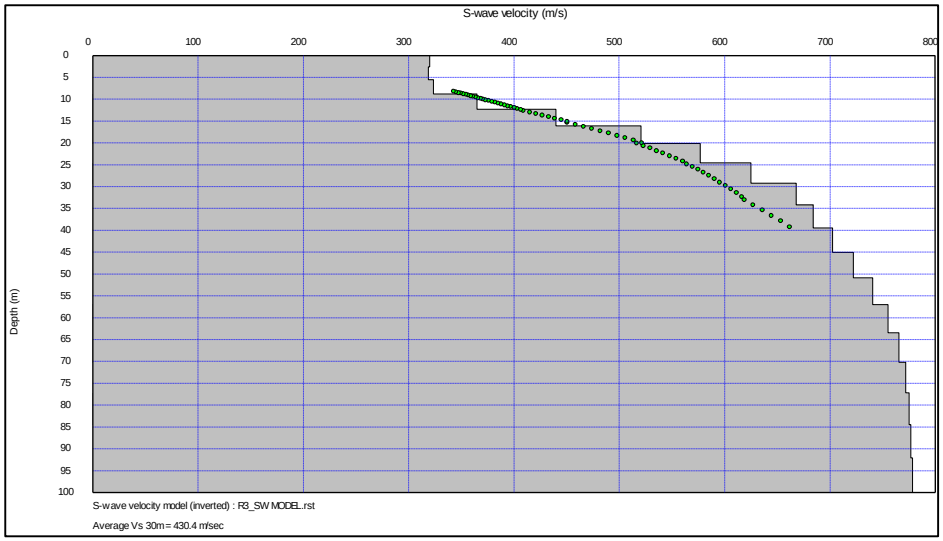

5.56	323.48	1651.81	1.85	0.48	0.19	573.89
8.77	364.92	1696.69	1.86	0.48	0.25	732.54
12.28	439.73	1778.34	1.88	0.47	0.36	1069.43
16.08	520.52	1867.32	1.91	0.46	0.52	1507.12
20.18	576.70	1929.87	1.92	0.45	0.64	1856.98
24.56	624.75	1983.75	1.94	0.44	0.76	2185.68
29.24	667.70	2031.71	1.95	0.44	0.87	2501.02
34.21	683.90	2049.31	1.95	0.44	0.91	2620.71
39.47	702.29	2068.68	1.95	0.43	0.96	2758.79
45.03	722.14	2089.21	1.95	0.43	1.02	2911.48
50.88	740.35	2107.83	1.95	0.43	1.07	3054.75
57.02	755.02	2122.69	1.95	0.43	1.11	3172.41
63.45	765.41	2133.10	1.95	0.43	1.14	3257.01
70.18	771.70	2139.29	1.95	0.43	1.16	3308.64
77.19	775.06	2142.54	1.95	0.42	1.17	3336.37
84.50	776.75	2144.14	1.95	0.42	1.18	3350.32
92.11	778.20	2145.52	1.95	0.42	1.18	3362.40
115.79	778.20	2145.52	1.95	0.42	1.18	3362.40

R4

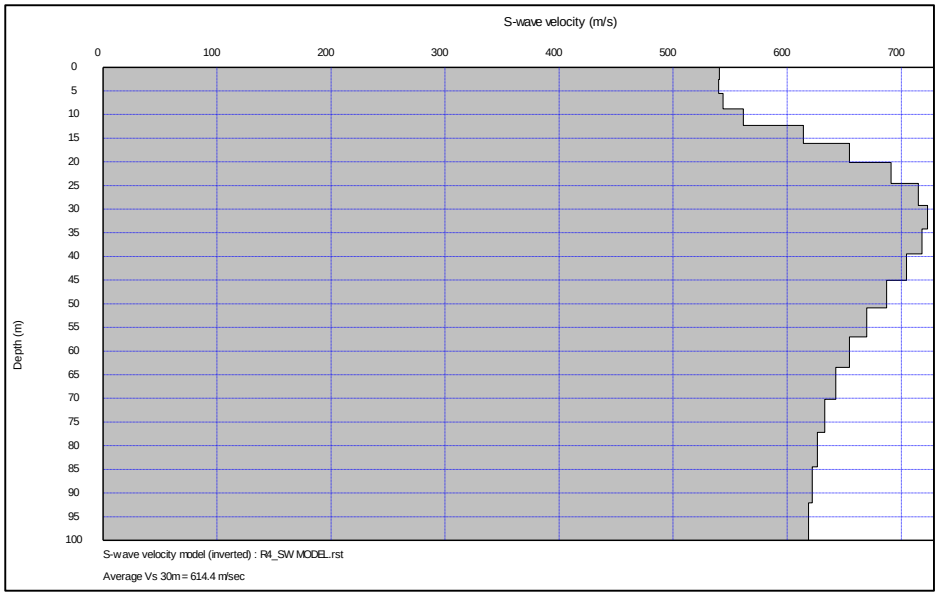

Depth (m)	S-wave velocity (m/s)	P-wave velocity (m/s)	Density (g/cc)	Poisson Ratio	Shear Modulus (Gpa)	Young Modulus (Mpa)
0.00	540.44	1896.17	1.93	0.46	0.57	1645.23
2.63	539.83	1895.57	1.93	0.46	0.56	1641.66
5.56	543.69	1899.57	1.93	0.46	0.57	1664.64
8.77	561.43	1917.66	1.93	0.45	0.61	1772.30
12.28	614.34	1973.38	1.94	0.45	0.73	2119.19
16.08	654.70	2014.71	1.94	0.44	0.83	2397.89
20.18	691.20	2052.37	1.94	0.44	0.93	2663.53
24.56	715.01	2077.33	1.94	0.43	0.99	2843.81
29.24	723.17	2086.51	1.94	0.43	1.02	2906.94
34.21	718.19	2082.24	1.94	0.43	1.00	2868.49
39.47	704.47	2068.83	1.94	0.43	0.96	2763.67
45.03	687.06	2051.41	1.94	0.44	0.92	2633.21
50.88	669.79	2033.88	1.94	0.44	0.87	2506.58
57.02	654.68	2018.35	1.94	0.44	0.83	2398.11
63.45	642.47	2005.75	1.94	0.44	0.80	2312.12
70.18	633.07	1995.98	1.94	0.44	0.78	2246.90
77.19	626.45	1989.04	1.94	0.44	0.76	2201.44
84.50	621.79	1984.11	1.94	0.45	0.75	2169.74
92.11	618.56	1980.66	1.94	0.45	0.74	2147.84
115.79	723.17	2086.51	1.94	0.43	1.02	2906.94

APPENDIX II

Coordinates of the measurement locations (WGS 84)

Name	x	y
S1	169512	9968943
S2	169631	9968902
S3	169821	9968800
S4	170166	9968642
S5	170488	9968495
S6	170665	9968411
S7	171095	9968227
S8	171360	9968111
S9	171747	9967984
S10	172053	9967933
S11	172553	9968114
S12	172836	9968217
S13	173466	9968528
S14	173711	9968604
S15	174048	9968679
S16	174543	9968802
S17	174730	9968645
S18	174930	9968537
S19	175109	9968512
S20	175654	9968553
S21	175833	9968583
S22	176044	9968643
S24	176298	9968689
S25	176902	9968685
S26	177265	9968591
S27	177395	9968544
S28	177604	9968453
S29	177776	9968380
S30	178055	9968266
S31	178349	9968142
S32	178684	9968022
S33	178890	9967916
S34	179047	9967847
S35	179263	9967758
S36	179445	9967679
S37	179558	9967635
S38	179676	9967582
S39	179808	9967531
S40	179980	9967457

Name	x	y
S41	180121	9967399
S42	180232	9967351
S43	180375	9967290
S44	180482	9967250
S45	180584	9967205
S46	180772	9967128
S47	180899	9967073
S48	181022	9967024
S49	181151	9966965
S50	181315	9966896
SHORT PROFILE		
Name	X	Y
R1	173124	9967964
R2	173202	9967672
R3	173273	9967408
R4	173313	9967241
R5	173247	9966732